NTNU
Norwegian University of
Science and Technology

Photochemistry of a Nucleobase Relevant to the Formation of Malignant Melanoma

Using Spectroscopic Techniques to Study the
UV-Induced Damage of Thymine on MoS_2

Jakob Vinje

Nanotechnology
Submission date: June 2016
Supervisor: Justin Wells, IFY

Norwegian University of Science and Technology
Department of Physics

Das Volumen des Festkörpers wurde von Gott geschaffen, seine Oberfläche aber wurde vom Teufel gemacht.

Wolfgang Pauli

God made the bulk; surfaces were invented by the devil.

Wolfgang Pauli

This thesis is typeset using LaTeX 2_ε and the KOMA-Script book-class. Sketches and illustrations are created with the PGF/Ti*k*Z-package and plots using PGFPLOTS.

The thesis is intended to be printed in colours.

Abstract

Paring of nucleobases in deoxyribonucleic acid and the subsequent transcription of genes is arguably two of the most important processes for life. When subject to ultra violet (UV) light, one of the nucleobases, thymine, can dimerise with a neighbouring thymine forming cyclobutane pyrimidine. This reaction is known for its ability to affect the replication of healthy epithelial cells and causing cancer of type *malignant melanoma*.

In this project the dimerisation between two pure thymine molecules was studied using X-ray Photoelectron Spectroscopy (XPS) and X-ray Absorption Spectroscopy (XAS). The experimental results have been interpreted by means of *ab-initio* calculations using second order Möller-Plesset perturbation theory.

Empirical data suggests that thymine undergoes severe changes upon exposure to high intensity UV light. The molecular modifications are primarily attributed to chemical changes in the functional groups around the pyrimidine, rather than breaking of the ring structure in the molecule.

The two oxygen and the two nitrogen atoms in thymine was found to evolve from being fairly equivalently bound in the molecule to show large bonding differences. A fact that is seen in the core level spectra from oxygen and nitrogen respectively. The photoemission spectra of the peaks both show significant asymmetries after exposure, in contrast to the situation before exposure.

A suggested explanation for the observed change in the experimental data is the tautomerisation of thymine. UV light is known to perturb the keto-enol equilibrium of some molecules, an equilibrium which defines the relative proportions of the different molecular tautomers. The agreement between experimental data and calculations indicate that UV light shifts this equilibrium for thymine as well.

Sammendrag

Base-paring av nukleobaser i deoksyribonukleinsyre (DNA) og den påfølgende transkripsjonen av gener kan påstås å være to av de viktigste prosessene for levende organismer. Når tymin, en av nukleobasene i DNA utsettes for ultrafiolett stråling kan disse dimerisere og danne syklobutan pyrimidine dimer. Denne reaksjonen er kjent for dens evne til å påvirke replikasjonen av sunne epitel-celler og forårsake kreft av typen *malignt melanom*.

I dette prosjektet er dimeriseringen mellom to isolerte tymin studert ved bruk av to typer røntgenspektroskopi: en metode basert på den fotoelektriske effekt (XPS) og en basert på absorpsjon av røntgenstråling (XAS). De eksperimentelle resultatene har blitt tolket ved hjelp av kalkuleringer fra førsteprinsipper ved bruk av andre-ordens Möller-Plesset perturbasjonsteori.

Empiriske data indikerer at tymin gjennomgår store endringer under eksponering av ultrafiolett lys. De molekylære forandringene tilegnes primært til endringer i de funksjonelle gruppene rundt tymin-ringstrukturen, heller enn brudd på ringstrukturen i molekylet.

De to oksygen- og de to nitrogen-atomene i tymin har blitt funnet til å gå fra å være tilnærmet likt bundet i molekylet til å være ulikt bundet. Dette kan sees fra endringer funnet i elektronenes bindingsenergi før og etter eksponering. Fotoemisjonsspektra av elektron-orbitalene viser store asymmetrier.

En foreslått forklaring på de observerte endringene i de eksperimentelle data er basert på prinsippet om tautomerisering. Ultrafiolett lys er kjent for å påvirke keto-enol likevekten i andre molekyler, en likevekt som angir den relative proporsjonen av de forskjellige tautomere. De presenterte eksperiementelle data og kalkuleringene indikerer at denne sammenhengen også gjelder for tymin.

Preface

This thesis concludes my five years of studies at the Norwegian University of Science and Technology (NTNU). The work is submitted in partial fulfilment of the requirements for the degree Master of Science in Nanotechnology at the Department of Physics.

The experimental work described in the following was performed as a cooperation between Federico Mazzola and the author, whereas the text of this thesis belongs solely to the author himself. Certain parts of this thesis are inspired from the authors Specialisation project (Autumn 2015). Some illustrations are reused with slight modifications. All of these are, unless otherwise explicitly stated, created by the author himself.

The first principle calculations were performed by M.Sc-student Merete Falck.

Acknowledgements

Even though only my name appears on the cover of this thesis, several people have contributed to its production. I am grateful to everyone who helped me in finishing this thesis concluding my studies at NTNU. I will look back at my studies, especially the final year, with gratitude and many good memories.

Particularly, I have to thank my thesis supervisor Associate Professor Justin Wells. His support and thoughts have been of great importance during the writing and work with this thesis . His open attitude and including personality has made me feel very welcome in his research group. Justin's educative way of speaking and interest in others success has shaped me as a person and made me interested in pursuing an academic career.

I am also very grateful to Federico Mazzola. His help during preparing the work, performing the work and when doing data analysis has been valuable to me. Federico has motivated me during the work and made me really believe in myself!

Simon Cooil is acknowledged for providing me with valuable tools for doing data analysis and for many good advises. In addition am I thankful for all fruitful discussions with Lars Grønmark Holmen. He has to be thanked for helping me with tips and tricks, and for making all the hours spent working and writing really enjoyable.

Despite the short cooperation, am I indeed very thankful to master student Merete Falck for supplying me with the valuable insight from the first principle theoretical calculations. The thesis would be incomplete without her additions.

Lastly, I have to thank my sister Elise for being a motivating person with great care for others. Her help and comments are of high value to me. Other family members and friends have to be thanked for their continuous support as well.

Contents

Figures and Tables

List of Figures

List of Tables

Abbreviations

ASTRID Aarhus STorage RIng in Denmark

BCC Basal-cell cancer

CHA Concentric Hemispherical Analyser

DNA Deoxyribonucleic acid

ESCA Electron Spectroscopy for Chemical Analysis

FWHV Full-Width at Half Maximum

IMFP Inelastic Mean Free Path

KFPM Kelvin Force Probe Microscopy

LN, LN_2 Liquid nitrogen

MP2 Second order Möller-Plesset perturbation theory

NEXAFS Near Edge X-ray Absorption Fine Structure

NMSC Non-melanoma skin cancer

NTNU Norwegian University of Science and Technology

PES Photo-Electron Spectroscopy

SCC Squamous-cell cancer

SNOOP Same Number Of Optimized Parameters

TMDC Transition Metal Dichalcogenides

TSP Titanium Sublimation Pump

UHV Ultra High Vacuum

UPS Utraviolet Photoelectron Spectroscopy

XAS X-ray Absorption Spectroscopy

XPS X-ray Photoelectron Spectroscopy

Chapter 1.

Introduction

1.1. Background

All living organisms have genetic information which contains information regarding most aspects of cellular life. Most of this genetic information is stored in a strand-like molecule named deoxyribonucleic acid, more famously known as DNA. A DNA strand commonly consists of two individual strands coiled up to form a double helix form.

Each of the strands are composed by smaller units termed nucleotides. These nucleotides are again composed of three main parts: a nucleobase, a monosaccharide (sugar) and a phosphate group. The nucleobases are found in four forms: cytosine, guanine, adenine and thymine. By combining nucleobases in different sequences, information can be stored in the DNA. Such information, commonly referred to as *genes*, is the fundamental information about a living organism life and properties.

Replicating the DNA is done by paring the bases. The two pyrimidines adenine and thymine are paired, and the two nucleobases cytosine and guanine are paired, these are known as purines. Replication of DNA is a process that happens in all living organisms, and is arguably one of the most important processes for cellular life. Replication is done at a blistering speed at all times [2]. Mostly the replication processes proceed just fine. Genes may be replicated many times before any problems occur.

Genes are dynamic structures. They are subject conditions which may alter the process of replication. Carcinogens are known to either change a nucleobase itself or to introduce alternations in the bonding process to other nucleobases. In addition, subsequent nucleobases on a single strand may interact and cause the replication process to halt. Most DNA lesions[1] are corrected by an intricate biological system in the organism itself, however, in some cases this is not sufficient. When this is the case, a patient is said to have cancer and medical therapy is needed. Such therapy is commonly done by chemotherapy or radiation treatment.

[1] A lesion is a change in a biolocial molecule such as cell tissue or DNA.

In this project an alternation in the DNA replication process is studied. as well as the effect UV light has on thymine. More precisely, when two subsequent thymine nucleobases are subject to ultra violet (UV) radiation, they may covalently bond together and interrupt the replication of the gene. In these reactions, a pyrimidine dimer is formed. Throughout the thesis, the mechanisms for this process are elaborated and an analogue to a pyrimidine dimer is tried investigated using X-ray Photoelectron Spectroscopy (XPS).

The goal of this thesis is to contribute to the understanding of the photo-activated reaction between thymine nucleobases. This reaction is responsible for the formation of *malignant melanoma*, more commonly known as skin cancer, a health issue many humans encounter throughout their life. Ultimately the goal of the project is to make way for understanding the reverse reaction, that is to be able to reverse the process of skin cancer formation.

For understanding these reactions, Photoelectron Spectroscopy (PES) is combined with the usage of X-ray Absorption Spectroscopy (XAS) by trying to investigate analogous molecules. In addition the project tries to artificially and controllably dimerise thymine adsorbed onto a molybdenum disulfide (MoS_2-surface) by using synchrotron generated X-ray and UV-photons to both study and induce the molecular changes.

1.2. Previous work

Due to its impact on society and individuals, cancer is a thoroughly investigated field by scientists. A vast array of studies have been completed on most aspects of cancer, its prevention and treatment. Cancer is, as with many other topics, an interdisciplinary topic of research. It can be studied in the frames of medicine, social medicine, biology, chemistry and physics amongst others.

As with cancer in general, photo-activated reactions between thymine nucleobases leading to malignant melanoma have been meticulously studied in the past. However, to the writer's best knowledge, detailed studies on the formation processes, physical properties and photochemical activation of the pyrimidine-dimer using spectroscopic techniques lack. The literature found on this subject is scare and often focuses on one small part of the subject: the biological principles behind the reaction.

Light plays a fundamental role in the universe. It stands behind both the origin and evolution of all living organisms on our earth. Recently, a European research group suggested that life on earth originated from interstellar ice analogues that were exposed to UV light [66]. They found that photochemical and thermal treatment of cosmic ices could be a potential pathway for forming biologically relevant molecules. Via their work, the group has presented an interesting theory for how the life on our *Tellus* originated. In one way this

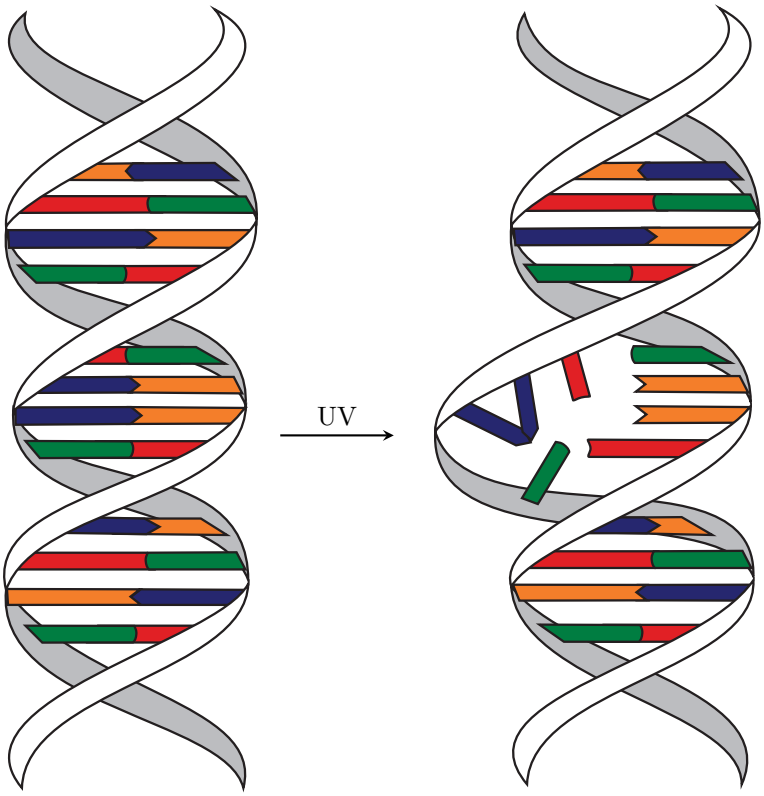

Figure 1.1.: Schematic of double stranded DNA where two thymine nucleobases covalently bond to form a pyrimidine dimer. The two thymine (blue nucleobases in the figure) may covalently bond when the DNA is subject to ultra violet radiation, through a well documented reaction. As illustrated, this causes an enlargement of the DNA at the site, and this is shown to inhibit correct DNA replication [22].

thesis builds on their work, as mutation of genes is one of the mechanisms for evolution of life.

1.3. Thesis overview

In order to contribute to this field, this thesis tries to elaborate further on the physical and chemical effects ultraviolet light has on thymine bases. Additionally, the aim of this thesis is to investigate if it is possible to induce these photochemically activated reactions in artificial conditions using synchrotron radiation.

The thesis is organised in several chapters. The first chapter contains an introduction to the subject as well as the thesis and explains the scope of the work presented herein. Chapter 2 is a brief introduction to the basic theory needed to understand the presented subject, with focus on photochemistry, genes and a basic introduction to the physics behind the experimental techniques used. In Chapter 3 the basic knowledge regarding the equipment and apparatus used in the work is presented. This is done to make the reader be more confident in understanding the results of the practical work presented in Chapter 4. In Chapter 5 are the experimental results presented and discussed. Here *ab initio* calculations are compared to the experimental results as well. Ultimately, a short summary and a conclusion is presented in Chapter 6. The conclusion also contains a suggestion for further work.

Chapter 2.

Theory

This chapter gives fundamental insight into some theoretical aspects of the work presented in this master thesis. First a short introduction to the field of photochemistry is presented. Here the focus is on trying to establish a framework for discussing photochemistry, by introducing basic concepts of light as well as three important laws in the field. Following this is a short introduction to genes, DNA and the formation of skin cancer, where the latter is considered to be a result of "photochemical reactions", as described earlier in this section. Then, a short introduction to two-dimensional materials is presented. The goal of which is to make the reader understand why molybdenum disulfide (MoS_2) was chosen as a template material for doing the investigations presented in later chapters. Lastly, the fundamental physical principles of the used experimental techniques are presented.

Even though, a complete and thorough coverage of theory is outside the scope of this thesis, the author has made an effort in writing an independent theory section. It is built up by introducing some important concepts in the beginning, before these concepts are applied in describing other parts of this thesis background information.

2.1. Photochemistry

Arguably, one of the most important concepts of chemistry is the use of light[1] as a source for supplying energy to drive chemical reactions. Humans do experience photochemical reactions frequently. An example is the chemical reaction of photosynthesis. Photosynthesis is based on plants conversion of solar energy into carbon dioxide (CO_2) and sugar. Without the constant supply

[1] Normally, when one talk about light one refers to a small range of the electromagnetic spectrum between 400 nm to 700 nm. This is only the for humans visible part of a large spectrum of electromagnetic radiation. However, some ambiguousness exist when talking about "light"; it could be the visible part only, or sometimes the whole spectrum. In this thesis, several terms are used interchangeably. For example is no difference intended between "UV-light" and "UV-radiation".

of energy from the sun, life on earth or rather the absence thereof, would look quite different than today. Another example of the utilisation of light, is the activation of vitamin D in the human liver and kidney. Here the energy from the sun is used to introduce a hydroxyl group (–OH) into the organic compound of vitamin D, in a process known as hydroxylation. In other words: chemicals reactions driven by energy from light is a fundamental part of our lives and even for most of earth's life.

2.1.1. The concept of light

Understanding the nature of light is essential in order to understand how photochemical reactions occur. Light has been around since the beginning of time, and scientists and philosophers have tried to describe it almost since the start of civilisations [7]. Considering the scientific description of light since the 1700s, one can distinguish between three paradigms[2]. Sir Isaac Newton had in the late 1600s founded classical mechanics by publishing of his book "Philosophiæ Naturalis Principia Mathematica". Newton explained light as a stream of point particles, analogous to the description from his very successful description in classical mechanics. Newtons large reputation as a scientist, not convincing experimental work, led to this sight being the ruling description of light for many years. Throughout the 1800s, several new experiments demonstrated properties of light that contradicted Newtons description, most notably the phenomena of interference. Some years later Maxwell formulated his hypothesis of light being "a field of electromagnetic charges with properties of waves". In addition he formulated some elegant equations, describing exactly this: light behaving as a wave. Maxwell's theories were challenged in the late 19th century, when it was found that the theory of light being a wave contradicted with the measured electromagnetic spectrum emitted by black bodies. Max Planck developed a theory explaining the radiation, a theory which was based upon light being emitted in discrete packets. Such packets, termed quanta, were later suggested by Einstein to be regarded as real particles.. These light quanta, or photons, were found to have an energy given by,

$$E = hf = \frac{hc}{\lambda}, \tag{2.1}$$

where h is a fundamental constant called the Planck[3] constant, f is the frequency, c is the speed of light and λ is its wavelength. Later it was proposed

[2] According to the Oxford English Dictionary a paradigm can be explained as: *a conceptual or methodological model underlying the theories and practices of a science or discipline at a particular time; (hence) a generally accepted world view* [82].

[3] Named after the German theoretical physicist Max Planck who first recognised the constant in 1900.

that light exhibit both wave and particle properties, known as the "wave-particle duality". Following this was the suggestion from Heisenberg that there was a certain limit for how precise one could measure given fundamental physical parameters such as position and momentum. The Heisenberg uncertainty principle states that

$$\Delta x \Delta p \geq \frac{\hbar}{2}, \tag{2.2}$$

where Δx and Δp is the uncertainty in particle position and momentum respectively and $\hbar$ is the reduced Planck constant, which is defined as,

$$\hbar = \frac{h}{2\pi}. \tag{2.3}$$

2.1.2. Basics of photochemistry

From the expression of the photon energy in equation (2.1), is it obvious that the photon energy is dependent on the wavelength. It is imaginable that light can carry energy and even transfer energy to matter it expose; as when dark objects become warm when subject to sunlight. The heating is due to transfer of energy via photon absorption in the material [98, p. 434]. When the photon is absorbed it may excite the molecule, that is by supplying energy to a bonding electron such that this is lifted to a higher energy level. Conceptually, this can be written as,

$$X \xrightarrow{h\nu} X^*, \tag{2.1}$$

where X is the ground state form of the molecule, and X^* is the excited state after supplying electromagnetic radiations with energy $E = h\nu$.

The excited molecule may give away energy through several different mechanisms. Firstly, the supplied energy may be given away as heat (Q) until it is cooled down to the temperature of the surroundings. Secondly, absorbing a photon can lead to changes in the electronic structure of the absorbing molecule (or an neighbouring molecule), creating "excited electronic states", possibly with physical and chemical properties deviating from the ones of the ground state. Lastly, the energy can be given away with light ($h\nu$), through the processes of fluorescence or phosphorescence. These three processes can be summarised through the following simplistic reactions respectively;

$$X^* \longrightarrow X + Q \tag{2.2}$$

$$X^* + Y \longrightarrow Z \tag{2.3}$$

$$X^* \longrightarrow X + h\nu \tag{2.4}$$

There are no general rules how a molecule react when brought in to an excited state. Excitation can, however, open different reaction pathways, such

that the molecule react in an unexpected way relative to the ground state molecule. Studying the mechanics of excited states and how they react is in the realms of the field of photochemistry. Formulated sixty years ago, Noyes [81, p. 50] description of photochemistry still summarises the field quite well:

> The primary photochemical process comprises the series of events beginning with the absorption of a photon by a molecule and ending either with the disappearance of that molecule or with its conversion to a state such that its reactivity is statistically no greater than that of similar molecules in thermal equilibrium with their surroundings. There may exist several different paths for loss of the absorbed energy and not all of these may result either in dissociation or in conversion of the absorbing molecule to a new molecular species. [81]

2.1.3. The laws of photochemistry

A basic introduction to photochemistry can be followed by three laws describing the fields fundamental concepts. The first law of photochemistry states that only light absorbed by a molecule can produce a change. In other words; for a photochemical reaction to occur, does the molecule need to absorb photons with an energy the source can deliver. Even though irradiated with light, no excitation occur if the molecule cannot absorb the photons.

The second law of photochemistry, known as the Stark-Einstein law states that each photon absorbed causes one molecule to be photochemically activated. Differently said: a single photon is responsible for *one* molecule reacting photochemically [3, p. 10].

The third law, named the Bunsen-Roscoe Law of Reciprocity state that the photochemical effect is dependent on the total energy dose (in $\mathrm{J\,m^{-2}}$). According to Bunsen and Roscoe, the effect should be independent on the irradiation time (given in seconds) and the irradiation power (in $\mathrm{W\,m^{-2}}$), but rather depending on the product of the two [3, p. 18]. For ideal conditions, this is true, but for many biochemical reactions, the relationship fails [36].

2.2. Genetics and mutations

The following section gives an introduction to the field of molecular biology and to the concept of genes. It has to be noted that the field is fascinatingly intricate and that no complete description is provided in this thesis. Aiming for the goal of making the reader able to understand the main biological concepts of the work, a quite broad and qualitative introduction is presented. Many of the biological processes encountered is presented in a simplified manner, this to avoid the reader to become too buried in the small details. Nevertheless

emphasis is on the details that is most relevant for the reader to understand the work presented. As a "complete" description is somewhat outside the scope of this thesis, motivated readers should consult the literature [87].

2.2.1. Deoxyribonucleic acid

A wide range of living organisms express their genes in form of deoxyribonucleic acid, or DNA. DNA is a long polymer consisting of repeating monomers termed *tides*. A detailed structure of an example DNA strand is depicted in Figure 2.1. The nucleotides consists of three main components: a nucleobase, a deoxyribose sugar and a phosphate group. Together these three units build up the repeating monomers that contain the genetic information in the majority of living organisms [18].

Nucleobases are nitrous compounds that are the basic building block of the DNA. They come in four forms: adenine, guanine, cytosine and thymine, where the former two are termed "purines" and the latter two "pyrimidines". The nucleobases or bases, are often described with their abbreviation, A, G, C and T respectively. Bound to the nucleobases are a sugar-phosphate backbone that builds the structure of the DNA-strand. Figure 2.1 displays the molecular structure of the four nucleobases in DNA.

The DNA-strand is a polymer of nucleotides, where the ordering of the nucleotides hold the genetic information. By alternating the order of adenine, thymine, guanine and cytosine, genetic information can be stored. A gene is a part of the DNA containing both an coding and a non-coding element. The former determines what the gene codes for, whereas the latter non-coding part determines when the gene is expressed. Summarised, a gene holds information about how a living organism build and maintain their cells. When a cell is divided, its DNA is copied in several very complex processes to the new cell [18].

Most commonly DNA is observed in a double helix structure where the bases on one DNA-strand is bound to a complementary DNA-strand. Here the bases are paired with their complementary base, such that Adenine+Thymine (A+T) and Cytosine+Guanine (G+C) are bound together by hydrogen bonds. From the chemical structure it is possible to estimate the number of bonds between the nucleobases. Cytosine and guanine form three hydrogen bonds when they bond. Adenine and thymine form two hydrogen bonds. The C+G bonding is thus expected to be stronger than the A+T bonding [102].

The genome of an organism or cell is the total genetic information it possesses. All genes in an organism are stored on one or more chromosomes and the total of all genes form its genome. In other words; a chromosome consists of a very long DNA strand containing genes at given positions or loci[4].

[4]The Latin word *loci* is plural for *locus* meaning "place" or 'position".

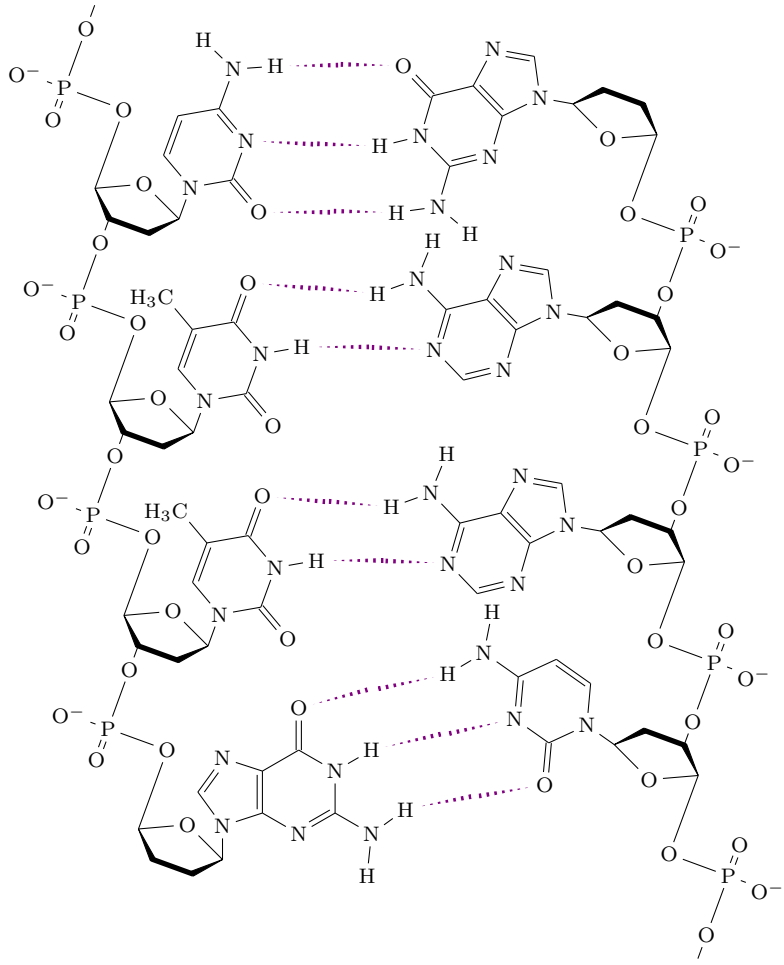

Figure 2.1.: A detailed picture showing the constituents of a double stranded DNA. The leftmost strand consists of the nucleobase sequence: guanine, thymine, thymine and cytosine when counting from the top. Complementary to these bases are the nucleobases on the right strand. Between the nucleobases, hydrogen bonds are indicated.

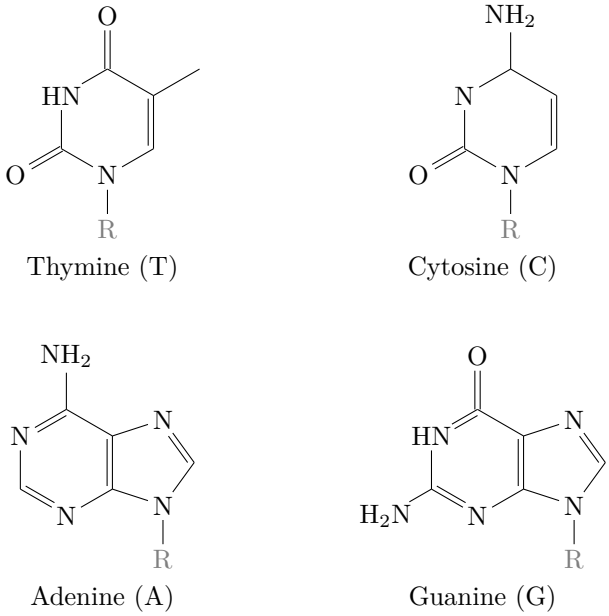

Figure 2.2.: Illustration of nucleobases found in DNA. The nucleobases are connected to a sugar-phosphate backbone, which is indicated on the figure as an arbitrary group, R. Strictly speaking, the "'R-group" is not included in the nucleobase, but it is drawn here to indicate where the bases are bound to the backbone. Thymine and cytosine are known as pyrimidines, whereas adenine and guanine are known as purines.

2.2.2. The dynamic nature of DNA

As with other molecules, also biological molecules such as the DNA is dynamic. They can change over time, either in a predefined or random manner. A human genome consists of approximately 20.000 to 25.000 genes [35], and DNA-damage occurs at a rate of 1000 to 1 000 000 lesions per cell and day [60]. Compared to the number of bases in the human genome, approximately 3 000 000, this is a relatively small number. However, unrepaired lesions in important genes can induce large alternations in the cell build up and maintenance processes. If a cell is not able to repair such a lesion, it could drastically interfere with the cell behaviour and even lead to tumour formation [10, 14]. A normal working cell has numerous mechanisms for identifying and correcting these damages. These mechanisms are often based on the fact that a DNA damage only affects one of the DNA strands, and these enzymes can therefore "proof-read" the DNA by comparing the two. If damages remain unrepaired, important cell functions such as DNA transcription and cell replication may be blocked, and the cell could potentially die.

In addition to the DNA damages, mutation of genes occur. Such mutations involves a change of the DNA sequence on both strands, and can therefore not be recognized by enzymes [18]. In other words, no proof-reading is possible when both nucleobases in a base-pair have changed. Mutations can lead to a small or large change in the cell function. When undergoing cell division, the mutation is transferred to new cells. Although, it is possible to distinguish between DNA damages and mutations, they are related since DNA damages may cause problems in DNA synthesis during its replication. Issues throughout this replication is a major origin of mutations.

It is a relevant question how these DNA damages and mutations effect the organism during its lifetime. As un-repaired DNA damages are accumulating over time, such problems are significant for slowly or non-dividing cells. In addition, for cells with a fast division rate, non-repaired damages contribute to cause problems with replication and thus causing mutations in the new cells. Most mutations are neutral; i.e. they do not effect the function of the gene product. Of the mutations which indeed make a difference to cell function, a large portion have a negative effect; they have a tendency to be destructive for a cells life [89, p. 305]. A result of this being that mutant cells tend to not survive in a population with healthy cells without mutation.

Nevertheless, in some cases, the mutation gives the mutated cell a survival advantage over the non-mutated cells. In these cases, the mutated cell group grows more than the cells around. For the living organism as whole, such a process is very unfavourable, as it could lead to *cancer* formation.

2.2.3. Spontaneous and induced mutation

The molecules that make up the DNA in living organisms are not fully stable, and thus undergo spontaneous changes continuously. These changes at low frequency originates from the instability of purines and pyrimidines and from errors during DNA replication [59]. In addition, the natural presence of given environmental effects may also lead to these spontaneous mutations. Mostly these mutations are kept at a low level due to the low probability and frequency.

On the other hand, treating a cell with certain elements can lead to a rapid increase in the mutation frequency. These mutations, known as induced mutations can be caused by both chemical and physical factors. Such factors are known as *mutagens*. Many of the chemical mutagens are alkylating agents or azides [51]. Alkylating agents are chemicals that substitute alkyl groups C_nH_{2n+1} for hydrogen atoms on another molecule. Azides are compounds containing the azide anion, $N_3{}^-$. Physical mutagens include both ionising electromagnetic radiation[5] and particle radiation[6].

2.2.4. Skin cancer and malignant melanoma

When a cell and its DNA is exposed to mutagens many different mutations may occur [13, 109, 110]. One cancer with high occurence rate is skin cancer. In the white population skin cancer is now the cancer type with the highest incidence rate, and the number of occurences is continuously increasing. It is therefore crucial understanding the mechanism behind the formation of skin cancer.

Skin cancer is a term including three main types of cancer: basal-cell cancer (BCC), squamous-cell cancer (SCC) and melanoma [67]. BCC and SCC are together referred to as non-melanoma skin cancer (NMSC). NMSC skin cancer types constitute the majority of skin cancer diagnoses, but are seldom life threatening for the patient [48]. The opposite is the case for melanoma, as this cancer can become life threatening if not treated early [104]. If treatment is lacking, melanoma may spread into the rest of the body, in other words it can become metastatic[7]. Therapy is then difficult and the patients prospect for healing drops. Melanoma only accounts for about 4% of all skin cancer diagnoses, it is however responsible for about 80% of skin cancer caused deaths. Metastatic melanoma has a five year survival rate of only 14%. In other words: insight into understanding melanoma can ease the life for many [5].

It is known that the risk of melanoma formation is greatly enhanced by

[5] Includes UV radiation, X-rays and gamma rays

[6] Beta and alpha particles being examples hereof.

[7] Metastic cancer is cancer that has transmitted to other parts of the organism via blood vessels or the lymphatics.

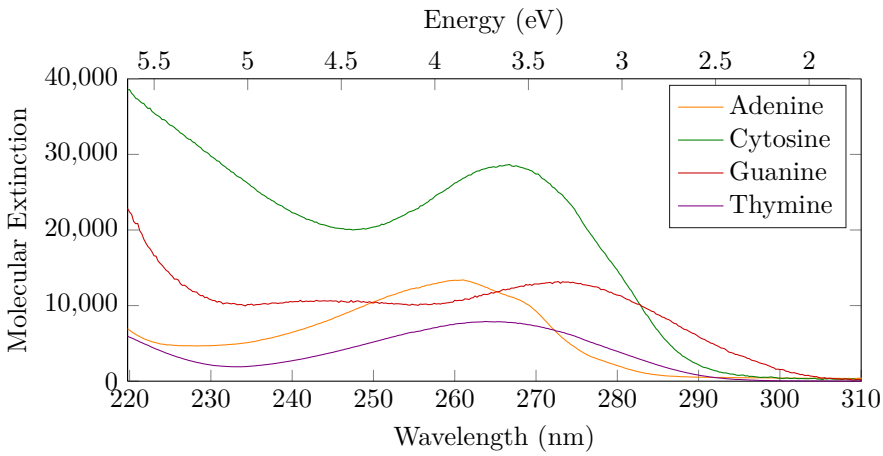

Figure 2.3.: Absorption spectra from the four DNA nucleobases. The molar extinction, given in $cm^{-1}\,M^{-1}$, is plotted for all four bases as a function of both energy and wavelength. The data is from the literature [21].

UV-exposure [25]. In addition to this, some genetic disposition does also influence the probability developing melanoma [68], as well as a previous case of melanoma seems to increase the risk for being affected again [88]. Taken these facts into account, the focus in this thesis on understanding thymine and its changes upon UV exposure is both relevant and important.

2.2.5. Absorption of ultraviolet light in DNA nucleobases

As mentioned in section 2.1.3 for any photochemical reaction to occur, the relevant molecule needs to be absorbing light. More specifically, it needs to absorb light with an wavelength that is provided by the light source. In the case of the dimerisation of thymine, light in the UV range must be absorbed by the thymine molecule. Figure 2.3 shows the absorption spectra for the four DNA nucleobases in the low energy part of the UV range.

From Section 2.2.1 the structural differences and similarities of the nucleobases are evident. They all consists of rings of atoms with alternating single and double bonds. Their absorbance of UV-light is measured experimentally [6] and predicted theoretically [91]. Each of the four nucleotides has absorption spectra which vary a little. If examining the absorption spectrum of DNA, one would fine that the absorbance is some combination between the individual absorbency of the nucleobases [103]. Comparing the energy distribution in

light supplied by the sun, it is evident that some sunlight can be utilised in photochemical reactions in the nucleobases.

2.2.6. Pyrimidine dimers

A pyrimidine dimer is a type of DNA lesion formed when two adjacent thymine nucleobases bond together via a photochemical reaction. The exposure to UV-light promote a formation of covalent bonds between the the thymines, via reactions happening at the C=C double bonds. Via a cyclobutane, the two nucleobases bond to each other forming a pyrimidine dimer. This reaction is indicated in figures 2.4 and 2.6.

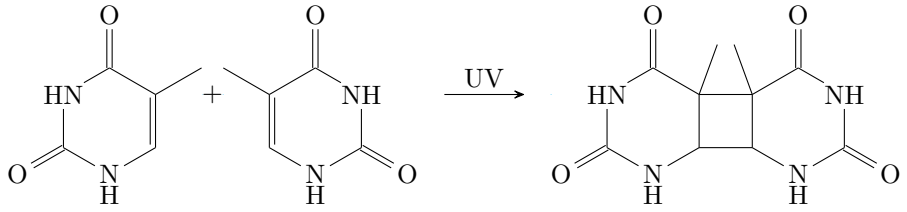

Figure 2.4.: Photochemically activated reaction between two thymine nucleobases forming pyrimidine dimer.

As is the case with many chemical reactions, the reaction form byproducts. In the case of the photoreaction between thymines, one alternate product termed pyrimidine pyrimidone or 6,4-photoproduct is formed. An overview over such a reaction is indicated in Figure 2.5 and proceeds with a rate of about one third of the pyrimidine-dimer formation rate.

Previously explained is the lethal and mutagenic effect of pyrimidine dimer

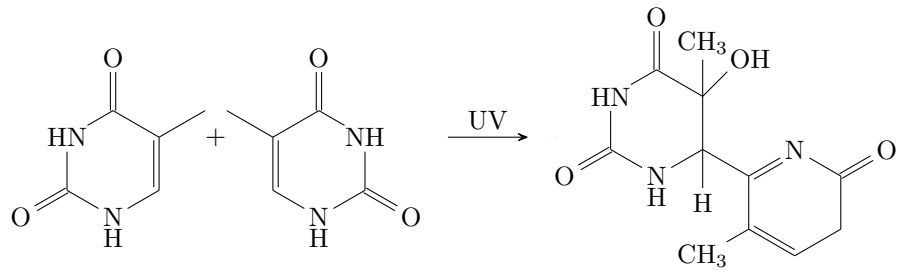

Figure 2.5.: Photochemically activated reaction between two thymine molecules forming the alternate product pyrimidine pyrimidone.

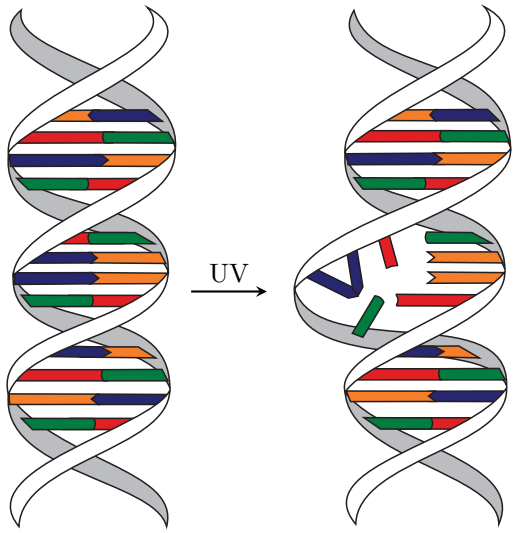

Figure 2.6.: When a double stranded DNA-strand is exposed to UV light, two adjacent thymine bases may covalently bind together forming a pyrimidine dimer. The process is schematically depicted in the figure with the nucleobases thymine, adenine, cytosine and guanine coloured. Please note that the process is exaggerated for illustration purposes.

on biological systems. Compared to this, pyrimidine pyrimidone has a similar effect on biological systems [57, 70]. It is mutagenic and may alternate the replication of DNA in a biological system. However, since the formation rate and thus the presence of the pyrimidine dimer is higher, this molecule can be regarded as more central in the formation of skin cancer for many patients.

2.3. Substrate material

2.3.1. 2D Materials

As templates for doing measurements, several groups of materials can be used. The material is normally chosen based on different aspects, e.g. properties and price. An example of a substrate material is molybdenum disulfide. Known as MoS_2, the material is a important one in a relatively new field of materials. This category known as “two dimensional materials” or 2D materials, represent a group of materials which are novel in many aspects. They are made out of

strictly 2D atomic crystals, that is crystals extending only in two directions. Such materials give rise to interesting properties [32, 77, 77].

These materials often have strong covalent intra-layer bonds, that is strong bonds inside *one* layer. On the other hand, the interlayer bonding, that is the bonding *between* layers only are the relatively weak van der Waals forces [69]. The interlayer van der Waals bonding is reflected in the alternate name for such materials; van der Waals layered materials. Many of these materials exist, the most notable of them being graphene, of which discoverers earned the Nobel Prize in Physics in 2014 [29].

The aforementioned properties give rise to interesting characteristics. First and foremost, 2D materials are as the name suggest infinitely thin. These materials can have an elastic modulus higher than bulk materials we today consider to be strong [9]. They may have breaking strength of many times that of stainless steel, and when this is combined with flexibility, robustness and chemical inertness, a material category of superlatives is born [30, 80].

Two dimensional materials are represented in various kinds of materials. They may have metallic, insulating, semiconducting, ferroelectric or even superconducting properties. Some materials do even posses multiple characteristics based on which direction is investigated; these materials are said to be highly anisotropic [69]. As two dimensional crystals strictly speaking don't have a "interior" or "bulk", they are highly tunable via surface doping of the material [46]. In addition to this, it is possible to alternate the stacking of 2D-layers to give even better control over the properties [58, 115].

From an application point of perspective, the 2D materials can be imagined to be applied in many fields, ranging from semiconductor physics to food industry and fashion. Such materials can be applied in biomedical applications, drug delivery, photovoltaics and electronics amongst others [8, 83, 92, 95]. 2D materials are attractive for these applications both because of their physical properties and that it is relatively easy to fabricate quite complex structures from them [106].

2.3.2. Molybdenum disulfide, MoS_2

One heavily investigated two dimensional material is molybdenum disulfide or MoS_2. As the name suggest it contains both a transition metal cation and a chalcogenide anion leading it to be placed in the families on transition-metal dichalcogenides or "TMDCs". MoS_2 is appearance similar to graphene [44]. They can both be exfoliated from layered 3D material crystals, that is from molybdenite and graphite respectively [75]. MoS_2 is relatively unreactive [100] and inert to acids and oxygen. These properties makes it suitable for doing experiments where the surface should be fairly unreactive. Being inert, the number of contaminants on the surface can be reduced by cleaving the

molybdenite in ultra high vacuum. On the other hand, if the substrate material is too un-reactive, it will be difficult to deposit molecules onto it. The proper degree of "inertness" is therefore a trade-off between several different effects.

In reality, several 2D layered van der Waals materials can be chosen to do photoemission experiments. Multiple materials are suitable when it comes to inertness and stability. Its inertness makes e.g. graphene a good candiate for studying processes where the surface is primarily there as a inactive substrate. However, graphene is a carbon based material and when studying organic compounds, the photoelectrons from the sp^2 bonded carbon in the graphite would make the analysis much more complicated. To avoid this, alternate materials such as MoS_2 is typically chosen when doing photoemission experiments of organic molecules.

Molybdenum disulfide consists of a 2D dimensional honeycomb lattice [69]. Two layers of sulphur atoms arranged in a two dimensional lattice are stacked. In between these layer molybdenum atoms are placed in a trigonal prismatic geometry, in other words each molybdenum atom is bound to six sulphur. A schematic drawing of two monolayered MoS_2 is depicted in Figure 2.7.

MoS_2 is a semiconducting 2D material. Its bandgap ranges from 1.2 eV for bulk material, to 1.8 eV for one monolayer (ML). Interesting enough, not only the magnitude of the bandgap changes when going from bulk molybdenum disulfide to the monolayer case. A transition from having an indirect band gap to having a direct band gap is seen when one monolayer is isolated. In other words, the properties of MoS_2 is interesting from several scientific perspectives.

2.4. Theory behind experimental techniques

In the following, the nature of absorption of electromagnetic radiation by materials and the subsequent spectroscopic analysis techniques is elaborated. In general, a spectroscopic technique is a technique where a response by a system is investigated as a function of energy. Changing the energy either on the incident beam or by detecting a variable energy of the outgoing beam, may give insight into different aspects of the system under investigation.

As spectroscopy is a general term, spectroscopic techniques are very varied. In this section only techniques where electromagnetic radiation is used to induce changes in a materials electronic structure, so called photoelectrons are discussed. The following introduces a semi-classical approach to absorption processes in materials and subsequently discusses some relevant analytical techniques based on this fundamental physics.

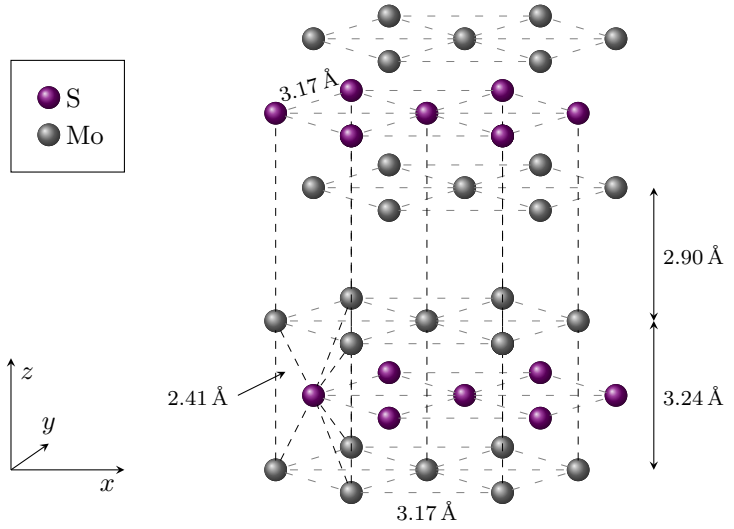

Figure 2.7.: Crystal structure of molybdenum disulfide, MoS_2, is shown in this schematic. Also shown are Mo-Mo, Mo-S and S-S bond lengths and the distance between planes of S. Each plane of molecules are strongly bound, whereas different atomic planes (at different z values) are loosely bound by van der Waals forces. The lengths are according to [37, 45, 55].

2.4.1. Absorption of electromagnetic radiation: a semi-classical approach

When a photon with energy $E = \hbar\omega$ is absorbed by an atom, the energy can be transferred to an electron. Depending on the energy, the electron is either ejected from the atom, or promoted to an higher energy bound state in processes referred to a photoelectric and resonant absorption respectively. Describing the absorption quantitatively can be done by using the linear absorption coefficient [4,63]. The intensity attenuation through an infinitesimal thickness dz of a material can be described by,

$$-\,\mathrm{d}I = \mu I(z)\mathrm{d}z, \tag{2.4}$$

where I(z) is the intensity at position z in the material, μ is the linear absorption coefficient. By integrating the function, one can express the intensity as a function of position inside the material. The equation was originally made famous by Johann Heinrich Lambert and August Beer, and is thus known as the Beer-Lambert equation,

$$I(z) = I_0 e^{-\mu z}. \tag{2.5}$$

The linear absorption coefficient is a material specific parameter. It is also dependent on the photon energy used as well as the atomic number of the absorbing material. μ is defined as the inverse of the attenuation length, i.e $d = 1/\mu$ which is the thickness of a material needed to reduce the intensity of a beam to $1/e$ of its original intensity.

The linear absorption coefficient can be expressed via more fundamental properties of a material,

$$\mu = \rho_{at}\sigma_a = \left(\frac{\rho_m N_A}{M}\right)\sigma_a, \tag{2.6}$$

where ρ_{at} is the number of atoms per unit volume, ρ_m is the density of the material, N_A is Avogadro's number and M is the molar mass of the sample.

The absorption coefficient often has a sawtooth shape when plotting it against the photon energy. The abrupt increase in absorption is due to the fact that the photon energy suddenly is sufficient to ionise an electron up to a new energy level, as seen from Figure 2.8 where $\hbar\omega_2$ is sufficient to ionise the atom. This is also seen when the absorption cross section, or σ_a is plotted as a function of energy. Figure 2.9 shows the total cross section for certain atomic species relevant for this masters thesis. A detailed quantum mechanical description can be found in Mandl's textbook [62] or in other equivalent sources.

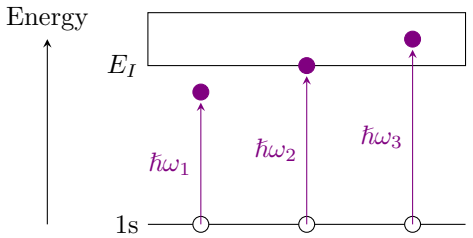

Figure 2.8.: Schematic of electron absorption in a material. The photons have an energy $\hbar\omega$, and their energy determines the strength of absorption. 1s is the core levels from which electrons are promoted, whereas E_I is the energy needed to reach the continuum of states.

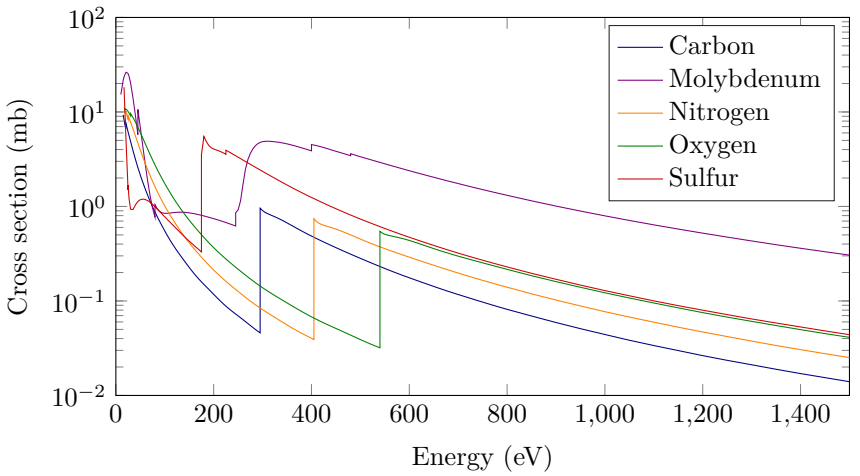

Figure 2.9.: Semi-logarithmic plot showing the total cross section for certain "isolated" atoms relevant for this master thesis. Note that the plot is semi-logarithmic, with the energy on a linear scale and the cross section given in "millibarn" (mb), with $1\,\mathrm{mb} = 10 \times 10^{-31}\,\mathrm{m}^2$. The absorption data are according to calculations previously made [112]

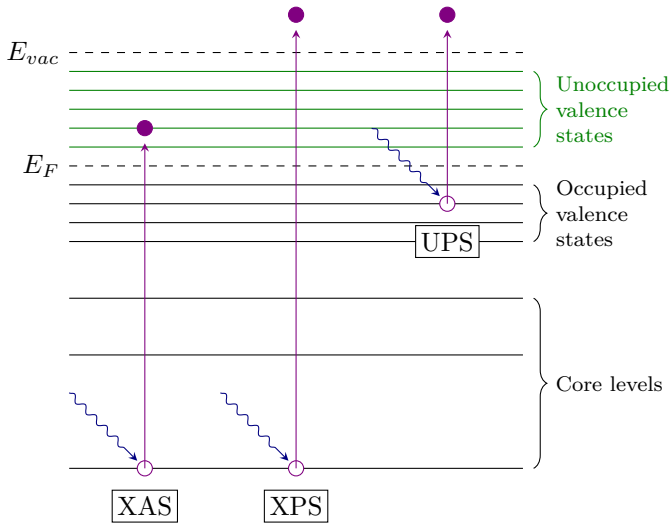

Figure 2.10.: Schematic of spectroscopy-processes where an photon with given energy is used to supply an electron energy. E_F indicates the Fermi level and E_{vac} indicates the vacuum level. Depending on the initial and final state, different properties of the specie is probed. Here, the schematics behind X-ray Absorption Spectroscopy (XAS), X-ray Photoelectron Spectroscopy (XPS) and Ultraviolet Photoelectron Spectroscopy (UPS) is drawn schematically. Note that the energies figure are not to scale.

2.4.2. X-ray Absorption Spectroscopy

From Figure 2.10 it is apparent that the energy, $\hbar\omega$, of the absorbed photon directs which type of electronic transition that occur in the material. If a photon has certain energy, it may be absorbed in the material. As a result of the absorption an electron is promoted from a core level state to an unoccupied state in the valence band. The following section explains the basic theory behind these processes, as well as some practical aspects regarding the usage of X-ray Absorption Spectroscopy (XAS) as a novel characterisation technique in surface physics.

Theoretical description of XAS

As with many physical processes, the total energy is conserved during an absorption process, in other words the energy difference between the final and

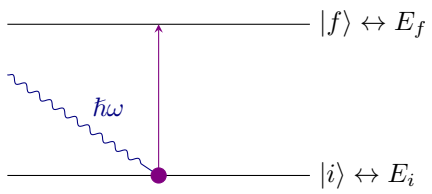

Figure 2.11.: Fundamental principle behind promotion of an electron from an initial to a final state by a photon. A photon with energy $\hbar\omega$ excites an electron from state $|i\rangle$ to state $|f\rangle$. The states are separated by an energy corresponding to the photon energy.

initial state has to be given by the absorbed photon with energy $\hbar\omega$,

$$E_f = E_i + \hbar\omega, \tag{2.7}$$

where E_f and E_i is the energy of the initial and final quantum states respectively. This is schematically depicted in Figure 2.11. Pauli's exclusion principle states that no two fermions, such as two electrons, can occupy the same quantum state. In other words, the final state had to be unoccupied prior to the transition. Further on quantum mechanical calculations yields that the transition probability is proportional to the square of the transition dipole matrix element. Written with Dirac formalism, this is

$$P_{i\to f} \propto |\langle\Psi_f|P_{dip}|\Psi_i\rangle|^2. \tag{2.8}$$

Written in a more direct way this is the same as stating that,

$$P_{i\to f} \propto \left|\int \Psi_f^* P_{dip} \Psi_i \mathrm{d}V\right|^2. \tag{2.9}$$

For a given photon energy there may be other transitions between different quantum states. Due to this, the total absorption probability for a certain photon energy has to include all transitions with the same energy difference. This gives the total probability at a given photon energy as,

$$P_{abs} \propto \sum_{i,f} |\langle\Psi_f|P_{dip}|\Psi_i\rangle|^2 \delta\left(E_f - E_i - \hbar\omega\right). \tag{2.10}$$

Summarised, XAS probes the unoccupied density of states (u-DOS) of the material, given certain assumptions. The unoccupied density of states is highly sensitive to the local electronic properties of the material. This is evident when comparing two absorption spectra from the same electron state in two different

samples. An example is the absorption around the K-edge (1s electron level) in carbon, where the spectra will be dependent on how carbon is coordinated to its neighbours. When qualitatively comparing spectra form diamond [111] and from an organic molecule of porphyrin-type [12], differences are visible. In other words: X-ray absorption spectra from the same element may differ strongly depending on the state of the element.

2.4.3. Near Edge X-ray Absorption Fine Structure (NEXAFS)

The calculated cross sections, visualised in Figure 2.9, are for single and isolated atoms. The precise structure of the steps in the cross section, is highly sensitive to the chemistry of the absorbing atom, that is its formal oxidation state and stoichiometry and the coordination environment. Studying the shape of the absorption edge, can therefore give important information about the element measured [33]. Such a study is termed Near Edge X-ray Absorption Fine Structure (NEXAFS)[8].

In line with other X-ray Absorption Techniques techniques, NEXAFS probes the electronic transition from core levels to unoccupied, but still bounds states. By changing the photon energy, and measuring the absorption strength, it is possible to investigate the absorption around a given absorption edge, yielding valuable insight into the sample. A NEXAFS spectra may consist of three main parts: a pre-edge, an edge and oscillations at higher kinetic energies [74].

At lower energy than the edge, a pre-edge peak may be found. Representing the transition from uonccupied, but bound states, the transition probability (and thus the absorption) is governed by the dipole operator in equation (2.8) and thus therefore include the dipole selection rules [15]. The pre-edge may give information about the local coordination environment and the oxidation state of the absorbing element [15]. Secondly, the edge defines where ionisation from cores to the continuum of states starts. As with the pre edge, the edge is dependent on the oxidation state, where a chemical shift can change the shift the binding energy to higher values with increasing oxidation state. Third, at even higher photon energies, the outgoing photoelectrons have low kinetic energy, and observe multiple scattering events with the surroundings. This is due to the increase in electron inelastic mean free path (see section 2.4.4) at low photon energies. NEXAFS spectras are thus sensitive to a ‘large” area of atomic positions. From these oscillations in the signal, information about the inter-atomic distances and bond angles in the sample is possible to obtain.

Summarised, NEXAFS has several advantages, it may give lot of valuable insights into the sample, it is sensitive to low elemental concentration and the

[8] Also known as X-ray Absorption Near-Edge Structure (XANES). The two acronyms have traditionally been used interchangeably. In this thesis NEXAFS will be used exclusively.

experimental set-up is relatively simple. Obtaining qualitative data, such as oxidation state, coordination and local positioning of the absorbing atom is relatively easy. However, due to multiple scattering events, the theoretical description of NEXAFS signals can be quite tricky. Simultaneously, quantitative analysis of such spectra is mostly omitted, and the spectra are primarily qualitatively analysed.

2.4.4. Photo-Electron Spectroscopy (PES)

A natural extension of the previous discussion follows when one consider the situation at higher photon energies. In the late 19th century Heinrich Hertz discovered that materials illuminated with ultra violet (UV) light created electric sparks more easily [38]. About 20 years later, Albert Einstein published his famous paper on the quantisation of light into discrete packets [24], and explained the phenomenon that became known as the photoelectric effect. Einstein discovered that upon absorption of a photon, electrons can be emitted from the sample with an maximum energy of

$$E_{kin} = h\nu - \phi_s, \tag{2.11}$$

where $h\nu$ is the photon energy[9] and ϕ_s is the work function of the material, that is, the barrier the electrons at the surface need to overcome to escape the material. The work function is discussed in detail later in this theory introduction. Not all electrons escape the sample with the same energy. Causing differences in electron kinetic energy is that electrons are bound in different states in the sample. Therefore, the electrons emitting the sample have the a kinetic energy in vacuum of

$$E_{kin} = h\nu - E_b - \phi_s, \tag{2.12}$$

where E_b is the initial binding energy of the electron. The binding energy is referenced to the Fermi level. When the sample and analyser are placed in electrical contact (both being at ground potential), their Fermi levels align. This lead to a contact potential given by $\phi_s - \phi_a$, which again lead to an offset in the measured kinetic energy of the photoelectrons given by,

$$E_{kin} = h\nu - E_b - \phi_s + (\phi_s - \phi_a) \tag{2.13}$$

$$= h\nu - E_b - \phi_a. \tag{2.14}$$

In other words, the kinetic energy of the photoelectrons is measured relative to the analyser's vacuum level. Thus, the work function of the analyser has to be known to correctly calibrate the binding energy scale [19, 94, 99]. A schematic of the process described in the previous, is shown in Figure 2.12

[9] For clarity: $h\nu = \hbar\omega$. The equality comes from the definition of the reduced Planck constant, $\hbar = h/2\pi$. In other words $\nu = 2\pi\omega$.

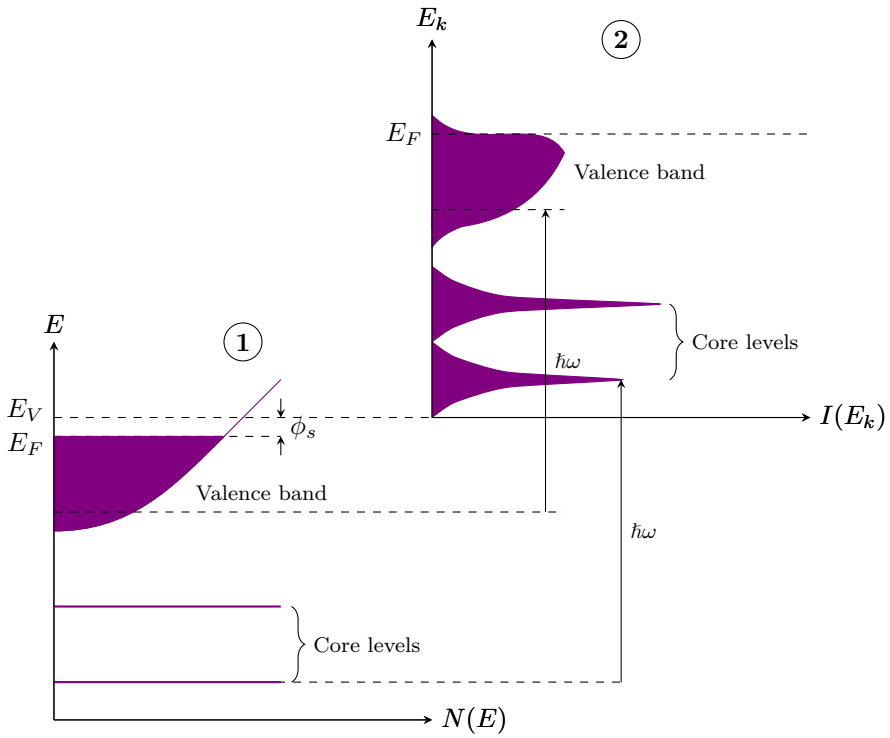

Figure 2.12.: Energy scheme of photo-electron spectroscopy processes. The figure shows the distribution of electrons as a function of energy in the sample, (1) and how the measured photo-electron intensity spectrum, (2) depended on the energy of the detected photo-electrons. To the line width broadening both physical and experimental processes contribute, as described in the section about "Peak profiles". Note that the axis are off-scale, that the broadening of core levels are exaggerated and the processes are oversimplified for illustration purpose.

Fundamentals of PES

Photoemission spectroscopy has proven a valuable technique for investigating the chemical and electronic properties of a sample. The principle of photoemission has been known since the times of Einstein and Hertz, but theoretically describing the process and using it for accurate quantification of properties was not possible until the late 60s. Several models for theoretically modelling photo-emission has been presented [20]. One way is with a *three-step model*. This model involves, as the name suggests, three steps:

1. Excitation of a bulk atom into final state,
2. Transport of the electron to the surface,
3. Transmission of electrons through the surface and out of the material for detection.

Such a simple model and step-based is frequently applied to describe the photoemission from a solid, especially when the process is used to describe the band structure of a solid. However, from a quantum-mechanical view, the model oversimplifies the situation. Quantum mechanically, the three steps are entangled and occur at the same time. One therefore has to apply a *one-step model*. The one-step model is regarded as more close to the actual process during photoemission [20]. In the following the three-step description of the photoemission process is used as it gives a simpler phenomenological description of the process relative to the one-step process, which is more abstract for the reader.

The first step involves an excitation from an initial state, i, to a final state, f, in the material. It is described by the previously mentioned *golden rule* as,

$$w_{i\to f} \propto |\langle \mathbf{k_f}|P_{dip}|\mathbf{k_i}\rangle|^2 \delta\left(E_f - E_i - \hbar\omega\right), \tag{2.15}$$

where $\mathbf{k_i}$ and $\mathbf{k_f}$ are the wave-numbers of the electron in the initial and final states respectively, P_{dip} is the transition matrix element, E_f and E_i are the initial and final energies and $\hbar\omega$ is the photon energy. As seen from the equation, there will be no photo-electron emission unless there are unoccupied final states that match with the photon energy.

In the second step of the model, the electron propagates towards the surface of the material. Electrons travelling in a solid generally have a very short mean free path before they lose energy in collisions. This is the reason for the extreme surface sensitivity of photo-electron techniques. The mean free path of electrons in solids are described in section 2.4.4.

Finally, in the third step of the model, the photoelectrons are actually emitted from the material. During this process the electrons are travelling

against a potential and the electron momentum in the z-direction is no longer preserved. In the surface plane, there are however no potentials for the electrons to overcome, and the lateral momentum is therefore conserved. This, together with some assumptions makes us able to say something about the initial electron state in the material. Using this, photo-electrons spectroscopy has proven a valuable method for investigating the electronic properties of materials.

Work function

The work function, ϕ, of a material is defined as the difference in potential energy between the vacuum level and the Fermi level of the surface. Typical values for the work function are ranging from about 3 eV to 6 eV. For a given material the work function can vary, depending on many factors.

In reality, the work function is a surface parameter, that is, its magnitude is dependant on the crystal plane the electron is emitted from. There is a tendency that electrons in more dense surfaces require a higher amount of energy to be removed [49].

There are several ways to measure its magnitude, one of the most frequently used being the Kelvin Probe Force Microscope, or KFPM. This technique measures the offset between the tip and sample surface potential [78]. Another simple, albeit less accurate method is to measure the current leaving a surface subject to an excitational force. The method comes in three variations, dependant on the excitation source, thermionic emission where the source is heat, photoemission with photons as source, and field emission when a strong electric field is applied. In all cases, the work function can be related to the emission current.

Surface sensitivity of PES based techniques

One property of X-rays are known to many; the ability for these rays to penetrate deep into or even pass completely through a material [4]. When a sample is exposed to light, photons will excite atoms and create photoelectrons according to the process scheme described in the previous description. This will occur at different depths in the material, as the probability for a photo-ionisation process to occur at a certain depth is above zero. Created photoelectrons commonly have an energy of below some hundred electron volt[10] (eV) and are very reactive. Due to their reactivity, they cannot travel far before they lose their energy due to interactions with constituent atoms in the sample.

The length between two scattering processes (i.e. collisions) are characteristic for a sample and a given photoelectron energy, and is known as the inleastic mean free path (IMFP). When looking at the electron movement for a large

[10] 1 eV = 1.602 176 53 J.

number of materials and electron energies, the IMFP is found to follow an universal curve. According to literature [93] the inelastic mean free path of elemets are governed by,

$$\lambda_e\,[\mathrm{nm}] = \frac{538a}{E^2} + 0.41a^{3/2}\sqrt{E} \tag{2.16}$$

where E is the electron kinetic energy in eV and a is the mean atomic distance given by

$$a = \left(\frac{M}{\rho N_A}\right)^{1/3}. \tag{2.17}$$

As seen from equation (2.16) and equation (2.17) the IMFP weakly depends on the atomic specie, but strongly on the electron kinetic energy [41].

PES-techniques are in general highly surface sensitive, a feature attributed to this very short inelastic mean free path. Only electrons emitted above some depth will be allowed to escape the material and reach the detector. Usually a *sampling depth* is defined as the depth of which 95% of the photoelectrons arise. This thickness is defined to be given by,

$$t \equiv 3\lambda_e \cos\theta_e, \tag{2.18}$$

where λ_e is the inelastic mean free path of the photoelectrons and θ_e the photoelectron emission angle, defined as the angle between the surface normal and the detector. The correction factor $\cos\theta_e$ accounts for when the photoelectrons have to travel a longer distance to escape from a tilted sample towards the detector.

Variations of spectroscopy

In principle, many PES based techniques are available. This is due to the fact that both the analyser, source experimental set-up can be constructed in such a way that they can vary several parameters. If one imagines an ideal analyser, this can resolve the electron energy (E_{kin}) and the electron emission angles (θ_e and ϕ_e). In addition the spin polarisation of the photoelectrons can be detected in a spin-resolved detector.

Source and experimental set up can be constructed such that they ensure variable photon energy ($h\nu = \hbar\omega$) at a variable incident angle (θ_p and ϕ_p). Some sources may also have an variable light polarisation (ϵ).

Summarised, the measured intensity will be a function of all these parameters, in other words, $I = I(h\nu, \theta_p, \phi_p, \epsilon; E_{kin}, \theta_e, \phi_e, \sigma)$. From this, several PES based techniques are imaginable, with some of the most widespread being;

- X-ray and Ultraviolet Photoelectron Spectroscopy (XPS and UPS)

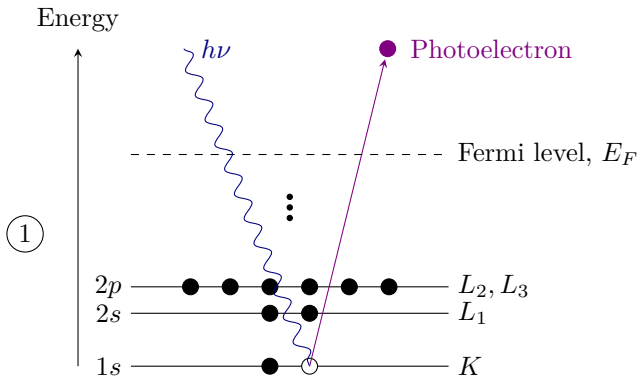

Figure 2.13.: Schematic description of photoemission from an energy perspective. A high energy photon is absorbed by an atom, and its energy is transferred to an electron. If this energy is high enough, the electron will be emitted as a "photoelectron".

- Spin-Polarised Photoemission (SP-PES)
- Angle-Resolved Photoemission Spectroscopy (ARPES)
- Photoelectron Diffraction (PED)

The interested reader should consult the literature [4, 108].

Features of spectroscopy spectra

A photoelectron-spectrum as mentioned earlier, a fingerprint of the occupied density of states (DOS) in the material. As Figure 2.12 suggests, the spectrum is not simply the DOS close to the surface region transposed up in energy by an amount of $\hbar\omega$. Several additional features is seen in a PES spectrum. The following describes certain features of such a spectrum based on one example spectrum in Figure 2.15. The discussion is kept short, and the reader is suggested to consult additional literature [4, 41, 108].

Direct photoemission peaks When a sample is subject to X-rays several processes may happen. If an incoming photon transfers its energy to an atom and an electron is emitted the process is termed "direct photoemission". The electron emitted, i.e. the photoelectron, have a certain energy and can be detected using an electron analyser. Such electrons have a detected energy depending on the binding energy in the material and the energy of the incoming

radiation, according to equation (2.14). Their core-level binding energy is independent on the photon energy used. Figure 2.13 shows a schematic of the process. When analysed in an PES spectrum, the core level electrons are named after the orbital left behind, such as 1s, 2p, *et cetera*.

Auger emission peaks An Auger process starts in the same manner as "direct photoemission". For the system to minimise its energy, the core-hole quickly fills after emission. The core hole is filled by an electron from another energy band and an electron with the transition energy is emitted. These emitted electrons are called "Auger electrons" and have a characteristic energy independent on the photon energy, $\hbar\omega$. The Auger process thus leads to a doubly ionised atom. Auger processes are named after the energy levels taking part in the process, an example being the KL_2L_3 Auger process, as shown in Figure 2.14.

Chemical shifts The exact binding of electrons in a material does not only depend on the "pure" core level, but also on the oxidation state of the material as well as the local chemical and physical environment. Due to this, seemingly similar electron orbitals, such as the 1s-orbital can be shifted to different binding energies. This shift is called "chemical shift", as its sensitive to the chemical state of the atoms, a fact that is the origin for the earlier name of XPS, Electron Spectroscopy for Chemical Analysis (ESCA).

When a photoelectron is emitted from an atom, the remaining electrons rearrange (relax) in order to minimise their energy, known as a final state effect as it happens after the electron promotion to the final state. On the other hand are initial state effects, that is a modification in electronic environment before emission. This effect can be view upon as a "true" chemical shift. In principle, chemical shifts originate from both effects, but in many cases it is a valid approximation to assume that the chemical shift is primarily due to the initial state effects.

One significant initial chemical effect is the oxidation state of the atoms. At higher oxidation states the binding energy seems shifted towards higher values. One simplified view for this, is that at higher oxidation states the interaction of inner shell electrons with the nucleus is higher. When a core electron is emitted, the effective screening of the nucleus potential is lower, leading to higher binding energy of the remaining core electrons. Another imporant chemical shift is the surface core-level shift. At the surface the electronic environment of the top atoms differ from that of the atoms in the bulk, leading to a shift in binding energy for the core levels [42].

Plasmon losses X-rays can penetrate deep into a material. When the radiation transfers its energy to an atom, a photoelectron is created at a certain

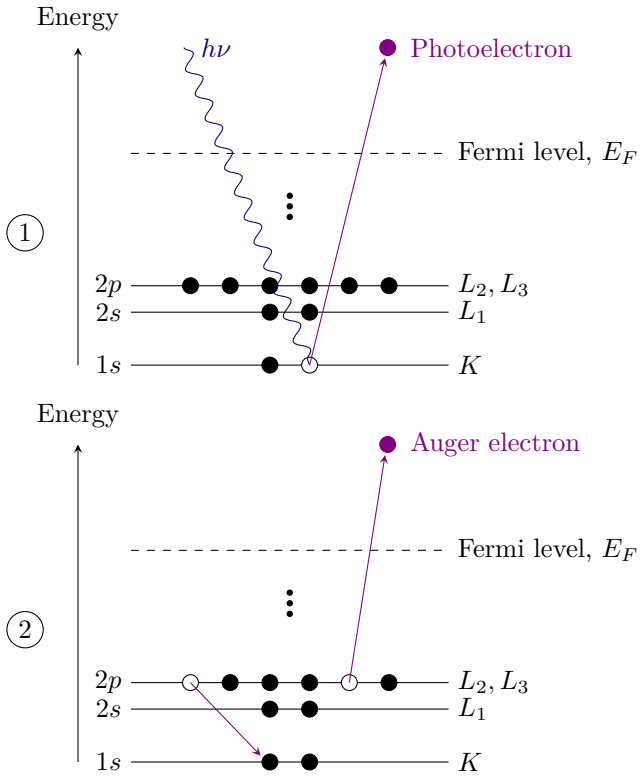

Figure 2.14.: Schematic picture of the Auger emission process. A high energy photon creates a core-hole with a finite life-time. When an electron from a higher lying orbital fills the hole, the energy is transmitted to another electron which leaves the atom. This emitting electron is called Auger electron.

depth. Such low electrons are known to interact heavily with the constituent material, as described in section 2.4.4. During inelastic collisions, the electrons transfer some of their energy to the material, and may induce collective oscillations of the electron gas in the material. Such oscillations are known as "plasmons", and will contribute to the signal at the low kinetic energy "tails" of the core level peaks. The plasmons have characteristic values for each material, and one or several plasmon peaks may therefore be found at the higher binding energy side of core-level peaks. In addition, since PES-techniques are highly surface sensitive, another process contributes [53]. Close to surfaces or interfaces, collective movement of the surface electrons can be excited [49]. Such an excitation is quantised in energy, where the energy, $\hbar\omega_{sp}$ is given by,

$$\hbar\omega_{sp} = \left(\frac{n\hbar^2 e^2}{m_e \epsilon_0}\right)^{1/2}, \tag{2.19}$$

where e is the elementary charge, m_e is the effective electron mass, n is the conduction electron density and ϵ_0 is the permittivity of vacuum. The surface plasma resonances will contribute to the measured spectrum as well.

Spin-orbit splitting In photoemission spectra certain peaks seem to be split into two peaks. This comes from an effect called spin-orbit splitting. When an unpaired electron is left in a degenerate orbital (in other words $l > 0$), the photons and the electron spin may interact in two ways, either in an parallel or in an anti-parallel orientation. This leads to the originally one energy level to split into two states corresponding to $j = l \pm 1/2$, analogous to $j = |\mathbf{l} \pm \mathbf{s}|$. For non-degenerate shells, such as the s shell, no splitting occurs [41]. Reason for the two states having different energies, is that the magnetic moments due to orbital motion and electron spin may oppose or reinforce each other.

The two peaks have different intensities and area in the PES-spectra as the number of electrons in the degenerate levels are changing from shell to shell. Calculating the peak area is possible by using,

$$r = \frac{2(l+s)+1}{2(l-s)+1}. \tag{2.20}$$

In other words, the states where the number of electrons are highest, will consequently have the highest intensity and area in the measured PES-spectrum. Electrons in p-orbitals have an area ratio of 1:2, d-orbitals 2:3, and f-orbitals 3:4. Details of this difference are presented in Table A.2 in Appendix A.

Satellites and ghost peaks Not all features in an spectrum can be attributed only to the electron structure of the sample itself. When accelerating electrons

towards an anode X-rays are generated. Based on the anode material, X-rays with characteristic wavelengths are generated. However, the resulting X-rays are not completely defined in energy, they have a spread, and several transitions in the material create X-rays of different energy. One of the lines is although often more bright. In addition to this, two of the most frequently used anode materials aluminium (Al) and magnesium (Mg) oxidises quickly, leading to a contribution from oxygen to the generated radiation. The peaks from different emission lines in one material are known as "satellite peaks". Oxygen contaminant contribution lead to peaks in the spectrum termed "ghost peaks".

As the different wavelengths generated using a certain material is known, it is in theory possible to attribute certain peak to different emission lines from each material. Their energy separation is given, and one can therefore assess the spectrum with this in mind. This applies for the contribution from oxidised surfaces as well. Detailed discussion on the generation of X-rays in X-ray tubes can be found in section 3.2.1.

The satellites and host peaks are in other words caused by the incoming X-rays having not only one wavelength. By using a monochromator, which filters the signal, such peaks can be avoided [4, 108]. These components are good for achieving a higher quality radiation beam, but have a large caveat: the beam monochromation leads to a considerable loss in beam intensity [4].

Analysis of spectra

Background models When measuring an emission spectra, the measured peaks always lie on top of a background signal. The background signal can contain useful information, but for simplification purposes, its normally subtracted from the signal. On one hand doing this is simple; a background signal is subtracted from the total signal. On the other hand; how is the background signal found? How can a background be modelled and which one of the models is closest to actual physics?

The background can be modelled in several ways, e.g. by using 1) a linear background model, 2) a Shirley background or 3) a Tougaard background. [42, 97] The linear background model is the simplest model, whereas both Shirley and Tougaard are more refined models accounting for more of the actual physics happening. The latter two are often considered to be closer to reality than when using a linear model. More detailed information on background subtraction can be found in the literature [42, 107].

Peak profiles The width of the photoemission peaks in a spectrum is largely determined by two contributions. A fundamental physical contribution comes form the natural linewidth of a core hole state left after photoemission, 2τ,

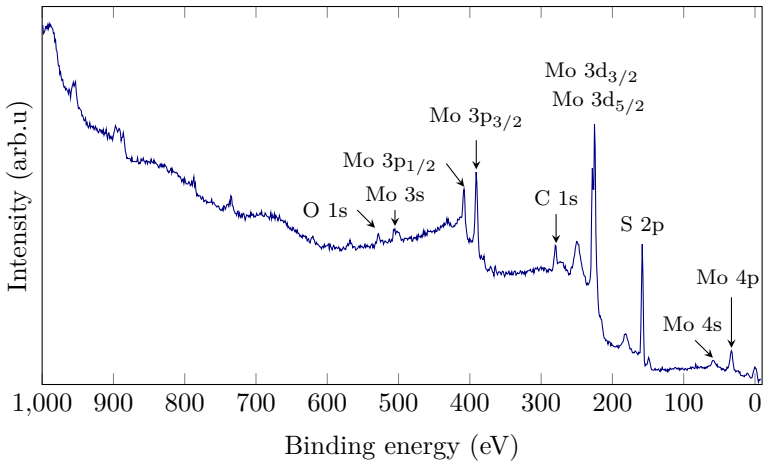

Figure 2.15.: Important characteristics of a PES spectrum presented with an widescan of a MoS_2-surface by using a Mg Kα X-ray lamp. Each detected peak is corresponding to one energy level in one of the atoms present in the sample.

known as lifetime broadening. By considering Heisenberg's uncertainty principle (as described in 2.1.1), one can estimate this broadening by

$$FWHM_{c-h} = 2\tau = \frac{h}{\tau} = \frac{4.1 \times 10^{-15}}{\tau}, \tag{2.21}$$

where h is Planck's constant, and τ is the time before the core hole gets filled, in other words the lifetime of the corehole. The intensity from a core hole is an Lorentzian function with a full width half maximum (FWHM) of 2τ and given by,

$$I(E) = I(E_c) = \frac{\tau^2}{(E - E_c)^2 + \tau^2}, \tag{2.22}$$

where E_c is the energy of the core hole, and E is the excitation energy. Using C1s or N1s with a lifetime of 6 fs, an estimate for the lifetime is about 0.68 eV [28].

In addition to the intrinsic lifetime broadening, one has to take broadening of the lineshape due to experimental contributions into account. Several factors may contribute, such as a broadening of the X-ray signal, Gaussian broadening due to atomic vibration and analyser resolution must be taken into account. These contributions add Gaussian broadening of the signal from the core hole. Summarised, the broadening (expressed by the FWHM) can be expressed as

$$\mathrm{FWHM_{tot}} = \left(\mathrm{FWHM^2_{c-h}} + \mathrm{FWHM^2_{analyser}} + \mathrm{FWHM^2_{X-ray}} + \ldots\right)^{1/2}. \tag{2.23}$$

The combination of these broadening profiles is therefore the combination of both a Lorentzian profile and possibly several Gaussian profiles. Such a profile is known as Voigt-profile, named after the German physicist Woldemar Voigt.

Other lineshape broadening profiles are possible as well. They can be based on different assumptions and may include other terms. In the end, the choice of profile is determined by personal preferences and which model fits best to the modelled peaks [41, 71]. In this thesis Voigt-profiles are used exclusively.

Detecting electrons

The previous has discussed emission of photoelectrons from a surface to high degree of detail. However, none of the discussed techniques would be useful without the ability to detect the photoelectrons, which may have different energies and momentum. A detection system mainly consists of two parts. First an analyser is used to control the momentum and energy of the electrons that reach the second component, namely the detector.

There are several different ways to analyse the photoelectrons, with one of the most popular being the concentric hemispherical analyser (CHA). As the name suggests, it consists of two concentric hemispheres with different radii. Between these metallic hemispheres, a potential difference is applied, leading to an electric field in between. When electrons enter the analyser, only the electrons with a given energy, E_0, will be able to reach the detector screen. Conventionally, this energy is referred to as the pass energy. Electrons with an energy different from E_0 will have an path leading to the loss of the electron. The optimum path corresponding to the correct energy is indicated in Figure 2.16. The figure shows an schematic drawing of a CHA [17].

Hemispherical analysers have different operating modes, with a common operation mode being the constant pass energy mode[11]. In this mode the pass energy is held at a constant value, and the lens system before the analyser is used to accelerate (or decelerate) the electron to the correct kinetic energy that is accepted by the analyser. To collect electrons with different energies, the lens systems is scanned over a range of voltages. In this mode the energy resolution is given by,

$$\frac{\Delta E}{E_0} = \frac{W_S + W_F}{4R_0} + \frac{(\delta\alpha)^2}{2}, \tag{2.24}$$

where W_S and W_F is the opening slit size for the entrance and exit into the hemispherical analyser, R_0 is the radii of the electron path in the analyser, and $\delta\alpha^2$ is a correction for the angular spread. From equation (2.24) one can

[11] The constant pass energy mode is also known as Fixed Analyser Transmission (FAT) mode or Constant Analyser Energy (CAE) mode.

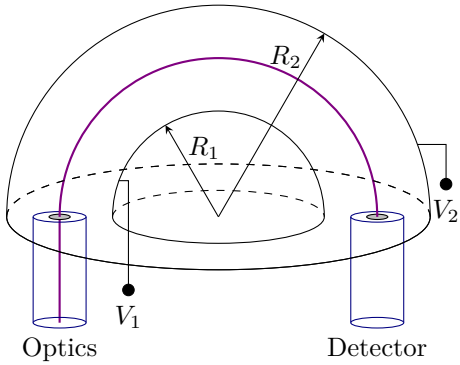

Figure 2.16.: Schematic of a concentric hemispherical analyser (CHA). Between the two hemispheres is the electron path indicated.

see that the resolution is determined by the pass energy. A lower pass energy yields better resolution, but also lower signal intensity and thus worse statistics. Quantitatively the pass energy ranges from 2 eV to 5 eV for UPS scans, through 5 eV to 30 eV for high resolution XPS measurement of specific core-level, up to 50 eV to 150 eV for wide energy XPS scans.

Chapter 3.

Equipment and Apparatus

The following chapter seeks to give an introduction into the equipment and apparatus used in the experimental part of the present thesis. First, a basic introduction to vacuum science is given, herein the basic principles of vacuum science with regards to pumps, pressure monitoring and sample preparation are presented. Secondly, a semi-detailed description on the creation of electromagnetic radiation, more specifically UV radiation and X-rays, is presented. Lastly, some instrumental aspects of the main techniques used in this work, photoemission- and photo-absorption spectroscopy, is presented.

Describing the instrumental aspects of the master thesis is important to the author as it makes the reader more able to interpret the results and follow the discussion presented in later thesis parts. Much of the work is highly sensitive to contaminations and it is crucial being aware of the right process steps, and a detailed description of these techniques are thus relevant. In addition, much of the practical work during the writing of this thesis was to understand and operate equipment in the laboratory both in Trondheim and in Aarhus.

3.1. Vacuum science

For many years, vacuum science in general and performing UHV experiments in special has been an important field of science. Vacuum conditions are characterised by a pressure lower than atmospheric pressure. The pressure range from atmospheric pressure down to the ultimate pressure achievable by humans covers many orders of magnitude. As the physics vary with varying pressure it is common to divide the wide range of pressures into different regions, as listed in Table 3.1. Defining pressure regions are done differently, and the table list one possibility. Table 3.1 mentions “perfect vacuum” as a pressure region, however is perfect vacuum rather a theoretical construct. Perfect vacuum refers to the total absence of any particles, which is unattainable in laboratory conditions.

The following part aim to explain the characteristics of such vacuum systems and how to achieve the low and controlled pressures needed for performing

certain experiments. As the following discussion will reveal; achieving ultra high vacuum conditions are certainly not trivial.

Table 3.1.: List containing pressure regions, their abbreviation, pressure and corresponding mean free path (MFP) of gas molecules. [50]

Name of region	Abbrev.	Pressure (mbar)	MFP (m)
Low vacuum	LV	300 to 1	10^{-7} to 10^{-4}
Medium vacuum	MV	1 to 10^{-3}	10^{-4} to 0.01
High vacuum	HV	10^{-3} to 10^{-7}	0.01 to 10^{3}
Ultra-high vacuum	UHV	10^{-7} to 10^{-12}	10^{3} to 10^{8}
Extreme high vacuum	XHV	$\leq 10^{-12}$	$\geq 10^{8}$
Perfect vacuum		0	∞

3.1.1. Vacuum chambers

As the name suggests, a vacuum chamber is a low-pressure closed volume separated from the surroundings. In the past, chambers were made out of glass. In modern time, glass has been replaced by chambers made out of stainless steel. Modern chambers have the advantage of being expandable with different types of components through flanges. These flanges are commonly sealed with metal gaskets[1], as they do not out-gas when subject to vacuum. A two knife edges on the flanges deform the gasket and thus create a seal by clamping the metal between them. Consequently, the metallic gaskets are only usable once. Other gasket alternatives are gaskets made out of vacuum compatible synthetic rubber materials, such as Viton. These can be used several times. Pumps are used to attain and keep vacuum conditions in the chamber.

One question arises quickly; why do we need vacuum conditions for doing these experiments at all? As previously described, photoelectrons emitted from a sample are highly reactive. If they were subject to a gaseous environment right after emission, it would be a finite probability for them to be absorbed and detection would not be possible. Despite this, the most advantageous feature of UHV-conditions is the ability to create a clean and controlled environment for doing analysis. For doing experimental procedures on the sample rather than on absorbed contaminants, the coverage of such has to be lower than a few percent of a monolayer. At atmospheric pressure, the gas molecules in the air hit the sample with a certain rate. Calculating this rate allows us to estimate the number of contaminants present on the sample surface at a given time.

[1] E.g. made out of oxygen free copper.

The pressure p determines the impingement rate of residual gas particles on a square centimetre of a sample per second. From kinetic theory of gases [47, 61] the flux of particles through a surface of unit area per unit time is given by,

$$\phi = \frac{n\bar{v}}{4}, \tag{3.1}$$

where n is the number density and $\bar{v}$ is the mean velocity of the particles. From kinetic gas theory, the mean gas particle velocity can be derived as well,

$$\bar{v} = \sqrt{\frac{8k_BT}{\pi m}}, \tag{3.2}$$

with k_b being the Boltzmann constant, T the temperature and m the particle mass. Using equations (3.1) and (3.2) together with the expression for pressure, $P = nk_bT$, from the ideal gas law, an expression for the flux can be found in terms of measurable parameters and constants as,

$$\phi = P\left(\frac{1}{2\pi k_BTm}\right)^{\frac{1}{2}}. \tag{3.3}$$

If typical values are inserted into 3.3, one would find that a pressure of 10^{-6} torr is sufficient to building up a monolayer of adsorbates per second. This value is defined as 1 Langmuir (1 L), in other words, a dosage of 1 L is the dosage corresponding to exposing the surface to 10^{-6} torr for 1 s. Using Langmuir[2] as a unit may give a more direct "perception" of the amount of absorbate coverage on a sample. At lower pressures the impingement rate of particles are much lower, and longer time are needed for attaining the same dosage, e.g. 1000 s at 10^{-9} torr.

As Table 3.1 suggests, *perfect* vacuum is not possible to attain in laboratory conditions. This is due to several processes occurring continuously in the vacuum chamber. The walls of the chamber may contain trapped gases, that over time are released into the chamber [84]. On the inside of the chamber walls, gas molecules may adsorb. An example is when breaking the vacuum; the content of H_2O in the air is enough to completely cover the inside of the chamber with H_2O-molecules over only a short time. At lower pressures, the gas molecules will desorb, and thus increasing the pumping load and increasing the ultimate obtainable pressure. The process of diffusion also works against vacuum scientists. Gas molecules may diffuse into the vacuum chamber through the chamber walls.

These processes all contribute to increase the pressure inside the chamber. In principle, with no leakage, the vacuum pumps can be switched of when low

[2]Named after the American chemist and physicist Irving Langmuir (1881 - 1957).

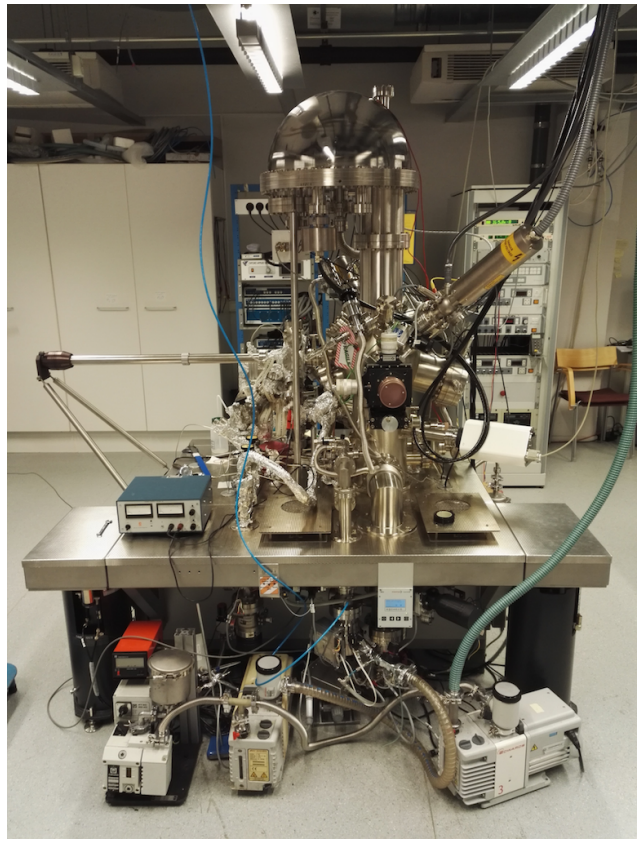

Figure 3.1.: UVH experimental chamber at NTNU. Below the chamber several pumps can be observed observed, more specific roughing- and turbo pumps. Below the chamber stand, hidden behind a metallic plate is an ion pump. The topmost part of the vacuum chamber is the concentric hemispherical electron analyser

pressure is reached. However, most vacuum pumps are run continuously to minimise the pressure at all times.

The experimental chamber in the NTNU Department of Physics lab is connected to multiple extensions and internal parts each with its own purpose. Being a vacuum chamber with standardised flanges, a wide array of equipment can be mounted onto the chamber. In this way, each experimental chamber may be different, depending on the activity performed in it. Table 3.2 summarises the connected equipment, its purpose and model number or name.

Table 3.2.: The table shows the components and instruments connected to vacuum chamber at NTNU. Each part is described by its purpose and a comment regarding e.g. the instrument model.

Equipment	Purpose	Comment
STM	Characterisation	Omicron VT-STM
LEED apparatus	Characterisation	Omicron Spectaleed SER 813
Mass spectrometer	Leak detection	Pfeiffer Vacuum QME 200
Sputter gun	Sputtering	ISE 100 Fine Focus Ion Gun
X-ray gun	Generating X-rays	SPECS XR-50 X-ray Source
UV-lamp	Generating UV-radiation	UVS 10/35
Electron analyser (CHA)	Filtering electrons	SPECS Phoibos HSA 3500
Detection unit	Detecting photoelectrons	SPECS PCU 300 MCD-9
Manipulator	Position of sample in chamber	Cooling possible on back of sample.
Evaporator	Evaporating of molecules	Mini e-Beam Evaporator 4
Growth chamber	Growth of structures	
Ion pumps	Pumping	Valcon Plus 300 Varian 60L
Titanium Sublimation pump	Pumping	Vacgen ST22 Sublimation Pump
Turbo pumps	Pumping	UHV obtainable
Mechanical pumps	Roughing pumps on turbo-pumps	Connected as backing pump for the turbo pumps or to pump gas lines.
Wooblestick	Movement of sample inside chamber	
Loadlock	Inserting samples	
Ion gauge	Monitoring pressure	High vacuum pressure gauge
Pirani gauge	Monitoring pressure	Low vacuum pressure gauge

3.1.2. Pumping

To achieve the desired pressure for doing experimental work, several types of pumps have to be used, the reason for this being differences in working principles, and thus their pressure operating range. As described in the following, pumps are designed to work at a certain pressure, and if they are operated outside this, their efficiency may reduce or the pump may even be broken.

Multiple pumps are applied when working with vacuum science, but some are used more frequently than others. In the following, four main types of pumps are presented. Their basic principles as well as operating range for pumping is presented briefly. Admittedly, there exist other pump types as well. For more detailed description of vacuum science in general and vacuum pumps in special, the reader is encouraged to consult the literature [39, 113].

Mechanical pump

A mechanical pump, is as the name suggest, a pump whose working principle is based on controlled compression and expansion of gases. A volume of gas is displaced by vanes attached to a rotor inside a cavity, usually refereed to as a stator. The rotor and stator centre is usually offset, leading to two eccentric plates. Into the rotor plates, one or more radial guides containing rotary vales, are mounted. These valves and the rotor plate divides the chamber into several parts. During rotation, the distance between the rotor and the stator changes, and to continuously divide the chamber parts, the valves are allowed to move in the guides. Usually proper lubrication, often oil, is needed to allow smooth running of the rotary valve. Due to this, some oil may flow back into the pumped volume, leading to so called *hydrocarbon backflow*. This can be prevented using several methods, where one well known is to use a filter consisting of activated alumina spheres [113].

In the rotary vane pumps, the inlet and the outlet has no direct connection to each other. As the rotation increased the volume of the inlet chamber, gas flow in to fill the volume. At a point later in the rotation, the section of the chamber is opened to the outlet. As the vane chamber decrease in volume, gas is forced to flow out through the outlet. Top performance rotary vane pumps can achieve an ultimate pressure in the order of 10^{-6} mbar.

Two rotary vane pumps are connected to the experimental chamber discussed above, their properties are summarised in Table 3.3 [23, 56]. These are included for the reader to get some example values for the properties of vacuum pumps. The interested reader should consult additional manufacturers for completeness.

As seen from Table 3.3, the rotary vane pumps are not able to create pressure lower than 2×10^{-3} mbar and 4×10^{-4} mbar respectively. From the above mentioned discussion, this indicates that pumps with even higher performance

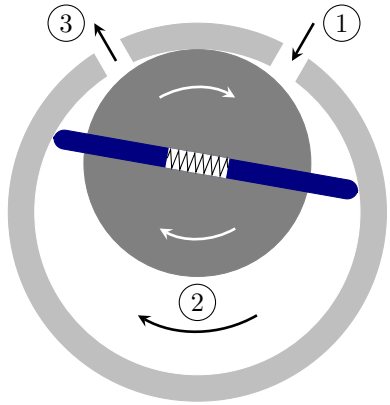

Figure 3.2.: Schematic drawing of a rotary vane mechanical pump. The black arrows indicate air flow from the reservoir (1), through the pump (2) and out of the pump (3). White arrows indicate the rotator rotating motion.

has to be used to attain even lower pressure. Using mechanical pumps as backing pumps for other pumps creating a rough vacuum, has led to them conventionally being called *roughing pumps*.

Table 3.3.: Important parameters for mechanical rotary vane pumps used in laboratory at NTNU [23, 56].

	Edwards RV 3	Trivac D 1.6 B
Pumping speed	$3.3\,\mathrm{m^3\,h^{-1}}$	$1.6\,\mathrm{m^3\,h^{-1}}$
Ultimate pressure	2×10^{-3} mbar	4×10^{-4} mbar
Nominal rotation speed	1500 rpm	3000 rpm
Motor power	450 W	100 W
Operating temperature range	12 °C to 40 °C	-
Noise level	48 dB at 50 Hz	-

Turbo-molecular pump

Mechanical pumps, as described in the previous section, represented by rotary vane pumps can obtain pressures up to 10^{-6} mbar. At this pressure, the number of molecules necessary to build up a monolayer hits the sample each second [61]. In other words: to avoid investigating the physics of adsorbed contaminants,

the pressure has to be even lower in the chamber. Achieving this is only possible by using alternate methods of pumping. Turbo-molecular pumps has become a frequently used pump type for achieving ultra high vacuum in recent years.

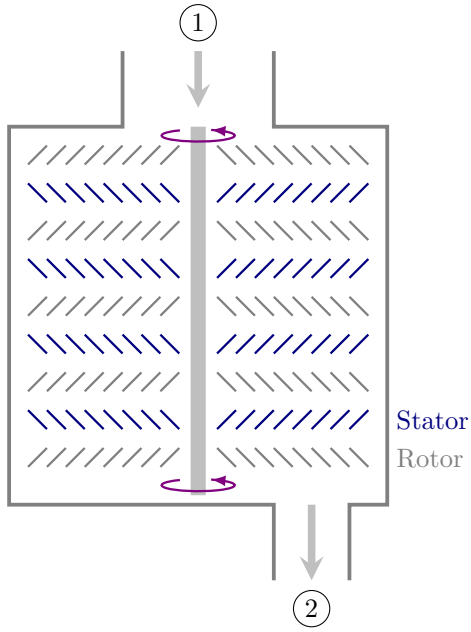

Figure 3.3.: Working principle of a turbomolecular pump (also known as turbo-pump). Gas molecules is pumped from a reservoir (1) by impact with the rotating rotor blades. They are given kinetic energy in the direction through the pump and out into a connected backing pump (2).

Turbo pumps have a design similar to conventional turbines, e.g. the ones found on aeroplanes. Multiple disks with rotor blades are placed in a housing. Between these rotors, stationary disks with blades, stators, are placed. When a gas molecule enters the housing, its given kinetic energy in the direction through the pump. After some time they hit the stator blades, and thus change their direction towards the rotor blades. Once again, the gas molecules are supplied with kinetic energy. These steps are repeated until the molecules have been transported through the pump and into a volume with low vacuum conditions created by a backing pump [85].

As the rotor blades transfer energy to gas molecules individually, it is

imaginable that it is some maximum pressure for the turbo-molecular pump to work. The turbo-pumps are designed to spin at a very high speed, typically somewhere around 1000 Hz. To achieve this, the rotor blades have to be precisely fabricated and balanced. If one exposes a running turbo-molecular pump to high pressure, the internal components of the pump may experience higher forces that they can withstand. In worst case, this may destroy the costly turbo pump [86].

Ion pumps

After operating roughing pumps and turbo-pumps for a time, the vacuum-chamber pressure is reduced. To further remove particles contributing to the remaining pressure, a third type of pump is used, the *ion pump*. In addition, hydrocarbon residues from the turbo-molecular and roughing pumps may be removed with the ion-pump. A schematic drawing of an ionisation pump can be seen in Figure 3.4.

When the pressure has been reduced sufficiently, a voltage is applied between the cathodes and ring shaped anodes inside the ion-pump. As an effect of the voltage, electrons are accelerated against the anodes. Their paths are however not straight, but rather in a helical path due to an applied magnetic field. Upon collision with gas atoms, ions are created. Through the magnetic field, the electron path length is increased and the ionisation probability correspondingly [86].

Positive ions created as a result of the collisions, strike the cathodes. These cathodes are commonly made out a chemically reactive material, as they react with the ions and trap them in the material. When colliding, some uncharged atoms are ejected from the cathode. Being without charge causes them to be unaffected by both the magnetic and the electric field. Their motion will therefore be directed by the ejection angle, and they may therefore deposit onto the anodes leading to a constant deposition of new anode material.

An ion-pump is a trapping pump. This means that the pumped gas molecules are trapped inside some part of the pump. At some point in time, the electrodes inside the pump thus have to be replaced. In other words: an ion pump has a maximum of atoms it can pump or "hide away". Taking this into account, the ion pump should not be used at too high pressure, as one would expect quick pump wearing due to this. In addition such high voltages can ionise the gas in an uncontrolled manner at higher pressures. Avoiding these sparks are crucial to stable operation of vacuum chamber electronics [113].

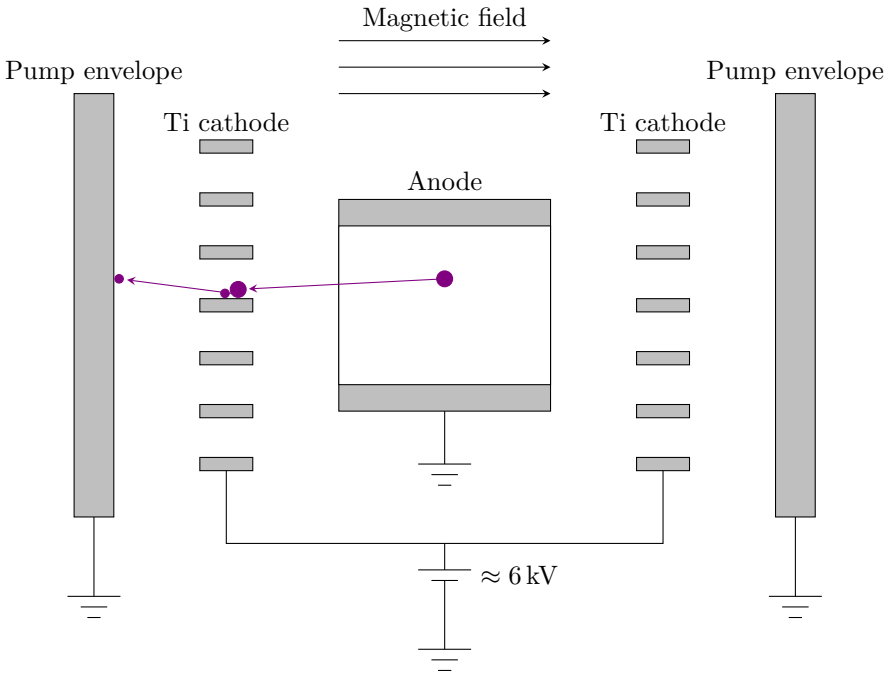

Figure 3.4.: Schematic drawing on an ion pump. Gas is ionised by a plasma discharge between anode and cathode. Ionised gas is attracted towards the cathodes, where they either get buried or react with the cathode material. The cathode material, eg. titanium, can then be sputtered off and deposit on other pump parts, enhancing the gas trapping here. The schematic drawing is adapted from [40].

Sublimation pumps

For further enhancement of the vacuum, sublimation pumps may be used. They are often set up to activate at predefined times with a certain periodicity, for example every eight hours. In essence, a sublimation pump is a simple construction, and the working principle is equally simple.

Through a wire a high current is passed, and due to Ohmic heating the wire temperature increases. By passing currents of several Ampere, the temperature reaches the sublimation temperature, which is somewhat lower than the melting point at 1660 °C. Above the sublimation temperature, the wire material undergoes a phase transition directly from solid to gas. One example of a frequently used wire material is titanium, resulting in the name Titanium Sublimation Pump or TSP.

Titanium sublimates and forms a thin, very reactive, layer on the chamber walls. When gas molecules now hit the chamber walls, they react with the reactive titanium and form solid by-product. The molecules are then incorporated into layers of titanium thus lowering the measured pressure in the UHV chamber.

Titanium pumps are thus only used for an additional pressure lowering in an already evacuated vacuum chamber. Other usage would lead to a much quicker wear on the pump. Different gas molecules can have different sticking coefficient on the reactive titanium film coated walls [34]. As such, the pumping efficiency of a TSP is dependent on gas type and other factors such as temperature.

3.1.3. Monitoring pressure

As previously mentioned, some of the vacuum equipment has requirements on which pressure range they can operate in. Operating outside these ranges can increase the wear on the instruments, or even lead to catastrophic failures. An example of this being to expose a turbo-molecular pump to a too high pressure. Thus, continuous monitoring the pressure is required to ensure a stable, reliable and secure operation of the ultra high vacuum chamber and its equipment.

Measuring the pressure in vacuum is possible in several ways, three variations/methods are presented here. They differ in the way they respond to a physical property of the gas that is dependent on pressure. One method is the group of mechanical gauges. One group is based on the fact that all gases exert a force on objects they hit. In the case of mechanical gauges this force is measured by looking at its ability to deform at thin wall. Secondly, thermal gauges relates the thermal conductivity of a gas to the pressure, for example by measuring the cooling rate of a heated object. A third category is ionisation gauges, also known as ion gauges. Here electrons are emitted from a filament, and subsequently they ionise the remaining gas molecules. Electrons

are then accelerated by an electric field to a detector. The current arising can be measured and related to the gas pressure.

3.1.4. Sample preparation

Despite having a good pumping system, good experimental results will be very hard to achieve if the actual sample is not clean. To attain this, preparation of the sample has to be done correctly. When performing photoemission studies is it crucial to use clean samples. As described in section 2.4.4, are photoemission techniques highly sensitive techniques to study amongst others the electronic properties of a system. As an effect of this, it is imaginable that keeping tight control over the system is critical.

When studying a sample using many modern techniques, carefully keeping the sample clean and uncontaminated is vital to obtain reasonable and reproducible results. When cleaning is done with nonchalance, one is running the risk of measuring properties arising from the contaminants, destroy the sample or even causing damage to the experimental set-up. However, how this cleaning is done is varying from sample to sample, and even from person to person. Similarly, care should be taken when doing other steps of sample preparation as well. In order to keep the samples of sufficient quality, the sample preparation has to be done correctly. In other words, performing the sample preparation correctly is crucial for performing many experiments, e.g. the photoemission studies described in this thesis. The following presents two methods for preparing suitable samples.

Cleaving 2D samples

When working with a sample, its crucial to know how to prepare it in order to get a nice, clean and reproducible sample for doing measurements. As described in previous sections, when a surface is subject to atmospheric pressures, it will eventually become covered in gas molecules from the air, that is molecules such as N_2, O_2, H_2O and similar. These species may absorb directly, or even incorporate into the sample. The bulk of the sample, will to a large degree be unaffected by this absorption. One way to overcome this is to create a new and clean surface. Cleaving samples, that is to cut the sample into two and make a new surface, is one way to achieve higher cleanliness. When creating a new topmost layer of atoms, and quickly inserting it into a vacuum chamber, the level of contamination is somewhat reduced.

Performing the actual cleave can for many samples be quite difficult. Getting a good cleave and a suitable sample size can, depending on the material, involve a lot of trial and failure. However, one category of materials is especially suited for the process steps: namely 2D materials. As described in section , they

may take the form of layers with strong intra-layer bonding, but with weak inter-layer bonding. This makes it possible to mechanically remove top layers by relatively simple means. In 2010, Konstantin Novoselov and Andre Geim received the Nobel Prize in Physics [80], for their isolation of graphene using the now acclaimed "Scotch-tape method". Using adhesive tape, they isolated single layers of graphite, known as graphene. Nowadays, this technique is a quick and easy way of cleaving 2D-dimensional samples such as graphene, MoS_2 and WSe_2. The method is based on using adhesive tape to remove a number of layers from the 2D material. Exposing new and atomically flat layers of the material is ultimately the goal [96].

If sample cleanliness is crucial, for example when doing very sensitive measurements, cleaving the sample in vacuum is advantageous. The basic principles are the same as when done in atmospheric pressure. 2D samples can be cleaved by using the Scotch-tape method inside the vacuum chamber. However, as doing the actual process inside a steel chamber is much more difficult than it is outside, only relatively simple cleaving processes are feasible in the UHV-chamber.

Sample heating and degassing

All gas molecules present around a sample, have a finite probability for adsorbing onto the sample surface. Before a sample is inserted into vacuum conditions, it may be subject to a relatively high pressure of gas. An example is exposure to air during storage or transport. Due to this, the constituents of the gas may adsorb onto the surface. In the case of exposure to air, contaminants such as H_2O or CO_2, may adsorb onto the sample.

Thus it is necessary to remove these gas molecules. One method for doing this is to heat the sample to increase the volatility of the gas molecules. When heated to a certain temperature, the gas molecules may desorb and can then be pumped away. How high the evaporation temperature is depends on both the adsorbate and the absorbent.

There are two main methods for heating an sample, the "direct" and "indirect" heating processes [65]. These two processes are depicted schematically and simplified in Figure 3.5. Direct heating involves passing high current through the sample. Due to finite resistance in the sample, heat is created and the sample temperature increases. Using this approach, samples can be heated to high temperatures, where the temperature is controlled by the current as well as heating time. Indirect heating involves heating an external source, which again warms up the sample. Compared to each other, direct heating needs a more robust sample with correct conductivity, whereas indirect heating is somewhat more versatile.

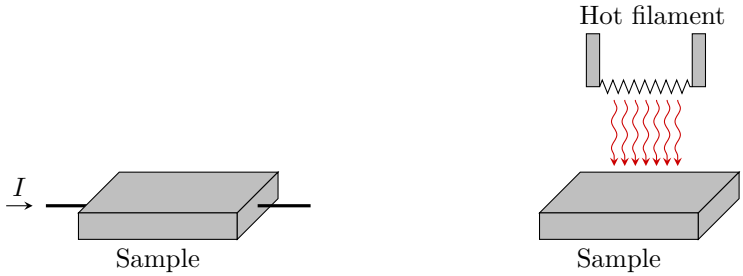

(a) Direct heating (b) Indirect heating

Figure 3.5.: Principle sketch of direct and indirect sample heating. Direct heating is based on passing a current, I, through the sample, whereas indirect current is based on a hot filament heating the sample.

3.2. Generating electromagnetic radiation

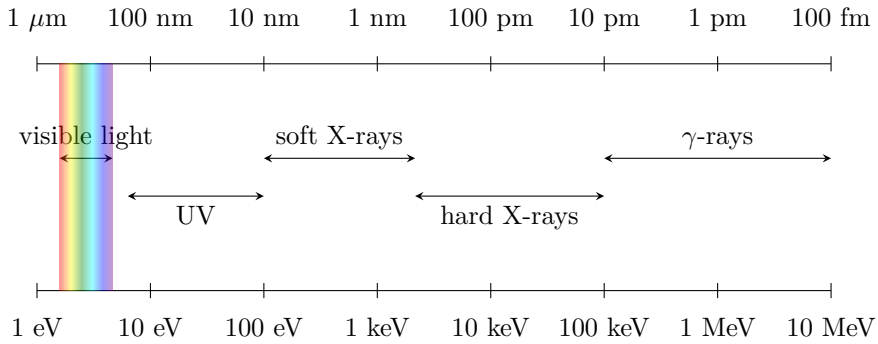

Figure 3.6.: Indicated are the different areas of the electromagnetic spectrum relevant for the analysis techniques mentioned in this thesis. Please note that people define the ranges in different ways.

As Chapter 2 reveals; particles with a particular energy are frequently used in many analysis techniques. This applies to the usage of photons, electrons or other types of particles. In the case of photons, often energies in the X-ray range (see Figure 3.6) are used. This can be attributed to two closely related effects. Firstly, the wavelength of photons in the X-ray regime is typically about some Ångstrøm ($1\,\text{Å} = 10^{-10}\,\text{m}$), a length that is comparable to the inter-atomic

spacing in many materials [31, 49]. Secondly, the energy of such photons, $\hbar\omega$, is typically enough to ionise the core levels of the elements. Following from this is the usage of the resulting photoelectrons in a range of different analysis techniques.

When working with these analysis techniques, it is important that the particles have specific properties. Properties such as wavelength (or energy), spectral distribution and intensity should be closely controllable. Following from this, is the notion that the creation of such rays has to be done in special ways to ensure that the properties are right, consistent and controllable. In the following text, three methods for creating rays of photons with a given energy is described. The first two methods are *lab based*, meaning that the instrumentation can be placed in a small laboratory. Another possibility is using a particle accelerator termed synchrotron does need more physical space.

3.2.1. X-ray tubes

Over time, X-rays have had and do still have a tremendous impact on both pure and applied science. A reason for this is attributed to the characteristics of the X-rays. However, without a convenient source for generating such photons, one could assume that X-rays based techniques could not have contributed to the same extent as they have.

One quite simple method of creating X-rays is by taking advantage of the "inverse photoelectric effect". A high current is passed through a filament and electrons are thus emitted by thermionic emission [4]. When a potential difference is applied to the filament (cathode) and a target (anode), the electrons are accelerated by the high voltage difference [71]. With a considerable speed and energy the electrons hit the target and subsequently creates X-rays having a characteristic energy depending on the material used as target. Both electrodes seat on an evacuated tube for several reasons. Firstly, the permeability of vacuum is lower than if gases are present. In this way, the probability for sudden electrostatic discharges (i.e. sparks) is lowered at low pressures. Secondly, the electrons would interact heavily with any residual gas particles. This would make it difficult to achieve reproducible and stable emission.

With a set-up as described above, the high voltage and the current can be varied almost independently. The limiting factor is the maximum power the anode target can withstand. Upon impact from an electron, most of the energy is converted into heat. To compensate for this, cooling water is circulated through the anode to prevent it from melting [4].

The materials for the electrodes can be chosen to suit the experimental requirements. As cathode material, tungsten (W) is often used, whereas pure metals such as molybdenum (Mo), copper (Cu), magnesium (Mg) and aluminium (Al) are used as target materials. By changing the target material,

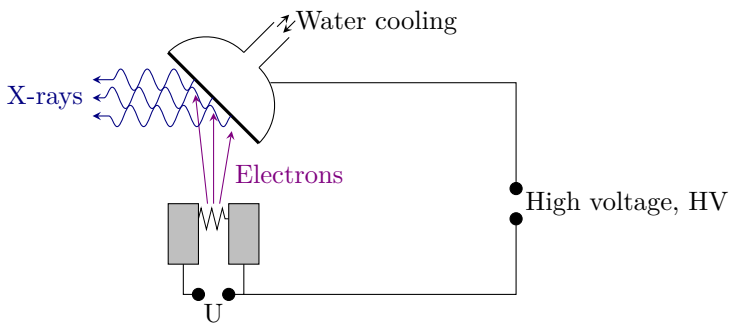

Figure 3.7.: Schematic layout of a conventional lab X-ray source

one can change the characteristics of the emitted X-rays.

As previously mentioned, it is advantageous to have a narrow spectral distribution when examining energy levels using X-rays. Having a broad distribution would smear out fine details in the spectrum and make data analysis correspondingly harder. To achieve a narrow distribution, is not necessary straight forward with an X-ray tube. However, it is possible to install an monochromator which filter out only certain wavelengths, albeit with a loss of intensity.

The X-ray tube is typically isolated from the main chamber with a window. Beryllium has a low absorption in the X-ray range, and is therefore a good material for making such windows. Another alternative is aluminium, as it also has a low absorption to X-rays [4, 108].

3.2.2. Gas discharge lamp

Some experiments need photons with a lower energy than in the X-ray range. An example is the usage of ultra violet or UV-radiation in PES, in a process named ultraviolet photoelectron spectroscopy or UPS. For examining valence band states, i.e. electron states that are more loosely bound than the core levels, ultra violet light is sufficient [31]. In practice, such radiation is indeed preferred, since the photo ionisation cross section has a tendency to be higher at lower photon energies. Summarised, such experiments are based on the measurement of energy spectra of photoelectrons emitted by solids that have absorbed ultra violet radiation. From these photoelectrons, we amongst others obtain valuable insight into the electric properties of a sample.

A frequently used way to generate UV photons in laboratory conditions, is the usage of gas discharge lamps [114, p. 36]. Gas discharge lamps generate light from a gas (plasma) that is located in a glass tube between two electrodes.

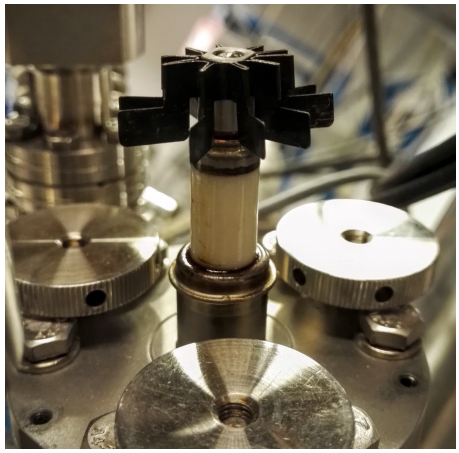

Figure 3.8.: Gas discharge lamp connected to the experimental chamber at NTNU. The helium gas is contained in the white cylinder, and the topmost black part is the electric contact and heat dissipation unit.

A voltage is applied between the two electrodes, and electrons will thus flow from the cathode towards the anode. During their travel, the electrons gain kinetic energy, an energy which is transferred by inelastic collisions to the gas atoms, through excitation or ionisation processes. Gas in an excited state is unstable and will inevitably relax sooner or later, via radiative de-excitation processes. The energy of the radiation is related to the energy gain, E, the atoms got upon excitation. The wavelength, λ of the radiation is given by,

$$\lambda = \frac{hc}{E}, \tag{3.4}$$

where h is the Planck constant and c is the speed of light. Since the energy gain in the excitation processes is atom dependent, the gas contained in the tube determines which wavelengths are generated. An example of gas used is helium. From helium, several emission lines are possible. A summary of these are presented in table 3.4.

3.2.3. Synchrotron radiation

In specific cases, the X-rays created in standard X-ray tubes are not sufficient enough to meet the requirements made by the analysis technique. These rays

[3]Where 100 is set to be the intensity of the highest intensity emission line.

Table 3.4.: Helium emission lines [42]

Emission line	Energy (eV)	Wavelength (nm)	Relative intensity[3]
I α	21.22	58.43	100
I β	23.09	53.70	2
I γ	23.74	52.22	0.5
II α	40.81	30.38	20
II β	48.37	25.63	2
II γ	51.02	24.30	0.5

might not be intense enough or they may have a too broad spectral distribution. An example of this is when examining very fine energy details in materials. Using light with a narrow distribution is then needed to resolve the fine details. One possibility is to use synchrotron radiation, in essence radiation generated by accelerating electrons. Developed from the 40s and onwards, synchrotrons have proved to be a useful high-end substitute of the standard X-ray tubes. In the following, the basic principles of synchrotrons are briefly explained. As the discussion omits most of the details about their complex nature, the interested reader is advised to consult additional literature [4, 71, 108].

What is a synchrotron?

As mentioned, a synchrotron is a type of particle accelerator. It has been known for a long time that charged particles that are accelerated emit radiation [54]. Using this, it is possible to generate photons with a given energy and with very high intensity. In a synchrotron, electrons are accelerated to relativistic speed and when magnetic and electric fields exert on the electrons they emit radiation. Synchronised magnetic and electric fields are used to enforce the particles to travel along curved paths, through certain components and follow the path of the storage ring. These rings, which may have a circumference ranging from some metres to a few kilometres, contain the particles circulated at almost constant energy for a given amount of time [108].

Creating electromagnetic radiation in a synchrotron

Although not all synchrotron are equal, they are often designed using the same general principles. A synchrotron commonly has five important components: (i) electron source for supplying electrons; (ii) linear accelerator to increase the electron energy; (iii) booster synchrotron to further accelerate the electrons; (iv) storage ring where electrons are maintained on a closed path; and (v) radio frequency cavities to compensate for the energy loss of the electrons.

Supplying the electrons is typically done by thermionic emission from a hot filament. Thermionic emission is the emission of charge carriers from a hot surface, where thermal energy enables the carriers to overcome the work function and leave the material. Following this is the acceleration of the charge carriers in a linear accelerator, typically up to an energy of several MeV. When the electrons have reached a threshold energy, they are emitted into the booster synchrotron, where they are accelerated until they reach the velocity (and correspondingly energy), at which they circulate in the storage ring. In the storage ring, the electrons are kept circulating at "relativistic" velocities on a closed path at almost constant energy [33].

Sections of the storage ring contains different devices needed for ensuring correct operation. Two main categories of synchrotron components exist: magnets primarily to control the beam path and insertion devices to create useful electromagnetic radiation. Modifying the electron beam path is done by three types of magnets: dipole magnets for bending it, quadrupole magnets to focus it, and sextupole magnets to correct for chromatic aberrations[4].

Useful radiation is primarily created by insertion devices [71], comprised of a periodic array of magnets. In these arrays, the electrons are forced "undulate", i.e to oscillate gently in the plane of the storage ring. Resulting from this is a type of *slalom* motion around the straight line representing the electron trajectory without the undulation. Over a length of L a full undulation is completed, and this length is possible to relate to the emitted wavelength from the electrons. A schematic drawing of such an insertion device is presented in Figure 3.9.

Since the electron velocity is near to light speed, one has to take several relativistic effects into account when calculating the actual emitted wavelength. Both the time dilatation and the Lorentz contraction has to be included to understand the radiation correctly. The observed wavelength in the laboratory frame[5] from an insertion device can be given as,

$$\lambda_L = \lambda_S \gamma \left(1 - \frac{v}{c} + \frac{v}{c}\frac{\theta_L^2}{2}\right) = ... \approx \frac{\lambda_S}{2\gamma}\left[1 + \gamma\theta_L^2\right], \tag{3.5}$$

where λ_S is the emitted wavelength in the electron frame, θ_L is the viewing angle relative to the axis of the insertion device and γ is the Lorentz factor given as,

$$\gamma = \frac{1}{\sqrt{1 - \left(\frac{v}{c}\right)^2}}. \tag{3.6}$$

[4]Chromatic aberration is an effect caused by the energy spread of the electrons circulating. Quadrupole magnets used to focus the beam have different focusing strength for different photon energies, and this has to be corrected to achieve a properly focused electron beam.

[5]The laboratory frame is from the view of the laboratory, i.e it is stationary and not moving along with the particle

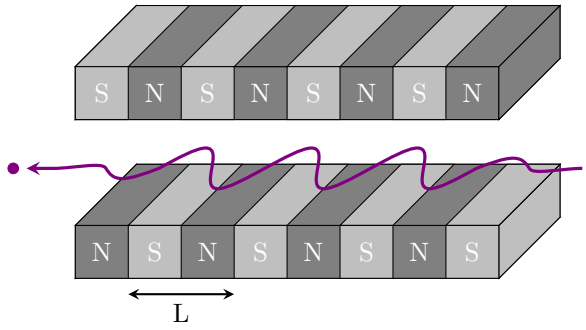

Figure 3.9.: Insertion device for creating electromagnetic radiation in synchrotron. The electrons are accelerated by a periodic array of magnets. Their magnetisation is indicated in this figure by N (= north pole) and S (= south pole). Resulting is an undulating electron path and thus the generation of electromagnetic radiation with wavelength (and conversely energy) depending on the insertion device parameters.

Using the definition of Lorentz force, acceleration and relativistic mass, the emitted wavelength in the laboratory frame from the moving particle can be expressed as,

$$\lambda_L(\theta_L, B) \approx \frac{L}{2\gamma^2}\left[1 + \frac{K^2}{2} + \gamma\theta_L^2\right], \tag{3.7}$$

with K known as the insertion device parameter,

$$K \approx 0.934 \times L\,[\text{cm}] \times B\,[\text{Tesla}]\,, \tag{3.8}$$

where the period L is given in cm and the magnetic field B in T.

From the K-parameter one usually makes a distinction between two types of insertion devices: undulators and wigglers. An undulator typically has a more narrow spectral distribution than a wiggler [4]. The K-parameter directs the energy of the light produced, and when necessary it can be changed to yield different energy profiles. Either permanent- or electromagnetic magnets can be used, and the method for varying the K-value can be changed by changing the separation and the current in the magnetic coils for the two types respectively.

Synchrotron advantages

Synchrotrons are spatially large and complicated to build. They can be extremely expensive to both build and operate and require a lot of knowledge

to operate. In other words: there have to be some good reasons for building such equipment.

One drawback of conventional X-ray sources, such as the standard Coolidge tubes, is that the technique depend on fundamental atomic transitions. They are therefore not tunable in energy. Whilst they can provide electromagnetic radiation at several energies, due to different transitions, they cannot be tuned continuous. Continuous tuning the energy would be advantageous for several experimental techniques.

Considering equation (3.7), one can appreciate that this limitation is overcome using a synchrotron. In the insertion devices the energy of emitted radiation can be tuned by changing the magnetic field magnitude, B. A change in the magnetic field is achievable by changing the separation between the array of magnets.

Another significant advantage of using a synchrotron to generate radiation is the intensity of the light shined onto the surface. By using high intensity light, most experiments can be performed faster, without any loss of statistics. One can include several properties to describe the quality of a photon beam[6]:

- Number of photons per unit time, F.
- Beam collimation, in other words the angular spread of the beam $\delta\theta_y$ and $\delta\theta_z$.
- Size of the beam source, σ_y and σ_z.
- Range of photon energies contributing to the intensity, Δ.

All of these parameters can be combined into one common parameter known as the brilliance defined as,

$$\text{Brilliance} \equiv \frac{F}{\delta\theta_y \delta\theta_z \sigma_y \sigma_z \Delta}. \tag{3.9}$$

Such a combined parameter makes it possible to compare the "quality" of different photon beams, from the ones made in simple laboratory equipment to the most advanced light sources. In general synchrotron light from undulators or wigglers has a brilliance of approximately nine orders of magnitude larger than the brilliance of conventional lab sources [11, 108].

Monochromator

Even though an insertion device in a synchrotron tends to generate radiation with a narrow spectral distribution, several measurements are taken to assure

[6] Here considering a beam travelling in x-direction, such that y and z are the two directions perpendicular to the direction of travel.

that the radiation delivered to the sample is of the highest possible quality. To achieve this well defined photon energy a monochromator is often used. Monochromatisation[7] of light is normally achieved by exploiting the principle of diffraction, pictured in Figure 3.10. Two common types, grazing and crystal monochromators uses diffraction from many objects in array to achieve constructive interference of the light with wanted properties [71]. If the incoming radiation to the monochromator contains multiple wavelengths, each wavelength λ creates a characteristic set of diffraction pattern allowing the exit slit to filter out desired wavelengths along a specific diffraction maximum [108]. When the light provided from the synchrotron is unfiltered by the monochromator the light is said to be of $\varnothing$-order, i.e. of zero order.

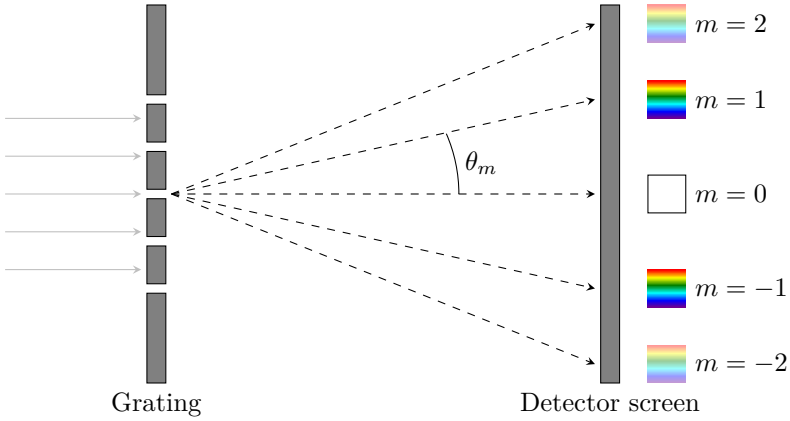

Figure 3.10.: Diffraction principle of light is the basis for a grating monochromator. Light with different wavelengths is split into its individual parts, and can thus be separated into the light one wants. Note: the incoming light is typically not consisting of wavelengths of visible light, as indicated here. This is done for illustration purposes, as UV light is tricky to depict in a figure. Point of the illustration is to indicate that the diffraction is dependent on the wavelength, and that light with a combination of wavelengths can be filtered using this principle.

[7] From latin "mono" meaning one, and chromo meaning "light"

Chapter 4.

Experimental

This chapter discusses the experimental methods and approaches performed in connection to this project, with the goal of studying the mechanism of UV induced change of thymine-molecules. First an experimental overview is presented in order for the reader to follow the thereafter following description. Then the sample preparation is described in-depth.

It has to be noted that the experimental work in this section was done in two main sessions. To begin with, the feasibility of depositing thymine (IUPAC: 5-Methylpyrimidine-2,4(1H,3H)-dione) onto the MoS_2-surface was tested. This was done to ensure that the experiment was likely to succeed before travelling to Aarhus for the more advanced analysis. Here the materials science beamline, Matline at the synchrotron light source ASTRID2 was used to get higher controllability of the radiation source and to get superior experimental resolution.

In essence, the experimental work performed in the laboratory at NTNU was a preparation for the work planned in Aarhus. Beam time at synchrotrons is usually scarce and having prepared the experiments in advance is thus crucial. Thus, the work performed in Aarhus, copied the initial lab work and took it some steps further.

The experiments are presented in chronological order, in other words: in the order the different parts were done. This reflects the way the experimental work was performed, as the way forward was chosen partly based on preliminary results obtained during the experiments. Additionally the goal of writing it this way is to make the reader follow the "track of thought" the author had when performing the measurements.

4.1. Initial studies of adsorbed thymine

The following describes the experiments done in the XPS lab at Department of Physics at the Norwegian University of Science and Technology.

These experiments were primarily being a "test of concept" for depositing thymine onto the surface. In order not to waste any valuable measurement

time at the ASTRID2 synchrotron in Aarhus, the idea was to try to do some of the experiments, at least the deposition of thymine onto the MoS_2-surface to check its stability. Being a sensitive instrumental setup, the synchrotron instrumentation cannot cope very well with sudden spikes in the pressure. Such unforeseen and immediate pressure increases could arise from the desorption of molecules from the sample. For testing this, thymine powder was deposited onto the sample at low temperature and the stability was tested.

4.1.1. Creating evaporation cell

Thymine was bought from chemical supplier Sigma Aldrich, and came in the form of powder. Evaporating the powder compound was chosen as this represents a quick and tunable deposition method. In addition evaporating the molecules is fairly gentle when it comes to keeping the molecular structure of the compound intact.

To evaporate the powder a simple evaporator was built. The evaporator consisted of a standard halogen light bulb produced by Philips, spot welded onto two electrodes. These electrodes were connected to an electrical cable feed through, which in terms were connected to a 2.75 in NW35 conflat (CF) mounting flange. Depicted in Figure 4.1 is the light bulb evaporator.

CF-flanges are flanges where both sides are equal, mounted together with six bolts holding the two parts firmly together. Materials used are typically stainless steel for the flanges, where the seal mechanism is based on a knife edge that is created below the flat flange surface. When the pair of flanges are tightened correctly, a soft metal gasket gets deformed when the knife-edges make trenches on each side of the gasket. As the knife edges deform the metal, an air tight seal is formed. Using airtight metallic seals are common in UHV equipment, as they tend to behave better in vacuum than polymer seals.

To make the actual effusion cell, a Philips dual pin single ended halogen light bulb[1], with a diameter of 0.5 in or 12.7 mm was used. By carefully mounting the light bulb on a bench vise, exposing the top part, and drilling a small hole into it, a cell for evaporating the powder compound was created. When making the particular care was made to avoid breaking the glass bulb. In addition, the delicate filament was kept under additional attention. Ethanol and acetone was used to clean the light bulb. For cleaning the other parts of the evaporator, ethanol was used.

In order to evaporate the powder compound, the light bulb had to be filled with powder. Using a paper funnel, it was filled with a small amount of thymine powder. For evaporating, a current was applied trough the light bulb using a variable DC power supply, Delta Elektronika EK030-10.

[1] Light bulb specifications: effect 35W, Designation T4, Voltage 12V

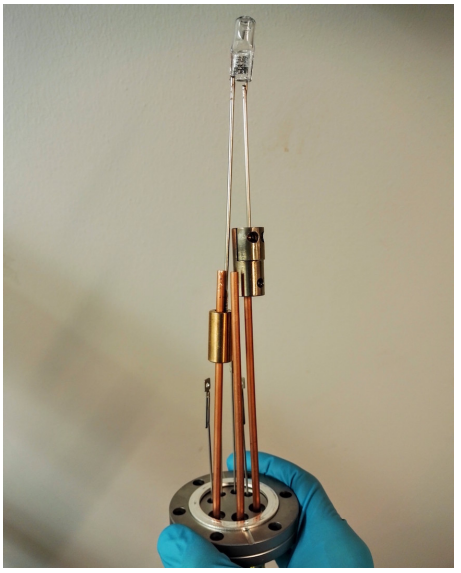

Figure 4.1.: Evaporator for powder compounds. Current is run through the bulb leading to heating of the powder. Subsequently evaporation occurs. The evaporation is primarily controlled by varying the current.

4.1.2. Sample preparation

The sample was prepared from a natural molybdenite crystal. Using natural crystals can raise concerns about the level of contaminations, as their formation often includes other atomic species as well. Ideal substrates, that is samples with no contaminants, are obtainable under controlled laboratory conditions. In some cases such are needed, but as the presented work did not require really high purity substrates, an inexpensive alternative bought on the Internet was a good option. A similar molybdenite crystal to the one used is depicted in Figure 4.2.

Molybdenite is a 3D crystal consisting of numerous layers of molybdenum-disulfide, MoS_2, stacked upon each other. Its look and feel is similar to that of graphite, as they both are 3D crystals created by stacking 2D layers and have similar properties otherwise [79]. One advantage of these crystals is that they can be cleaved with relative ease, as the 2D layers only have van der Waals forces bonding them together, as discussed in section 3.1.4.

Preparing the sample started by cleaving a small part off the 3D crystal using a scalpel. To ease the mounting onto the sample holder, the piece was

Figure 4.2.: Natural molybdenite crystal used as a substrate for doing the experiments.

thinned down additionally to a thickness of 2 mm to 3 mm. The sample was then mounted onto a sample holder made out of tantalum (Ta) using silver epoxy glue. The sample holder had dimensions of approximately 15 mm × 17 mm, and they were cleaned using ethanol and an ultrasonic bath in water prior to attaching the sample.

Silver epoxy glue is a two component glue suitable for usage in ultra high vacuum conditions. One part consists of the epoxy glue and the other part of a hardening compound. When mixed and left to dry, it will attach the sample firmly to the designated sample holder. This method of mounting the sample onto the sample plate has the advantage that its a quite gentle way of mounting delicate samples. Another frequently used method is by clamping the sample under metallic strips spot welded at the edges. For "weak" samples such as the 2D materials, using this method could potentially lead to crushing and flaking and potential difficulties performing measurements.

After the sample was mounted onto the sample holder, adhesive tape was attached to the sample. By gently attaching the adhesive tape to the sample, it was assured that it had a contact with as much of the substrate as possible. In order to remove the top layer or layers, the adhesive tape had to be removed. This was done by slowly peeling the tape of from one side to the other. Visual inspection was used to evaluate the sample quality. If the sample looked poor, i.e flaky or rough, the process was repeated until a satisfying result was obtained. Using the "Scotch tape method" involves a lot of trial and error, and training is needed to consistently obtain good samples.

Depicted in Figure 4.3 is this described cleaving process. As seen from the illustration, one could do the process both by using adhesive tape or by

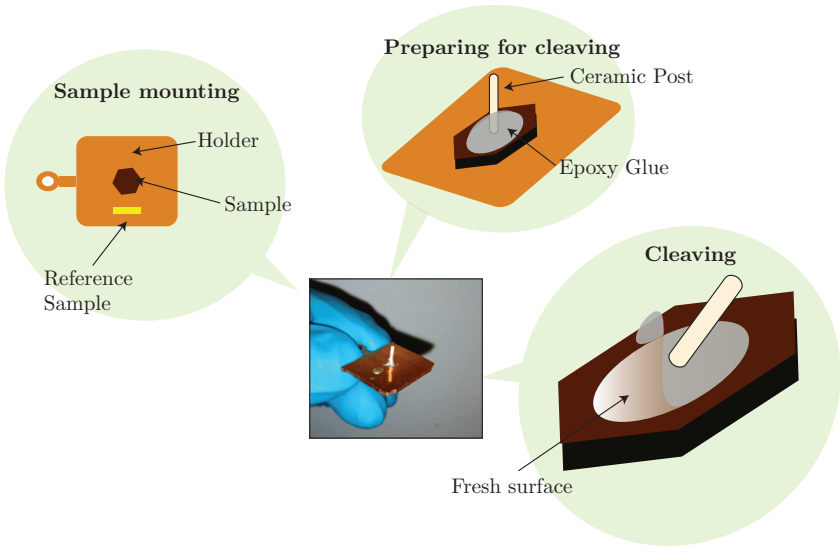

Figure 4.3.: Cleaving process schematic for 2D-materials. In the middle a sample holder with a mounted sample is depicted. Around the cleaving process is shown. First a sample is mounted onto a sample plate. Then some glue or tape is attached to the sample surface, before its removed and a fresh surface is exposed to the outside. From Mazzola's thesis [65], with permission.

attaching a ceramic post using epoxy glue to the surface.

Cleaving the sample was done in ambient conditions, that is doing the cleaving exposing the sample to air. Despite the contamination concerns this raised, the method has some advantages. Doing the cleaving outside a vacuum chamber, simplifies the practical aspects of the process considerably. First and foremost, as suggested above, the process had to be repeated until a satisfactory sample quality was obtained. As imaginable, doing the cleaving inside the UHV experimental chamber would involve an considerable amount of time for pumping the chamber between each trial.

Indeed, the sample cleaving in ambient conditions will lead to a higher degree of contamination onto the sample, such as adsorption of water contained in the air. However, as the goal of the study was to adsorb additional molecules onto to the surface and study how these molecules react in the UHV chamber, the presence of small amounts of contaminants on the surface should not be affecting the experiments to a high degree.

4.1.3. Alignment and clean sample analysis

The sample was then inserted into the experimental chamber through the load-lock. After leaving the load lock pumps pumping for some time, the valve into the main analysis chamber was opened. Using the magnetic drive, which use magnetic coupling to control both the linear and rotary movement on a shaft, the sample was transferred to the analysis chamber. Then it was inserted into the manipulator sample position.

In the analysis chamber, the sample was left for some time. Leaving the sample before starting measurements can help improve the quality, as some of the adsorbed gas molecules may desorb and be pumped away. Before inserted into the chamber, the sample had been exposed to ambient conditions, and therefore a wide array of gases. To remove additional gas molecules the sample was resistively heated. During the heating, particular attention was paid to the pressure to avoid possible spikes in the pressure. Avoiding such spikes is crucial to protect sensitive parts of the delicate equipment.

The clean sample was then moved into analysis position on the manipulator and the X-ray source (SPECS XR-50) was used to irradiate the sample. Both magnesium and aluminium Kα X-rays with energies of 1253.6 eV and 1486.7 eV respectively is possible using this source. Magnesium was chosen as the author had most experience using this source.

When using the X-ray Photoelectron Spectroscopy system X-ray source irradiates a large area compared to the sample size on the sample plate. Resulting from this is that the measured photoelectron signal in reality arises from both the sample, the sample plate and possibly the attachment solution as well. To account for this the electron analyser has slits for limiting the electrons entering and leaving the electrostatic lens system based on their emission position. To account for this, the electron analyser has slits selecting of electrons that can enter the electrostatic lens system, and those who are unable to enter the lens system. Both the beginning and the end of the lens system has slits to control the collection to a higher degree. Following from this is the importance of aligning the sample correctly. One wants the collecting spot to be on the top of the sample, if possible avoiding photoelectrons from the sample holder and clamping mechanism. All XPS measurements done in the laboratory at NTNU was performed using a 3 mm circular slit.

Inside the vacuum chamber, the sample is placed into a slot on the tip of a manipulator. The manipulator mounted sideways on the experimental chamber, has movement four degrees of freedom. All three dimensions, x, y and z can be varied independently, only limited by the internal components in the vacuum chamber. In addition, the sample can be tilted by changing the θ-angle, allowing for detection of photoelectrons at different emission angles.

For aligning the sample, all these positions have to be correct. Using

previously known analysis positions as a starting point, the sample was aligned. This was done by looking at the photoelectron signal from the Ag $3p$ core level. Silver was used for alignment, as this was a component in the mentioned silver glue used to attach the sample. As the glue was present on a larger area than the MoS_2 sample, minimising the silver signal would help identifying the actual position of the MoS_2 sample. Many quick alignment scans were done before finding a promising sample measurement position. By controlled varying the directions x, y and z the sample was placed in a position suitable for measurements. At a suitable measurement position, photoelectrons from silver is not seen.

At this position, a wide energy scan was done to get an overview over the state of the sample. In addition from this the goal was to identify the chemical elements and their approximate ratio of presence. Using an Mg Kα radiation as an source, the sample was exposed to X-rays and photoelectrons emitted according to the theory. Collecting the emitted photoelectrons was done by a Phoibos HSA 3500 150MCD-9 analyser. To further asses the sample quality and cleanliness core level scans of two common contaminants, oxygen and carbon, was performed as well. Some relevant scan parameters from the scans performed using the laboratory at NTNU is summarised in table B.1 in Appendix B.

4.1.4. Cooling, deposition and analysis

After a wide energy scan of the clean sample, a valve to the attached evaporator was opened, and the sample was moved to the deposition position on the manipulator stage. The goal was now to evaporate the thymine powder from the crucible, and deposit it on the surface.

From basic thermodynamics its known that the deposition rate on a surface is dependent on the sample temperature. Adsorption, the phenomena required for deposition, is directed by the temperature. Several factors are responsible for the temperature dependence and the interested reader should consult the literature [76]. Simplistically one can say that attraction forces exist between adsorbate and adsorbent, and from an adsorption process heat is released. The competing process, desorption thus therefore need to overcome an energy barrier. The energy is supplied by the thermal energy, k_bT, which is obviously temperature dependent. At lower temperatures, the thermal energy is lower, and may therefore not be enough to desorb the molecules. Consequently, cooling the sample could increase the efficiency of the adsorption process.

Cooling was done using liquid nitrogen[2] (liquid N_2) flowing through pipes and the manipulator cooling unit close to the sample at the manipulator head.

[2]Liquid nitrogen has a boiling point of $-195.79\,^{\circ}\mathrm{C}$ or $77\,\mathrm{K}$ and is a frequently used liquid for low temperature cooling.

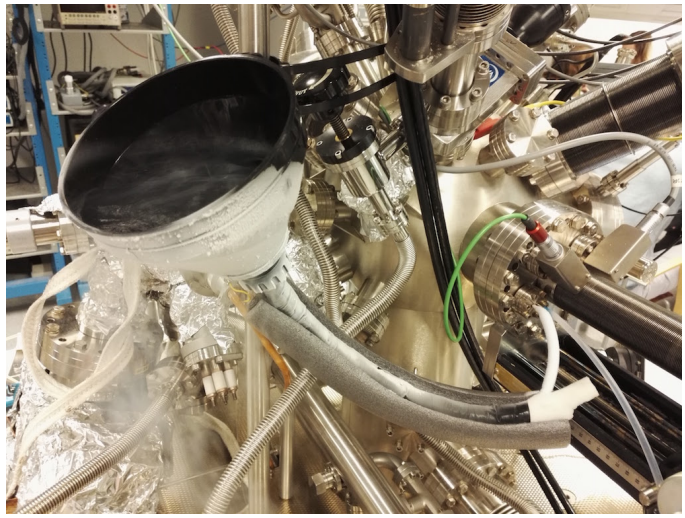

Figure 4.4.: System for cooling sample using liquid nitrogen (LN). The funnel was filled with liquid nitrogen, which ran through the pipes and on the back side of the manipulator tip. As the manipulator tip cooled, the sample temperature decreased as well, allowing the deposition of thymine.

The system consisted of a funnel, pipes connected to the manipulator and a pump pumping the nitrogen trough the pipes, see Figure 4.4. Supplying the cooling liquid was done by pouring liquid nitrogen into the funnel and topping it up periodically. Monitoring the temperature was done by a thermocouple on the manipulator head. It has to be noted that the thermocouple was mounted behind the sample, and thus introduce some errors in the temperature readings.

After some time, the cooling from the liquid N_2 and the heating from the surroundings reached an equilibrium. The evaporation cell described in section 4.1.1 was then connected to a power source, and whilst cooling continued, thymine was deposited. The power supply was of type EK 030-10 manufactured by Delta Elektronika. To perform the deposition, a current of 1 A and a voltage of 2 V was supplied by the current source for 5 min. Table 4.1 summarises process parameters for this process step.

In order to investigate the reproducibility of the deposition, thymine was deposited again. The cooling was therefore stopped and the sample left to heat up to room temperature. When room temperature was reached, the sample was resistively heated using to desorb the thymine. Using a current of 1.5 A and a voltage of 8.2 V, the heating was continiued until the thermocouple indicated approximately 100 °C.

When desorbing the molecules, they would contribute to an increased pressure in the chamber. By monitoring the pressure, it is therefore possible to get an indication if the deposited molecules are staying on the sample or if they are desorbing. Using this principle, the pressure was monitored over 10 min. During this time, the thermocouple temperature was kept reasonably stable between 98 °C to 102 °C.

To avoid rapid cooling of hot parts, the system (sample and equipment) was left to cool down to room temperature. During this time, the cooling equipment was again prepared, and active cooling started when the thermocouple read room temperature values. Supplying liquid nitrogen led to a drop in temperature to −80 °C and deposition was then started again. Column three in Table 4.1 shows the evaporation parameters for the second deposition.

4.1.5. Temperature-stability of thymine on MoS_2

As mentioned previously, the goal of the preliminary work at NTNU was to investigate the thermal stability of thymine on the MoS_2 surface. To get an indication on the stability the sample was left in the experimental chamber overnight without supplying any liquid nitrogen for cooling. When the cooling was stopped, the sample temperature would gradually increase.

From the discussion regarding cooling above, this could lead to desorption of the molecules at some temperature with a corresponding thermal energy. Before cooling was stopped, the sample had reached a temperature of −93 °C.

Table 4.1.: Thymine evaporation parameters. Voltage and current is run through the evaporation cell. Temperature is measured by a thermocouple behind the sample.

Parameter	Depositon 1	Deposition 2
Time	5 min	4.5 min
Voltage	2 V	2 V
Current	1 A	1 A
Initial temperature	−78 °C	−78 °C
Final temperature	−80 °C	−81 °C
Initial pressure	8.8×10^{-8} mbar	1.3×10^{-9} mbar
Final pressure	1.6×10^{-6} mbar	2.7×10^{-7} mbar

Thymine was then covering the surface according to the above mentioned deposition step.

4.2. Detailed studies using synchrotron light

The following section explains the experimental and practical parts related to the measurements performed using facilities at Aarhus University, most notably the Matline beamline at ASTRID2, a synchrotron at the Department of Physics and Astronomy. First the some practical aspects regarding the beamline is presented, before the core experimental work if this thesis is described.

Despite separate presentations, the two experimental parts, i.e. the work performed at NTNU and in Aarhus, were closely related. The work performed at NTNU was used as preparation for the work presented in the following part. As much of the experimental work is similar to that performed at NTNU, the presentation is kept quite short in the following. Emphasis is put on the areas which are not already covered in section 4.1.

In order to make the experimental process more clear to the reader, the author has made a flow chart. The visualisation of the process is shown in Figure 4.5. It contains the main parts of experimental work performed at Matline.

4.2.1. Matline at ASTRID2

The experiments in Aarhus was performed by using the Matline beamline, a surface science beamline with a Zeiss SX700 monochromator and two electron energy analysers. The monochromator has a maximum energy range from 20 eV to 700 eV.

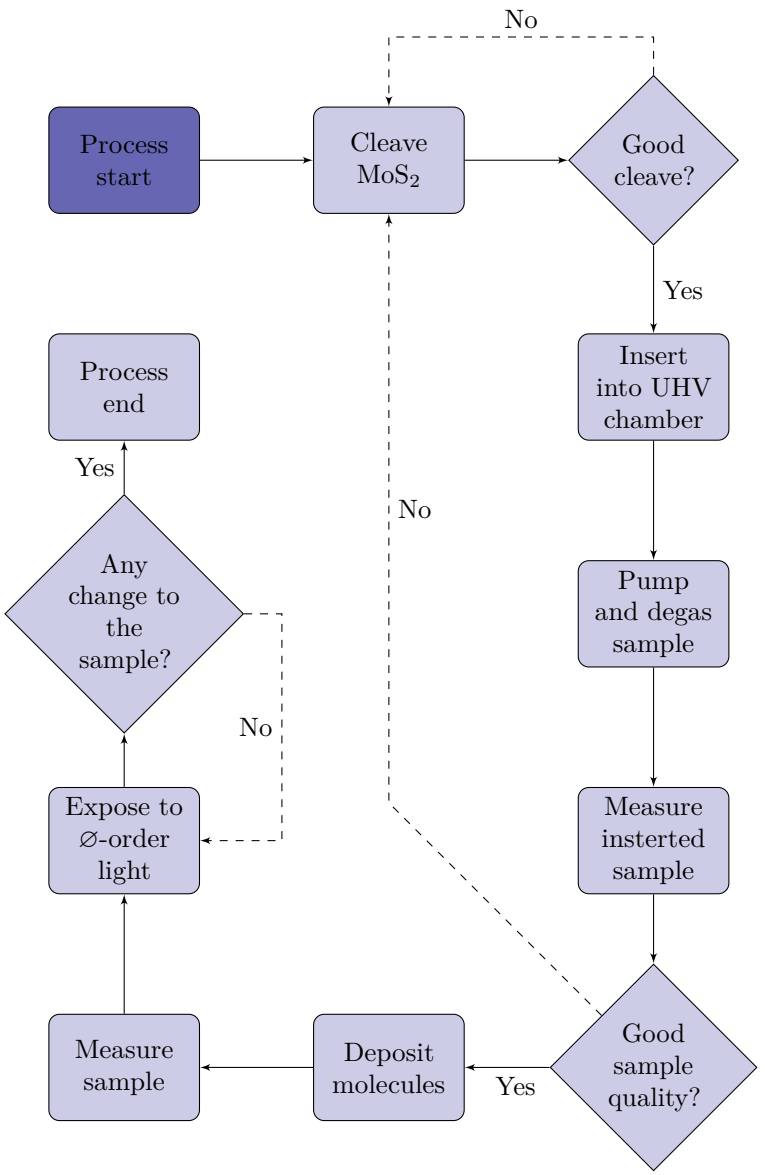

Figure 4.5.: Schematic drawing of the experimental process performed using the Matline surface science beamline at the ASTRID 2 synchrotron facility.

Compared to the conventional lab X-ray source used in the previous sections, the Matline beamline has the ability to deliver much higher flux of photons. Generating the photons is an insertion device in the ASTRID 2 beamline. More specifically, a multi-pole wiggler generates photons with an adjustable energy range from 20 eV to 700 eV. Here a strong magnetic field, up to 2 T is applied between two magnetic arrays separated by approximately 12 mm. Each of the magnetic arrays consists of periodically arranged magnets, where each period spans a length of 116 mm and six periods is present in total. When considering a 100 µm exit slit, photon fluxes of $10 \times 10^{10}\,\mathrm{s}^{-1}$ and $10 \times 10^{9}\,\mathrm{s}^{-1}$ at energies of 125 eV and 600 eV is measured respectively.

The sample holder has possibilities for electron bombardment heating, and cooling is possible via a liquid nitrogen flow cryostat. Mounting the sample is done on a sample manipulator with movement in x, y and z directions. In addition rotation is possible in two directions. Figure 4.6 shows the experimental chamber from the outside, whereas Figure 4.7 shows the sample mounted on the manipulator inside.

4.2.2. Sample preparation

Preparing the MoS_2 sample was done similarly to the procedure performed at NTNU. A block of molybdenite was cleaved with a pair of tweezers, followed by further thinning it down using micro-mechanical exfoliation. The sample was then attached to a tantalum sample plate using two-component silver epoxy glue. Previously the sample plates had been cleaned using ethyl alcohol.

As the molybdenite crystal was a natural crystal, and the author had limited experience with cleaving 2D sample, several cleaves had to be performed in order to obtain a satisfying sample. Determining the sample quality was done by visual inspecting it.

Ideally, a perfect MoS_2 surface would be desirable for doing the experiments. Such a sample would make the experiments more reproducible, as non-perfect surfaces could be different from experiment to experiment. However, as this was not possible, it was chosen to exfoliate the sample using the "adhesive tape method" until a good enough sample quality was achieved. Assessing the sample quality was done by visual inspection. After peeling of layers several times, a surface with satisfactory quality was obtained.

The sample plate was then inserted into a load lock. After pumping down the load lock to ultra high vacuum, its flange to the experimental chamber was opened and the sample transferred. The sample was then set to degas for some time[3]. Annealing was done by resistively heating the sample up to

[3]The precise time for degassing was determined by looking at the pressure in the experimental chamber.

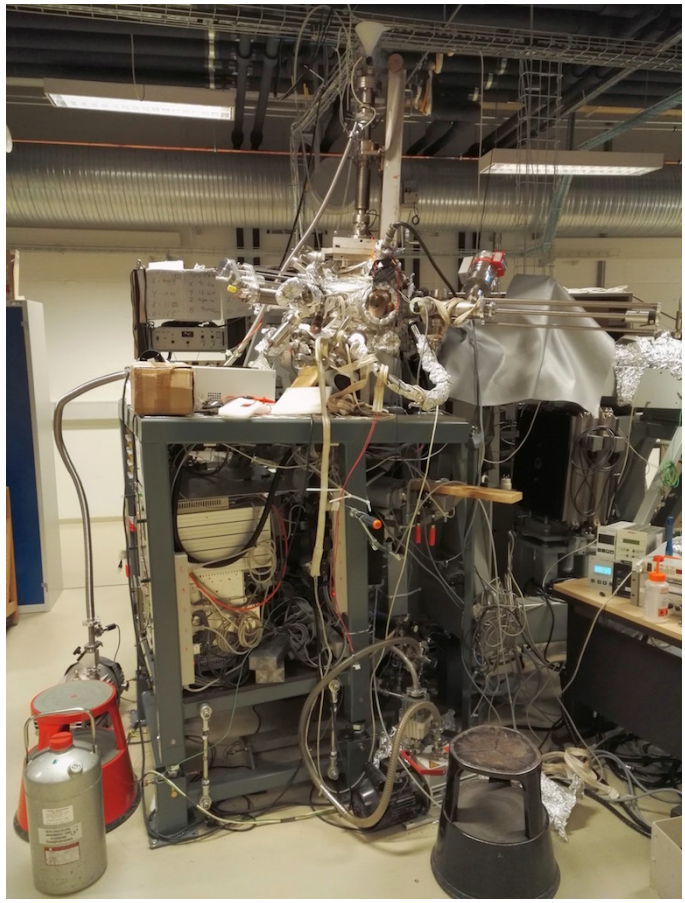

Figure 4.6.: Matline end station on the ASTRID2 beamline. Centred in the image is the experimental chamber seen. Below the chamber electronics and pumps is seen. Liquid nitrogen cooling is possible via a flow cryostat, where liquid nitrogen is supplied into the funnel at the very top of the chamber.

390 K for removing contaminants. At this point the sample was measured using XPS/UPS and XAS techniques. Details about the measurements are presented in section 4.2.5.

4.2.3. Evaporation and deposition

To evaporate the thymine powder, an evaporation cell similar to the one presented in section 4.1.1 was created. In other words; a hole was drilled in a standard halogen light bulb. The two light bulb electrodes were spot welded onto two electrodes, see Figure 4.1. Filling the light bulb was done with a funnel, and by carefully filling it, the filament was kept intact.

From the measurements at NTNU, the author had gained some knowledge regarding deposition parameters for the evaporation of thymine powder. Based on these parameters, evaporation was done for 10 min with a current of 1 A supplied from a current source.

After the deposition, some quick survey scans were performed to confirm that thymine actually had deposited. Thymine consists of carbon, oxygen and nitrogen atoms, such that high presence of these species would indicate that deposition was successful. When these measurements were done, measurements with higher energy resolution and longer acquisition times was performed. In order to get an idea of the thickness of the thymine deposited, the molybdenum 3d core level was acquired as well.

4.2.4. Exposure to high intensity UV light

Following the deposition of thymine was the exposure-part of the measurement. As mentioned in previous sections, the idea was to study the photochemistry of deposited thymine using synchrotron radiation. In theory, exposing the nucleobases to high intensity ultra violet light would emulate the UV light the DNA is subject to when exposed to sun light. In reality, the sun light intensity is much lower than in a synchrotron, but as described in section 2.1, the exposure dose is the relevant parameter.

To expose the sample to as much ultra violet light as possible, so called ∅-order light was used. ∅-order light is, as explained in section 3.2.3, all the light generated in the insertion device. Using all the radiation, without filtering it would quicken the time needed for exposure, as the needed dose could be reached faster. The Zeiss SX700 monochromator is not set to operate in an UV range below 20 eV, and using unfiltered (i.e. ∅-order light) allows us to reach low photon energies which is beyond the range of the monochromator.

As pointed out in Figure 4.5, the sample was potentially exposed to ∅-light several times. First only a few seconds were tried, in order not to overexpose the sample. Each exposure to the UV light was followed by a quick acquisition

Figure 4.7.: MoS_2-sample in the 5-axis manipulator inside experimental chamber at Matline. The sample plate is mounted to the manipulator with a clamping mechanism.

of the relevant core levels and the valence band states. The relevant core levels were chosen to be: C 1s, O 1s, N 1s and Mo 3d. The three first core levels were scanned to get an idea of how the thymine sample changed upon exposure. Photoelectron spectroscopy techniques are in general very surface sensitive. By looking at the molybdenum 3d level, the idea was to get an estimate of the thickness of the deposited layer. Thus, monitoring any changes in the intensity from molybdenum was done to get an impression if any changes in the thymine layer occurred.

Repeating the process was done several times with increasing length of exposure. First the sample was left exposed for only a few seconds, but exposures of 1 h and 6.5 h was performed as well. After each exposure step, core level and valence band scans were acquired.

4.2.5. Measurements

In the previous description it is evident that several types of measurements were done as a part of each experimental step. After inserting the sample into the experimental chamber, after depositing thymine and after exposing the molecules to ∅-order light the same measurements were done. The reasoning behind performing different types of experiments were that they give different type of information, and therefore may give different insight. For testing the reproducibility the whole experimental work was performed several times, as indicated in Figure 4.5.

Table 4.2.: Overview over measurements done after each process step at Matline

Measurement technique	Region	Photon energy
XPS	C 1s	380 eV
XPS	O 1s	620 eV
XPS	N 1s (+ Mo 3p)	529 eV
XPS	Mo 3d	350 eV
UPS	Valence band	100 eV
XAS	C 1s (K-edge)	278 eV to 302 eV
XAS	O 1s (K-edge)	520 eV to 545 eV
XAS	N 1s (K-edge)	390 eV to 420 eV

4.3. Deposition of other molecules

4.3.1. Depositing squared carbon directly: bromocyclobutane

After doing the thymine experiments, an additional experiment involving bromocyclobytane was performed. Bromocyclobutane is an organic compound containing one bromine atom covalently bonded to a cyclobutane ring. Its molecular formula is C_4H_7Br and its molecular weight $135\,\mathrm{g\,mol^{-1}}$. Figure 5.18 shows the simplified Lewis-structure of bromocyclobutane.

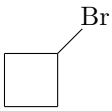

Figure 4.8.: Molecular structure of bromocyclobutane.

The idea behind the experiment was to investigate bromocyclobutane in a similar way as was done to thymine. Already containing a four-carbon ring, the goal was that bromocyclobutane could represent an analogue to the pyrimidine dimer. X-ray photoemission and X-ray absorption measurements of bromocyclobutane was thought to make the analysis of pyrimidine dimer easier. Correlating the measured effects from a "simple" molecule, could help the analysis of the quite complicated result of thymine dimerisation.

Bromocyclobutane was bought from Sigma Aldrich, and arrived in the form of a colourless liquid contained in a small glass capillary. To evaporate the liquid, a glass tube, as shown in Figure 4.9(a), was cleaned and 5 mL of bromocyclobutane was poured into the tube. The tube was then attached to a leak valve which was mounted onto the chamber, see Figure 4.9(b). Leak valves are valves used to control the flow of gases from an external source into a vacuum system

The MoS_2 sample, which had been resistively heated and confirmed to be clean, was now placed in the analysis position and the sample was checked for contaminants. To deposit molecules on the sample, the sample was oriented towards the position of the glass tube. Sample cooling by liquid nitrogen was again started. Heat tape was wrapped around the glass tube, as depicted in Figure 4.9(b). Current was then passed through the heat tape leading to a measurable increase in the temperature around the glass tube. As a method for controlling the deposition temperature the leak valve was used. It was opened two times, first for 6.5 min and then for 36 min. Between the two deposition attempts the sample was checked for any traces of bromine.

(a)

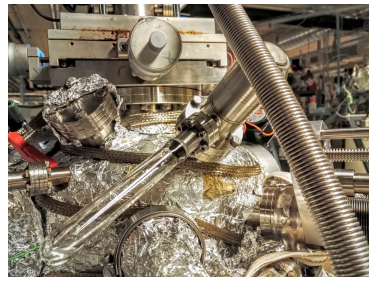

(b)

Figure 4.9.: Glass tube for evaporating bromocyclobutane. The tube is connected to the vacuum chamber. Around heat tape is wrapped and by passing current, the evaporation of bromocyclobutane can be controlled. Additional control is provided by a leak valve isolating the glass tube and the chamber.

4.3.2. An analogous molecule: biphenylene

In addition to the bromocyclobutane another molecule was planned used as a pyrimidine dimer substitution. The molecule pictured in Figure 4.10, contains a cyclobutane as the pyrimidine dimer has. Molecules with conjugated π-systems tend to form nice films on surfaces, and this should in theory help the deposition of the molecule.

However, the molecule did not arrive in time for the author to test the experiment with it. Further work should therefore include a study of biphenylene.

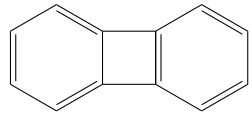

Figure 4.10.: Simplified Lewis-structure of biphenylene

Chapter 5.

Results and Discussion

The following chapter presents the results obtained from the experimental work described in the previous chapters, i.e. Chapter 4. The results are presented in two main parts. First the results from the experiments done in Trondheim is presented, followed by the experiments performed using synchrotron radiation in Aarhus. Whilst the experimental section was presented in a chronological order, the results are presented otherwise. Large parts of the results are most meaningful when compared to earlier observations, and the results is then presented with focus on comparison and changes.

As mentioned in Chapter 4, the scan parameters of each XPS, UPS and NEXAFS scan is determining the resulting signal. To avoid packing too much details into the following section, all scan parameters for the scans done are listed in Appendix B and Appendix C.

Using synchrotron radiation has the advantage that the experimental work can be done quickly and with high precision. Since it is possible to perform measurements in a short time, a high amount of results was obtained during the period using Matline to investigate the system. However, in order not to confuse or overwhelm the reader, only the core results from the work is presented in this section.

In this chapter, the experimentally obtained results are compared to the findings from first principle calculations on the thymine molecule. The goal of the reader is not to present a deep coverage of the computational work, but rather to give the reader an introduction to the calculations and to use them in describing and interpreting the effect between thymine as a result of ultraviolet exposure.

5.1. Initial studies of adsorbed thymine

As mentioned in the previous chapter was the goal for the preliminary studies using the facilities at NTNU to get an impression if thymine successfully could be deposited onto MoS_2, and if the molecules were stable enough on the surface to be used successfully as an adsorbate-substrate system in the synchrotron.

5.1.1. Cleaned sample

After the sample was loaded into the experimental chamber, was it left to degas for some time. Following this was resistive heating to try to evaporate contaminants. The cleaning procedure was followed by X-ray Photoemission Spectroscopy (XPS) scans to get an indication of the cleanliness level. A wide energy scan is presented in Figure 5.1. The sample was cleaved in air, and prior to the sample transfer it had thus been subject to atmospheric conditions[1] and possibly also effected by carbon compounds when outside the chamber. Indications of common contaminants such as carbon, nitrogen and oxygen was therefore to be expected.

Further investigation of these contaminants were done by performing more detailed core-level scans with a lower energy range. The core level scans, are as indicated in table B.1, performed with smaller energy steps and lower pass energy to give much higher energy resolution. Performing more detailed scans can lead to different results than what is obtainable with lower resolution. An example is the difference between the wide-scan and the detailed scan of the Mo 3d core level in figures 5.1 and 5.2. In the low-resolution wide scan, Mo 3d seems as one energy level in the material, whereas increasing the resolution in the detailed scans reveals the spin-orbit splitting of the band.

The MoS_2-sample was found having certain amounts of contaminants. From the wide scan, it can be seen that peaks arise at approximately 532 eV and 285 eV. These peaks in the signal can be attributed to O 1s and C 1s core levels respectively; in other words: both oxygen and carbon was present on the sample after loading it into the vacuum chamber. At 740 eV, a small peak is seen. From tabulated values, this is known to correspond to the oxygen KLL Auger transition, another sign that oxygen was present on the sample.

5.1.2. Thymine deposition

After deposition of thymine, a wide energy scan was performed in order to get an idea of the state of the surface. The wide scan presented in Figure 5.3 shows considerable changes relative to the corresponding scan performed before deposition. Two large changes can be observed between the two spectra. First and foremost, four large peaks not seen before deposition is seen. At approximately 290 eV binding energy the carbon peak has become much more intense relative to the background than before the deposition. Similarly, at 532 eV binding energy the O 1s core level is more intense relative to the surroundings. The increased intensity of the O KLL Auger electron peak is also

[1] Air is a combination of gases containing mainly consisting of N_2 (approximately 78%), O_2 (approximately 21%) and water vapour.

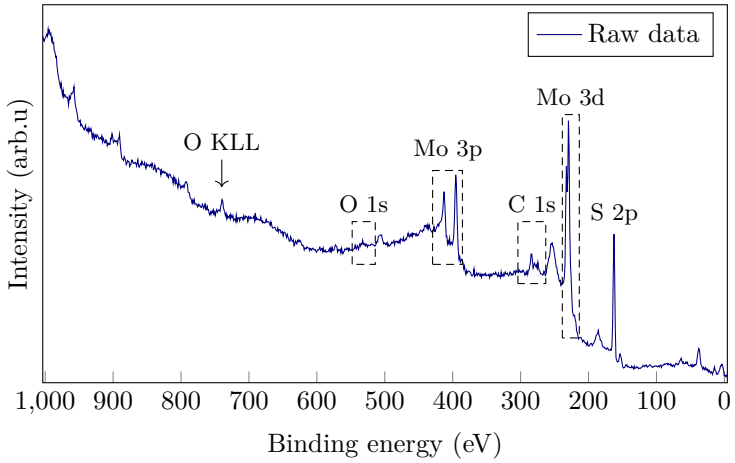

Figure 5.1.: Wide range scan of the MoS_2-sample directly after loading in into the vacuum chamber. The dashed rectangles on the plot indicates areas of which more detailed scans were done. These are presented in Figure 5.2

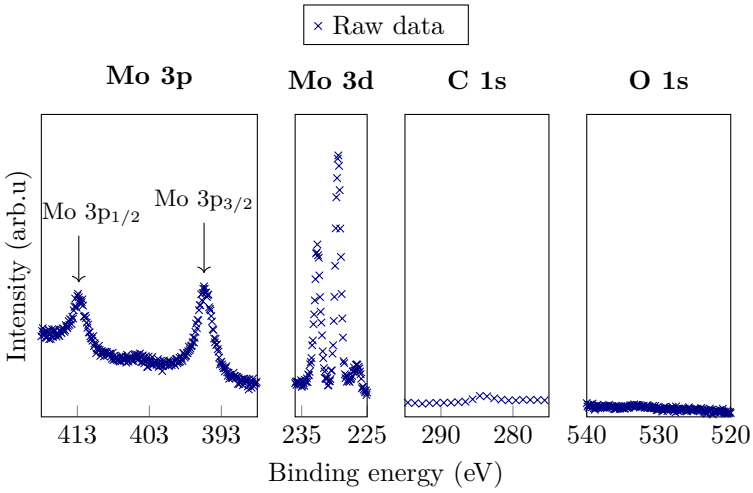

Figure 5.2.: Detailed core level scans of Mo 3p, Mo 3d, C 1s and O 1s of the sample as inserted into UHV chamber. All scans were done with a photon energy of 1253.6 eV, in other words the magnesium Kα transition. Three of the scans were done with a pass energy of 30 eV, whereas the C 1s scan was done with a pass energy of 100 eV

indicative of a higher oxygen content on the surface. In addition, a single peak is seen at the position in binding energy where Mo 3p was present previously.

5.1.3. Thymine temperature stability on MoS_2

The thymine was deposited onto the MoS_2-sample when cooled to a temperature of $-93\,°C$. From the figures 5.3 and 5.4 the successful deposition of considerable amounts of thymine is shown. Cooling was done by using liquid nitrogen flowing through the sample holder.

The thymine stability on the MoS_2-surface as a function of increasing temperature is also relevant. One could imagine that the thermal energy could be enough to desorb the molecules at some temperature. To test the thymine thermal stability on the MoS_2-sample, the liquid nitrogen for cooling was stopped after deposition, such that the sample temperature slowly increased.

Several hours after, the sample had reached room temperature, and photoemission spectra were taken. First a wide energy scan, Figure 5.5, shows that the situation is quite similar to that right after deposition. This fact was confirmed by the detailed core level scans of C 1s, Mo 3p + N 1s and O 1s core levels. These are presented in 5.6. Both the C 1s and O 1s scans were similar to the scans right after deposition, *cf.* Figure 5.4. Indicating a slight desorption of thymine is the presence of Mo 3p electrons in the N 1s spectrum. At binding energies of 411.6 eV and 395.4 eV the Mo $3p_{1/2}$ and Mo $3p_{3/2}$ are found respectively.

The presence of photoelectrons originating from molybdenum can be explained in two ways. One possibility is that the thymine layer actually is thinner than at the time of deposition. Since Mo 3d electrons are escaping from the sample, the layer has to be thinner taken the inelastic mean free path into account. Qualitatively said, the deposited layer had become thinner than the mean free path during the night, as electrons from the molybdenum was now collected by the analyser. However, the thymine, or at least some sort of the molecule were still present on the sample, as electrons from carbon, oxygen and nitrogen all was detected.

Another possible explanation is that the thymine molecules had clustered during the temperature increase. As the sampling area is quite big, one could imagine that the molecules cluster into clusters with a size smaller than the sampling area. When measuring one would then get signal from both the clusters and the substrate surface. As the vapour pressure of thymine is larger than zero at room temperature, the slow previously mentioned slow evaporation is expected. On the other hand; π-conjugated organic molecules tend to make uniform thin films when deposited, which is an argument against the clustering. However, disentangling and quantify the contribution from each effect is difficult, it is even possible that both occured simultaneously.

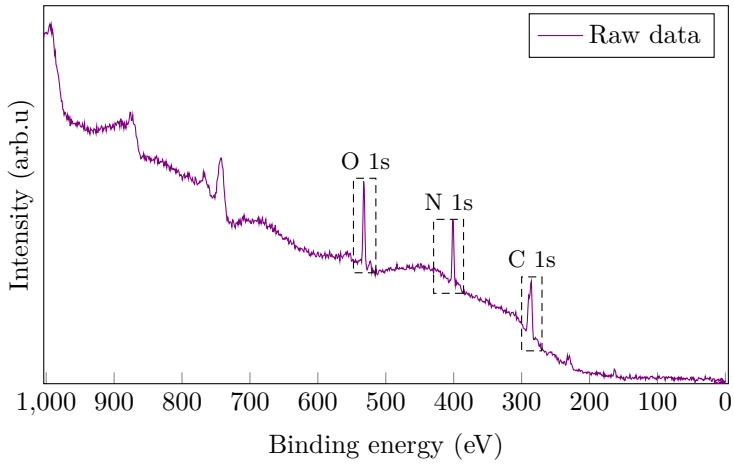

Figure 5.3.: Wide energy scan of thymine deposited onto MoS_2. The scan shows clear signs that thymine has been deposited onto the surface.

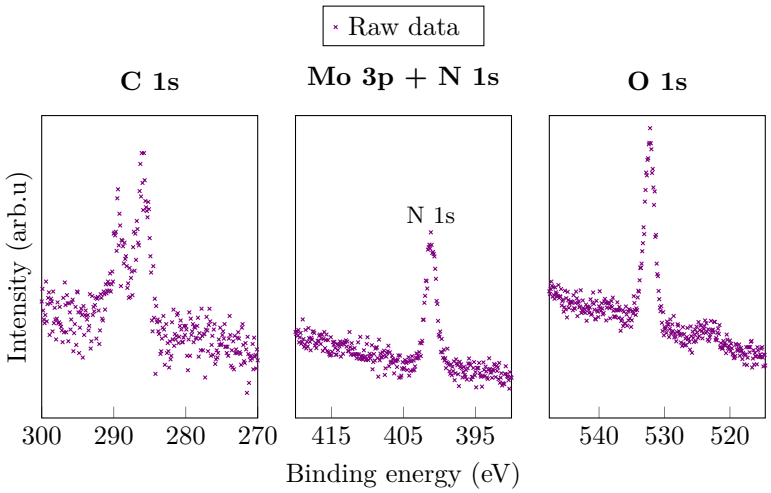

Figure 5.4.: Detailed core-level scans of C 1s, N 1s and O 1s after depositing thymine. All scans were done using a photon energy of 1253.6 eV and a pass energy of $E_p = 30$ eV, and a step size $\Delta = 0.1$ eV. Seen from the middle scan is the complete attenuation of the Mo 3p signal, *cf.* Figure 5.2, indicating that the deposited layer is thick, and may be regarded as a "bulk like" layer of thymine.

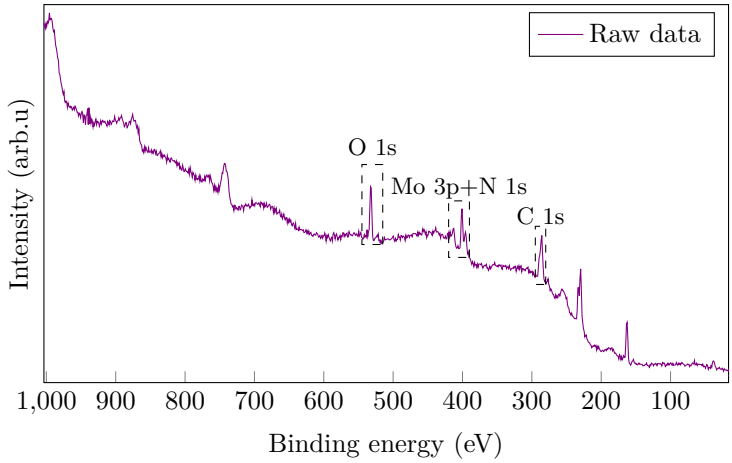

Figure 5.5.: Widescan of MoS_2-sample after slow temperature increase up to room temperature.

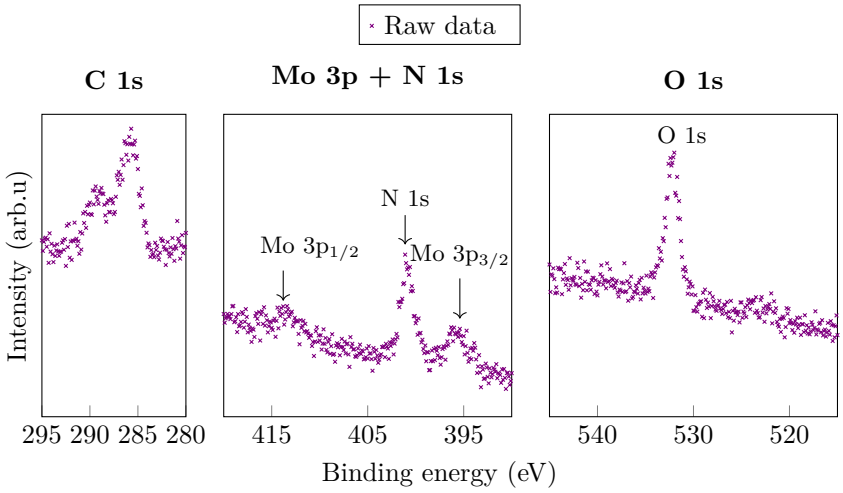

Figure 5.6.: Detailed core-level scans of C 1s, N 1s and O 1s after approximately 12 h with continuous increase in temperature from −93 °C to room temperature.

5.2. Reaction studies using synchrotron light

The following section presents the experimental results obtained using Matline in Aarhus. As earlier mentioned is this section built up by comparing similar measurements performed at different points in time. By presenting in such a way, the author hopes that it is possible to see the red thread in the experiments and follow the discussion more easily.

When collecting photoelectrons, the property detected is their energy. As was the case for the experimental work in Aarhus. In the following, the detected kinetic energy is plotted on the bottom x-axis of the plots, whereas the upper axis shows the calculated electron binding energy. The kinetic energy is shown, as this is the actual measured property. Including the corresponding electron binding energy is done for making the comparison to literature easier for the reader.

5.2.1. Core-level changes after exposure

After cleaving and insertion into the experimental chamber, initial characterisation of the sample was done. Figure 5.7 shows detailed core level scans of the sample after heating it to 390 K and letting it cool down. This shows that some contaminants was present on the sample, even after heating it. Most notable is the presence of carbon, represented with a C 1s peak at 96.9 eV. No nitrogen or oxygen was detected, which was favourable, as a presence of such elements could have made the analysis more difficult.

The detailed scan of the molybdenum 3d core level reveals to main peaks at 232.2 eV and 229.2 eV, which can be identified to be Mo $3d_{3/2}$ and Mo $3d_{5/2}$. The values are somewhat shifted from the tabulated values for the "pure" Mo 3d orbitals at 231.1 eV and 227.2 eV, but closer to values for MoS_2 reported by others [64]. This is not surprising, as the core level energy is known to depend on the chemical environment of the specie, as described in section 2.4.4. The spin-orbit effect is evident from the two peaks, and their separation correspond well to expected values. Left to the Mo $3d_{3/2}$ peak, a small peak corresponding to S 2s. S 2p has a ionisation cross section of 0.2661 compared to 4.195 for Mo 3d at an energy of 350 eV. In other words, the presence of the molybdenum peak dominates even though twice as many sulphur as molybdenum atoms is present in the material on average[2]. Sulphur is exposed to the outside, only being bound to molybdenum at one side, and a shift in the electron binding energies was therefore expected, measured was S 2p energy of 226.4 eV, compared to 230.9 eV as the tabulated value.

[2]This consideration neglects effects that it is a sulphur layer that is exposed to the top when looking at MoS_2 layered materials.

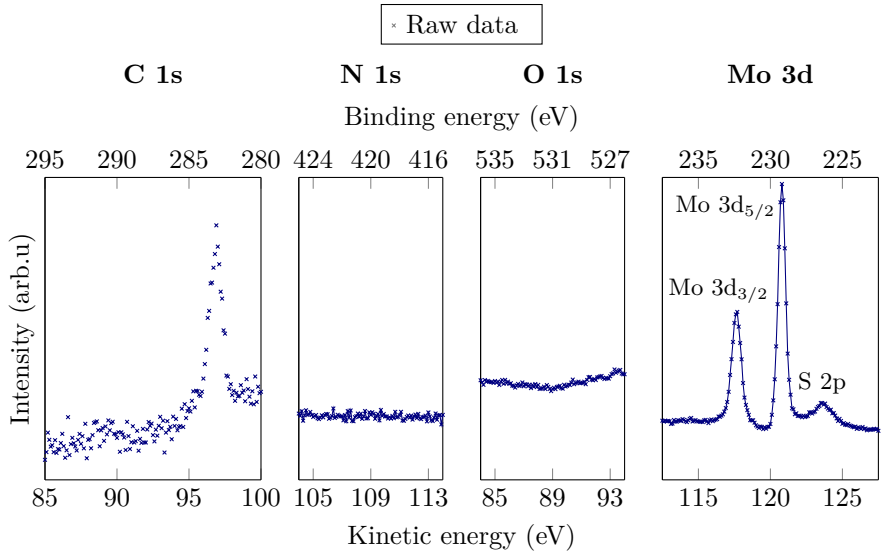

Figure 5.7.: Detailed photoemission spectroscopy measurement of C 1s, N 1s, O 1s and Mo 3d regions of MoS_2-sample right after inserting it into the vacuum chamber. The scans were done with photon energies of 380 eV, 529 eV, 620 eV and 350 eV respectively.

Following the thymine deposition onto the surface was the same scans. From the preliminary experiments performed at NTNU we expected the thymine to successfully stick to the surface. The high resolution spectroscopic measurements performed indicate this as well. Looking at the Mo 3d measurement in Figure 5.8 reveals an strong attenuation of the signal from the Mo 3d electrons. Using the first thickness estimation model provided in Appendix D gives an estimation of the deposited layer. By assuming an inelastic mean free path [1] of 1 nm and assuming that the cross sections is similar in the two materials the thickness of the deposited thymine layer is found to be 1.85 nm. It should be noted that the thickness calculations are based on many assumptions, and that it should only be used as a highly approximate estimate.

Three detailed core-level scans were done to characterise the deposited thymine, C 1s, N 1s and O 1s. The reasoning behind this was straightforward: carbon, nitrogen and oxygen are all present in the thymine molecule, and by looking at these core levels, the goal was to characterise the thymine at different times. These scans are shown in the three leftmost panels in the figure 5.8, 5.10 and 5.11. Thymine has molecular formula $C_5H_6N_2O_2$ and electrons from

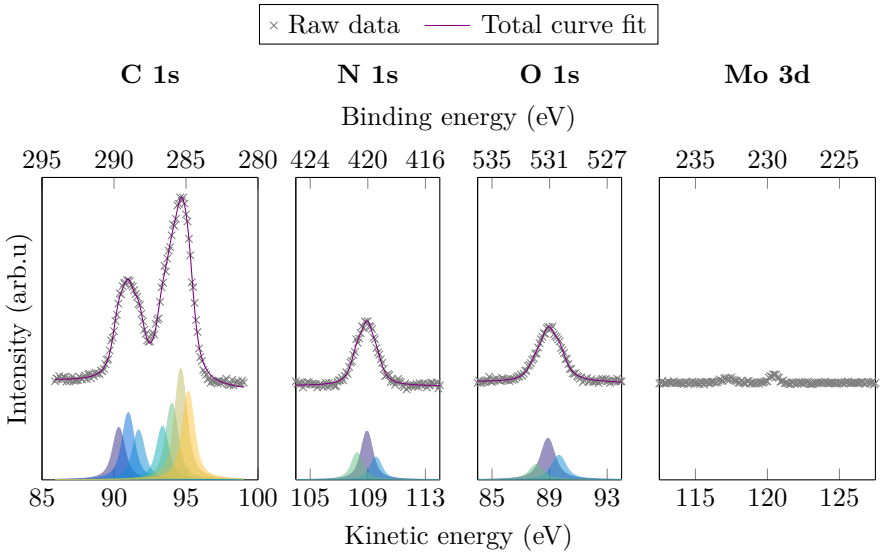

Figure 5.8.: Detailed photoemission spectroscopy measurement of C 1s, N 1s, O 1s and Mo 3d regions right after depositing thymine. The scans were done with photon energies of 380 eV, 529 eV, 620 eV and 350 eV respectively.

carbon, nitrogen and oxygen can all be measured in conventional spectroscopy measurement techniques. Already from the molecular formula, it is apparent that the analysis of thymine is complex.

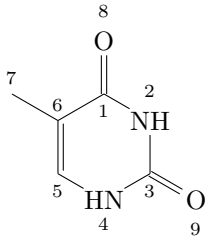

Thymine

Figure 5.9.: Molecular structure of thymine with atomic numbering. The atomic numbering corresponds to the atoms from which detectable photoelectrons arise.

Figure 5.9 shows a depiction of the thymine molecule. Numbered are all the atoms from which detectable photoelectrons arise[3]. Oxygen is present in two inequivalent configurations, namely atoms 8 and 9. Nitrogen is also present in two different configurations, in atoms 2 and 4. Carbon, which is the basis for all organic molecule is present in five configurations (atoms 1, 3, 5, 6 and 7) and a complicated photoemission structure was therefore expected when doing the detailed energy scans. The situation complicates additionally as the molecules can desorb differently onto the surface. Before deposition a C 1s peak from contaminants was observed, none of the peaks after deposition correspond to this peak.

In order to get an idea of the number of components in the scans, the well known χ^2-test (chi-squared) was applied. The test makes it possible to evaluate which number of components make the best fit to the dataset, and thus estimate the number of inequivalent electronic configurations for the atoms.

The core level scans showed that a considerable amount of thymine had been deposited onto the surface. Initially, the carbon scan seemed to contain two peaks, but expected from the molecular configuration is at least five different electronic configurations. The scan was therefore fitted with five, six and seven peaks, with seven peaks giving the best fit. Nitrogen 1s and Oxygen 1s both were found to be fitted best with three components.

Following the deposition was exposure to ∅-light. Despite the radiation exposing the sample being highly intense, the first exposures did not lead to any significant changes in the core level energies. Exposure was first done in small steps of some seconds[4], and later increased to 1 h. After the 1 h exposure changes in the core level signal became apparent.

Figure 5.10 shows the state of the core levels after 1 h exposure[5]. The core level scan of carbon revealed that the two peak structure had changed dramatically. Small changes was also observed for the N 1s and C 1s peak.

One could imagine that the thymine would reorder or even cluster when exposed to high intensity light. However, looking at the Mo 3d peaks, show no sign of the surface becoming more exposed. The signal from the Mo 3d orbitals were still low, almost completely attenuated by the topmost layer. This was an indication of no or low desorption or clustering of thymine from the MoS_2 surface.

The sample was exposed to additionally 6.5 h of ∅-order light, with the resulting core level scans presented in Figure 5.11. Qualitatively the results

[3] Atoms such as hydrogen and helium is not detectable by photoelectron spectroscopy as the 1s level in the molecules has a very low absorption cross section.

[4] The exposure was done with the following exposure durations: 1.5 s, 3 s, 5 s, 10 s, 20 s, 40 s, 90 s, 2.5 min, 5 min, 10 min, 15 min and 1 h

[5] The total exposure time was 1 h plus the short exposures made before the long 1 h exposure.

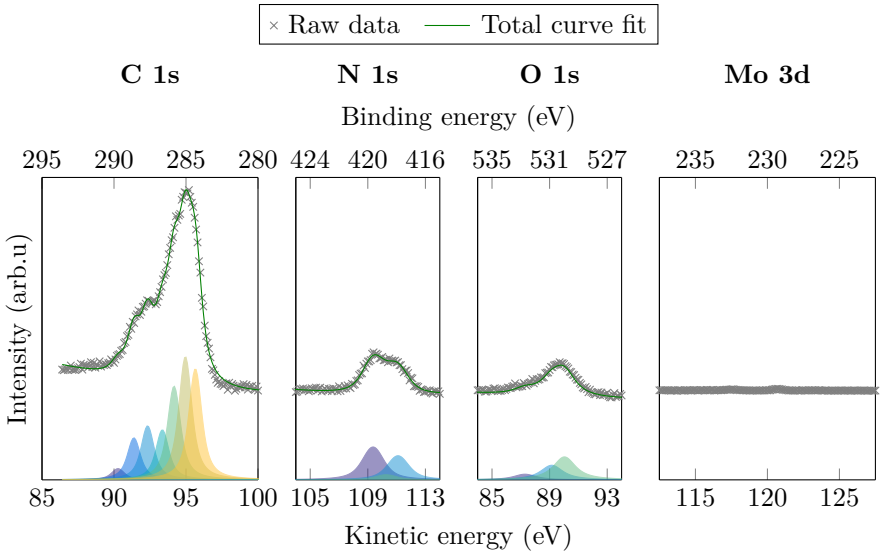

Figure 5.10.: Detailed photoemission spectroscopy measurement of C 1s, N 1s, O 1s and Mo 3d regions after exposure to approximately 1 h of ∅-order light. The scans were done with photon energies of 380 eV, 529 eV, 620 eV and 350 eV respectively.

seemed quite similar to the situation before the long exposure. Molybdenum was still not present, indicating that a bulk-like layer of thymine was still present on the MoS_2-surface.

To further investigate the differences between the electronic configurations in the three cases, the relevant core levels for the thymine molecule was plotted together in one figure, see Figure 5.12.

The carbon 1s core level scans show significant difference after deposition, after 1 h and after 6.5 h of ∅-order light. In the first case, a two peak structure was seen. After exposure, the higher binding energy peak of the two show gradual decrease until the component is barely visible after the 6.5 h exposure. Overall barely no shift is observed in the energy of the 1s level.

Nitrogen 1s was fitted with three components. Immediately after deposition the orbital exhibit a fine symmetry structure, with the three components constituting peak centred around a binding energy of 420.1 eV. As the thymine was exposed, N 1s shifts gradually towards lower binding energy. In addition the peak broadens, the fitted components spread out by some degree. This is seen in the peak shoulders observed after 1 h and even more after 6.5 h of

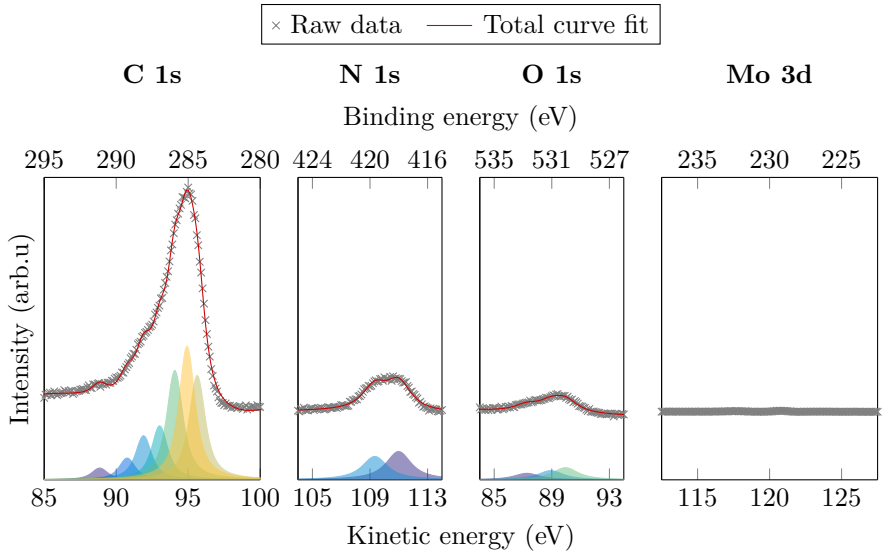

Figure 5.11.: Detailed photoemission spectroscopy measurement of C 1s, N 1s, O 1s and Mo 3d regions after exposure to approximately 6.5 h of ∅-order light. The scans were done with photon energies of 380 eV, 529 eV, 620 eV and 350 eV respectively.

exposure to ∅-order light.

Similar to N 1s, the oxygen core level shows both a shift and a spread after exposing it to ∅-light. Initially, that is immediately after deposition, the O 1s peak was centred at 531 eV. Upon exposure the peak shifted slightly towards lower binding energy, a shift quantified to be approximately 1 eV. O 1s show even higher spread than N 1s, and a clear shoulder towards higher binding energies occur.

Summarised, the core levels changed significantly upon exposure to high intensity light. The changes seen after 1 h of ∅-order light seemed to continue when exposed longer. All peaks are plotted in the individual core level scans presented in figures 5.8, 5.10 and 5.11.

In order to quantify the shifts in the fitted peaks are all peak positions recorded in Table F.1 in Appendix F. Here the precise peak position of C 1s, N 1s and O 1s fitted components are given before, after 1 h and after 6.5 h ∅-order light exposure. Note that the peak positions are given with some uncertainty. The numbering of the peaks are done from highest to lowest binding energy in all cases.

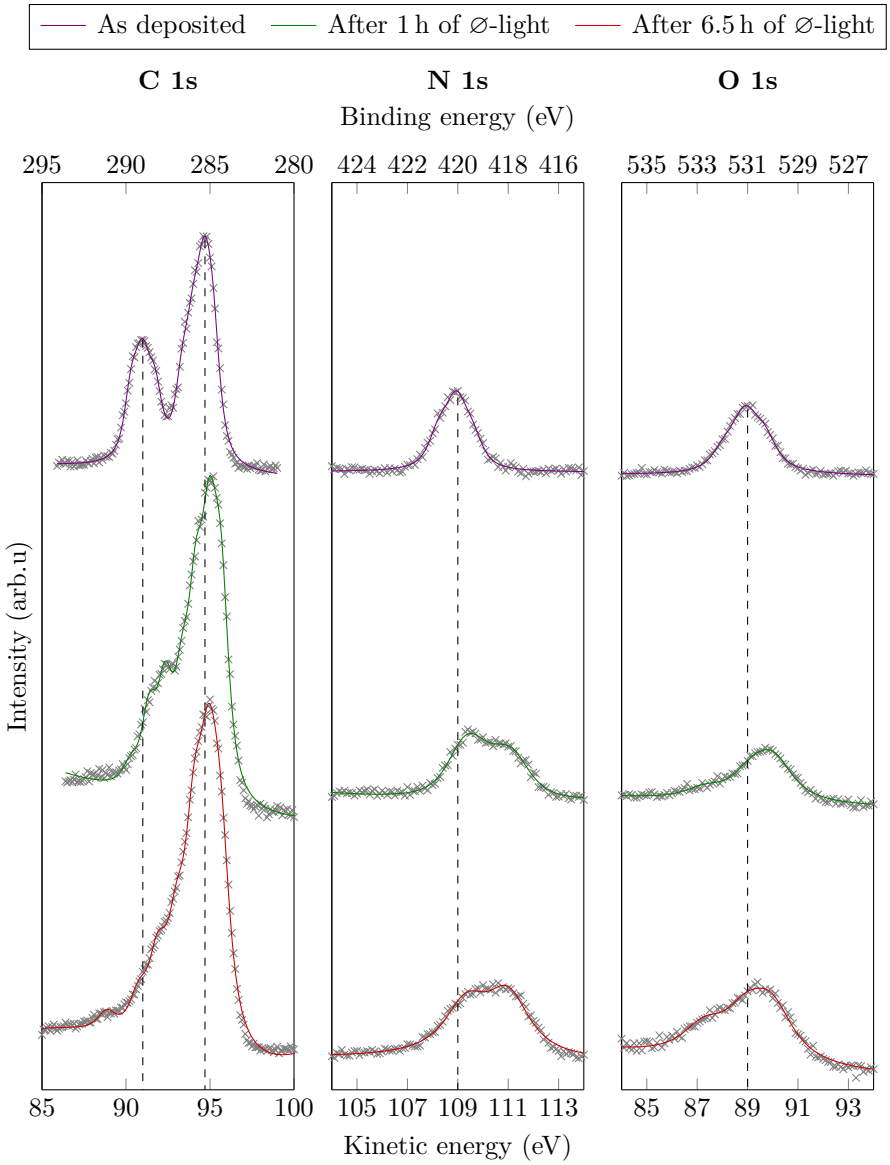

Figure 5.12.: Comparison between detailed core level scans of C 1s, N 1s, O 1s right after deposition of thymine, after exposing it to ∅-light for 1 h and 6.5 h. The measurements were done with photon energies of 380 eV, 529 eV and 620 eV respectively. Dotted lines from the centre of the original peaks are added to guide the eye.

5.2.2. Changes to the valence band due to exposure

Right after deposition, after a short exposure and after 1 h and 6.5 h of ∅-order light, the valenceband of the thymine was measured. Figure 5.13 shows the differences in the valence band between the different situations. From having a fine detailed structure, the valence band becomes smoother upon exposure. When considering the core-levels the exposure changed seemed to continue with more exposure, contradictory to the situation with the valence band. Even a short exposure for doing measurements induced a substantial change in the valence band.

Following the two largest feature during before and after exposure indicates that they have shifted towards lower binding energies. As the two features are shifted by approximately an equal amount, it is suspected that the shift is due to some form of doping of the material. One candidate for this doping is water evaporating onto the sample.

The loss of the fine structure upon exposure, could be due to several effects. One possible explanation is that the thymine molecules rearrange and that some of the features merge into the more prominent peaks. In other words a rearrangement where the differently oriented and bound thymine molecules changes into more a more regularly bonding configuration.

5.2.3. Absorption spectra changes due to exposure

As mentioned in Chapter 2, is NEXAFS an X-ray absorption technique very sensitive to the chemical environment and the coordination of the atoms in a molecule. Using NEXAFS could there potentially yield additional information about the system.

From the NEXAFS measurements presented in Figure 5.14, is it seen that the system change upon exposure, albeit to a low degree. The π^* resonances seen from approximately a kinetic energy of 284 eV up to 290 eV show the same general structure, but they smooth out, and the distinct peak structure seen before exposure is less clear. One possible explanation for the profile smoothing could be that the atoms become inequivalent in the molecule, or that some molecules react.

The presence of the same general structure before and after exposure could be explained by a preservation of the ring like structure in thymine, with only minor changes due to changes in the functional groups around the ring. Explaining these contributions is however, only done with “hand-waving” arguments, as a complete analysis of the NEXAFS spectra has to be followed by calculations [4].

NEXAFS is frequently used on organic molecules deposited on top of relatively inert surfaces. A central question is how much the presence of the substrate effect the system. Interactions with the substrates are often quite low, as the

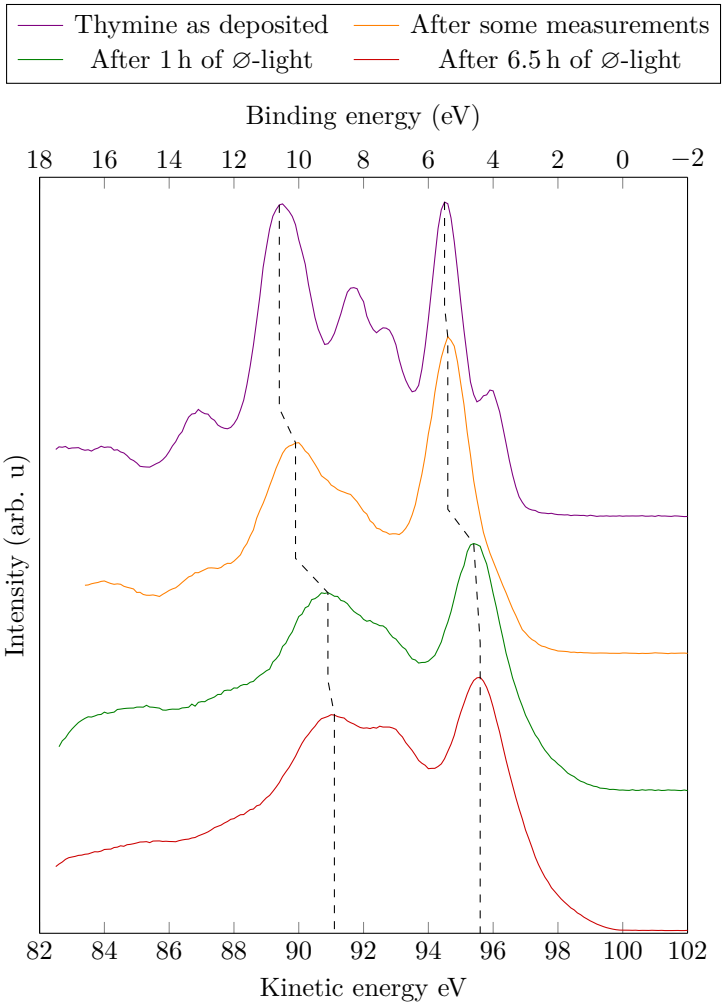

Figure 5.13.: Comparison between photoemission measurements of valence band taken at different moments. The scans were done using a photon energy of $h\nu = 100\,\text{eV}$ and a energy step of 0.1 eV. The detailed scans shows shifts in the valence band structure between the measurements. Dashed lines are added as a guidance to the eye for detecting the detailed differences in the valence band.

Table 5.1.: Core level binding energies of C 1s level in non-equivalent types of carbon atoms in thymine. The numbering and bond type characterisation is according to the literature [116]

Atomic binding	Atomic label	Graph label	Binding energy
CHC	6	a	284.6 eV
CN	5	b	285.8 eV
CN_2(CNO)	1	c	287.6 eV
CN_2O	3	d	289 eV

excited electronic states are found to have a large degree of its structure very similar to the one shown when isolated molecules are investigated [101].

Table 5.1 lists the different carbon related bonds and uses previously known bonding classification found in the literature [116]. The observant reader will notice that neither O 1s or N 1s absorption spectra is analysed any further. As the author found these spectra to noisy to analyse, it was not attempted. Additionally, for any NEXAFS analysis to be complete, appropriate calculations have to follow the experimental data.

5.3. Comparison to ab-initio calculations

The following section introduces the *ab-initio* calculations performed on two thymine molecules and relates it to the experimentally obtained results. Presenting the results is done in a basic way, with more focus on the found results rather than how the calculations are performed. Interested readers should consult other sources [72]. All calculations were performed by Merete Falk, and supplementary information is found in her thesis [26].

Summarised, the idea of the calculations was to be compared with the experimentally obtained results, and several calculations were thus performed in order to simulate different aspects of the experimental work. From previous discussions and presented results, it is apparent that some reaction occurred to the thymine molecules when exposing them to high intensity ultra violet light. Describing these reactions and their likelihood was the primary goal of the calculations.

5.3.1. Basis behind first principle calculations

For a given chemical reaction to occur, the participating molecules tend to be required to be in a given orientation. For thymine dimersation the double bonds in the ring structure need to be orientated properly [90] in order for the

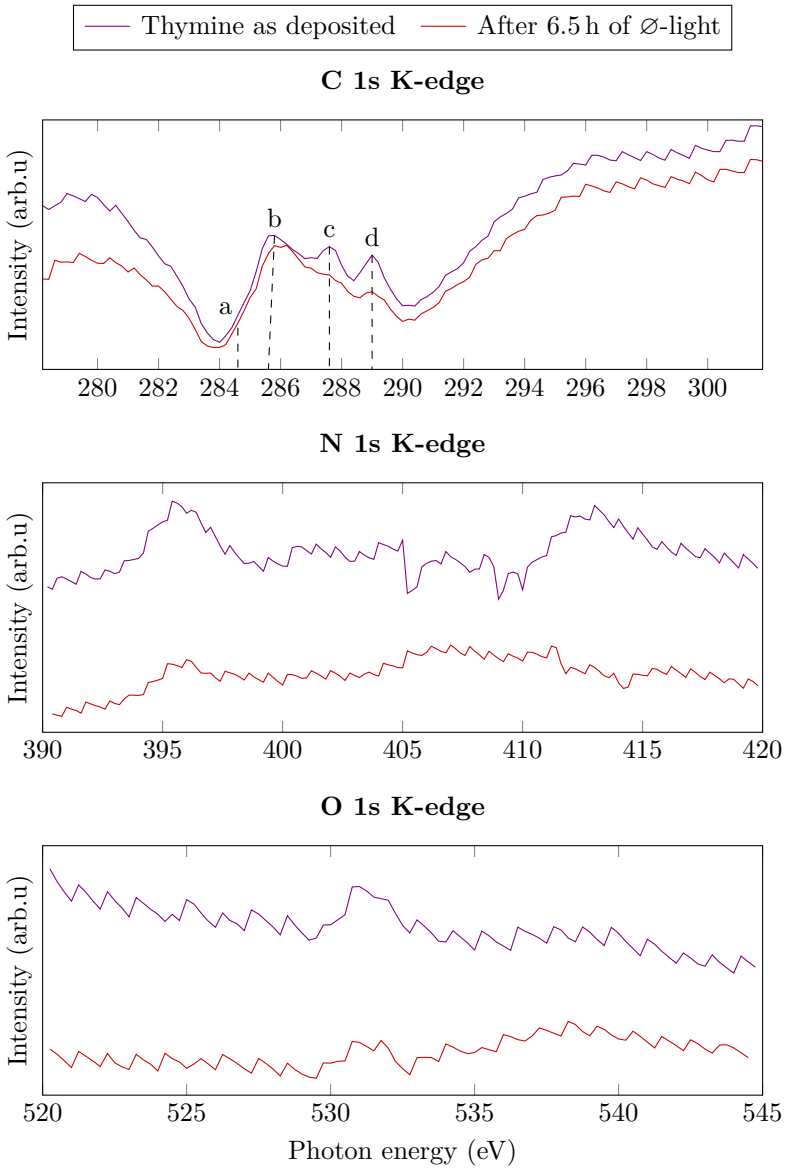

Figure 5.14.: NEXAFS of the K-edges of C, N and O in thymine before and after exposure to ∅-order light. The most prominent peaks are marked and their energy is described in Table 5.1. A background signal was subtracted from all spectra.

reaction to proceed. The relative orientation between the two thymine molecules participating in the reaction is affected by the interaction energy between the two thymine molecules. Where higher interaction energy is indicative of a more stable electron configuration and therefore a more probable orientation. Summarised, the interaction energies can be used as an indicator explaining the probability of a chemical reaction to occur.

In order to calculate the interaction energies the second order Möller-Plesset pertubation theory [72], MP2, along with the SNOOP-scheme [52] and the heavy-aug-cc-pVDZ basis. These theories combined builds on the Schrödinger equation, with some approximations. The SNOOP-scheme is a method for reducing the error of the computations and the basis is a description of the functions used to describe the electrons. For the calculations, a small basis is used, in order to limit the computational resources needed. Albeit, a simple model, these calculations have been found promising when compared to more complex calculations [26].

Due to its simplicity the calculations neglect some aspects. To lower the computational resources needed is only two thymine molecules was simulated, which is in contrast to the high amount deposited during the experimental work. Additionally, no substrate was included in the calculations. The substrate could effect the binding, as itself could effect the molecular orientation by molecule-substrate interactions. Lastly, the calculations are performed by assuming absolute zero temperature, i.e. 0 K. Combined all these assumptions make the interaction energies a theoretical construct, where the usable information lies in the relative differences in energy as well as the general trends.

5.3.2. Interaction energy between two thymine molecules

To calculate the interaction energy between two thymine, several relative orientations between the two "stacked" molecules were considered. This was done by fixing two thymine molecules parallel and calculating the interaction energy at different rotation. As the parallel orientation is a bit arbitrary, geometric optimisation gives more reasonable results. The angle between the two molecules presented in Figure 5.15 are thus the optimised geometries. All the geometries were optimised using the MP2 method and the cc-pVDZ basis.

Table 5.2 presents exact value of the calculated interaction energies. For dimerisation to occur is thymine required to be be oriented with 0° between the molecules [90]. The found interaction energy for this case is much lower than for other orientations, indicating that the thymine dimer does not prefer to be in the optimal conformation for dimerisation. Rather, the two thymine tend to be shifted relative to each other, by introducing an angle between the two methyl groups. Calculations give evidence that the methyl group creates steric hindrance and thus weaken the interaction for given conformations.

Table 5.2.: Interaction energy between two stacked thymine molecules at different orientations. The geometry of the orientations is depicted in Figure 5.15. Values according to Falck's calculations [26]

	Interaction energy	
Orientation	mE_h	meV
0°	-4.45	-121
90°	-18.55	-505
180°	-16.48	-448
270°	-17.90	-487

Table 5.3.: Interaction energy for different lateral orientations of two thymine molecules. The first principle calculations are performed by Merete Falck [26].

		Interaction energy	
Orientation	Figure	mE_h	meV
O1	H.1(a)	-19.12	-520
O2	H.1(b)	-5.26	-143
HB1	H.1(c)	-6.49	-177
HB2	H.1(d)	-7.99	-217

In vivo the thymine nucleobases may behave differently. Unlike in the case of free molecules, thymine in the DNA are bound to a sugar-phosphate backbone. This bonding may restrict or at least alternate the achievable orientations, giving one explanation why thymine dimerisation can occur despite the low calculated interaction energy and probability for the favourable conformation.

As the conformation needed for dimerisation was found to unfavourable compared to other conformations, other possible reactions and arrangements was considered. Placing thymine molecules laterally and making and educated guess of strong interaction and reaction relevant positioning, lead to the calculation of interaction energy for four different lateral position combinations. The four positions for which the interaction energies was calculated are depicted in Figure H.1 in Appendix H.

Without going too much into details, the calculations indicate that several orientations are possible. Which orientation that is relevant for a chemical reaction, is difficult to say without further analysis. However, as seen from the Figure H.1 in Appendix H and Table 5.3 the orientations could involve charge transfers and different bonding configurations.

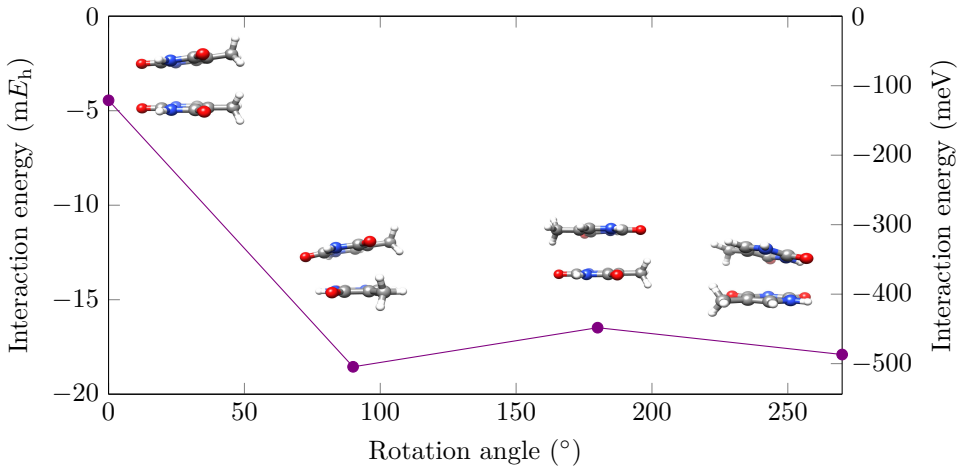

Figure 5.15.: Interaction energy between two thymine molecules at different relative orientations. It is seen that the most stable orientation, i.e. the one with highest interaction energy is when the two thymine molecules are orientated with the methyl groups at 90° to each other. The relative orientation is pictured in the molecular images above each data point.

5.3.3. Keto-enol-equilibrium

All ketones are found in the keto-enol equilibrium. Here the molecule switches between having a keto-group (C=O) to having a enol-group (C–OH). This principle is depicted in Figure 5.16 and is one process causing "tautomerism" [16]. Two isomeric forms of a molecule is said to be tautomers if they only differ by one or more such equilibria .

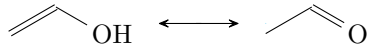

Figure 5.16.: Principle of keto-enol-tautomerism. The reaction proceeds rapid, resulting in the two forms being considered as two equal forms of the same molecule.

Thymine have two keto-groups in its structure, and several tautomers of thymine is therefore to be expected. Thymine has six tautomers including itself. These are depicted in Figure G.1 in Appendix G,. The switching between the isomeric thymine tautomers happens fast. Due to stability (=energy) reasons,

some tautomeric forms tend to more stable stable than others. Two of the tautomers are found to be the most stable, and thus occurring more frequently than the others [73]. Calculating the core level energies of thymine and its most stable tautomer was performed and presented in Table 5.4. Being a calculations with given assumptions, the absolute value of the energies should not be considered correct. The key aspect of these calculations is if the found core-level energy shift found experimentally could be interpret by the means of fundamental calculations.

Table 5.4.: Calculated ionisation energies for N 1s and O 1s. The CCSD calculations are performed by Merete Falck.

		Ionisation energy (eV)	
	Orbital number	Thymine	Tautomer
O 1s	1	542.03	544.80
	2	542.25	541.80
N 1s	3	410.25	410.48
	4	409.91	408.37

In order to compare the calculations to the experimental data, the calculated electron energies are plotted together with the experimentally measured energies. As the tautomer molecule contains two different nitrogen and two different oxygen atoms, all calculations were done assuming that the last fitted peak is a contribution from some other reaction. Such a reaction could e.g. be the interaction with the substrate.

Plotted together in Figure 5.17 are the experimentally obtained data and computational results. Calculations show a splitting of the two components of 1.7 eV and 3.2 eV for N 1s and O 1s respectively. From the experimental data the main components are found to be separated by 1.7 eV and 2.8 eV for N 1s and O 1s respectively. A hand-waving argument for the different calculated splitting is that some of the molecules react, but not all, contributing to a presence of photoelectrons originating from the "original" core levels. In addition is the effect from the substrate hard to account for.

Due to limited computational resources, C 1s an its ionisation energy was not calculated. These calculations remain to be performed, but they are assumed to indicate the same situation as was the case with N 1s and O 1s; a splitting due to the tautomerisation of thymine.

The deviation between calculation and practice can be interpret as an effect of other factors as well. While doing spectroscopy experimentally, several effects, some of which discussed in Chapter 2, contribute to the actual energy

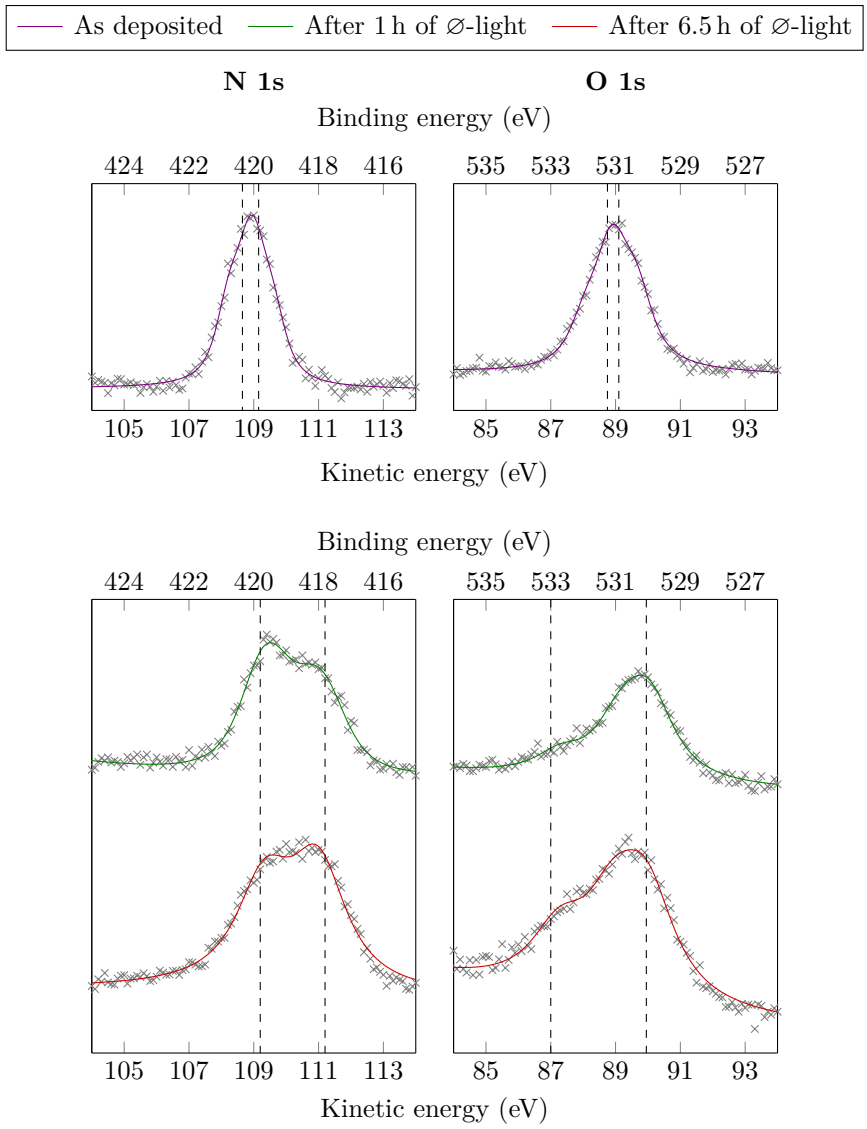

Figure 5.17.: N 1s and O 1s core-levels compared to calculated results [26]. Dotted lines are the calculated core-level energies for N 1s and O 1s with energy separations of 2.11 eV and 3.0 eV respectively. The graphed data are experimental data of the core levels after exposure to high intensity UV-light.

of the detected photoelectron. When doing spectroscopy of a non-ground-state photohole, the remaining electrons will try screening the photohole and reduce the energy.

How efficient this energy screening is, depends on the material, from very efficient screening in metals to low efficiency in insulators, i.e. the electron mobility is one important factor. Thymine as an organic molecule is suspected to be anywhere in between these extrema. Summarised, several effects are expected to contribute to the precise energy level in the molecule. Calculations are done without taking all aspects into account, and is therefore not necessary giving the right absolute values or the right splitting between the energy levels. However, the calculations help in interpreting the experimentally obtained results, and supports the belief that some charge transfers happens to the molecule upon exposure.

A relevant question is why the tautomer of thymine is not seen in the original core level spectra. Previously reported is that UV-light could perturb the keto-enol equilibrium described in Figure 5.16 in either of two ways [27]. Such an effect could be the underlying answer to this question. These equilibria are known to be dependent on pH and other factors as well [16].

Calculations also show that the reaction to create the pyrimidine dimer should proceed without any energy barriers, given that thymine is in the right conformation. The reaction is found to be complete within 1 ps, a time to short for rearrangements of the conformation after excitation. The calculations also show that it is more favourable for thymine to dimerise then for adenine to do it. Adenine is therefore often ending up in ground state without any reaction occurring [26].

5.4. Depositing bromocyclobutane on MoS_2

Bromide was tried deposited onto the MoS_2-sample two times. The Br 3d scan of the clean MoS_2, of the sample after the first deposition and after the second deposition is shown in Figure 5.18. The figure shows no signal of any photoelectrons coming from bromocyclobutane.

Four member carbons rings are rare, and due to the strain in the bonds, they tend to be unstable. At higher temperatures they become increasingly unstable as the thermal energy becomes higher relatively to the bonding strength. That bromocyclobutane did not stick to the surface was therefore not completely unexpected. Studying bromocyclobutane in general and the electronic properties of the square carbon ring in special, should therefore be done with a system with stronger interactions between molecule and substrate. However, this may alter the properties of the cyclobutane ring and make the study irrelevant.

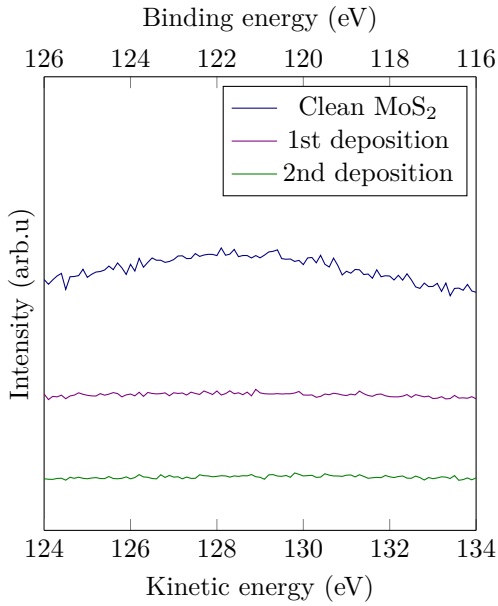

Figure 5.18.: Br 3d scan showing that bromocyclobutane was not possible to deposit on MoS_2.

5.5. Results summarised

An extensive part containing results have been presented in the previous text. In order to make the results more accessible to the reader, a short introduction of the results follows in this section. It summarises the results obtained when performing experimental work in connection to this thesis.

First it was found that thymine powder successfully could be evaporated and deposited onto a MoS_2-surface. The deposited thymine film was found be of appropriate thickness, and reasonable temperature stability was demonstrated.

Performing highly detailed studies using synchrotron light was done to shed additional light on the changes in thymine when exposing it to intense UV-light. The core electron energy levels showed a shift upon exposure. a shift seen after the first exposure to ∅-order light. A splitting of O 1s and N 1s core levels after exposure and the attenuation of one of the C 1s peaks was observed.

Valence band measurements indicated that some changes in the valence band occurred quickly when exposed to light. Even after some short measurement exposures a change in the structure and the loss of fine details was seen. X-ray Absorption Spectroscopy data suggest that some changes occurred to the

thymine, but that the general ring like structure was lost. As the

Calculations give additional insight into the experimental results. First principle calculations show that the optimal relative positioning of two thymine molecules is somewhat unfavourable, and that other reactions than the pyrimidine dimerisation should be considered as an explanation of the experimentally obtained results. Additional calculations was performed in order to investigate if tautomerisation could justify the asymmetric shape of the core levels after exposure. These calculations is in line with what was found experimentally and indicate, albeit with some uncertainty, that the UV light act as an perturbation on the keto-enol equilibrium between thymine and its tautomers.

Chapter 6.

Conclusion

In this work the DNA nucleotide *thymine* has been investigated using X-ray and ultra violet light generated from conventional lab sources and in a synchrotron. The work sought to gain insight into the photochemistry of thymine when exposed to ultra violet, as a way to artificially recreate the pyrimidine dimerisation process responsible for the formation of malignant melanoma.

Thymine dimerisation into pyrimidine dimers has been studied extensively in the past, using a plethora of different techniques. To the knowledge of the writer, spectroscopic techniques has not previously been used to study the reaction. Using synchrotron radiation it is possible to, in a controlled manner, study the conditions responsible contributing to the mentioned reaction.

Initial studies performed at NTNU show that molecules such as thymine can be deposited onto MoS_2 with relative ease. The molecules tend to stick to the surface without too much evaporation even when the temperature is increased up to room temperature.

Detailed results indicate that severe changes happen to the thymine molecules when exposed to high intensity UV light. The binding electrons in thymine undergo a severe change when exposed for long time, indicating a chemical alternation in the molecule. Looking at the valence electrons gives indications that another process, such as rearrangement happens quite quickly when exposing to light. X-ray absorption measurements indicate that the carbon nitrogen ring in thymine is intact after exposure to high intensity light. Breaking stable aromatic rings is known to require a lot of energy, and the measurements indicate that reactions occur to the molecular groups outside the main thymine ring.

Performing calculations can help understanding complex physical systems, and even simple models are often usable when the right approximations are done. In the case of this master thesis, *ab-initio* calculations were used to interpret the experimentally obtained results. The calculations support the notion that the keto-enol equilibrium in thymine is disturbed when exposed to high intensity light.

Even though it is questionable that actual pyrimidine dimers were formed, the experiments performed in connection to this master thesis helps us gain insight into the behaviour of thymine. In addition are the results in line with the expected behaviour of the molecules.

Despite being presented as a complete project, a lot of work remains to be done. Firstly, additional experimental work is advised to further investigate the photochemical reaction. A study of molecules already containing a four-atom carbon ring, and comparing it to the spectra obtained from the artificial created molecule, which is containing such a structure would be relevant. This could be done by using biphenylene or other similar molecules as a model-molecule. Secondly, the spectroscopic measurements should be complemented with additional numerical calculations. It would also be of interest to simulate the energy pathway for reaction of two thymine nucleotides.

In a broader sense, this work has shown the feasibility of using MoS_2-samples as a substrate for depositing organic molecules for studying with synchrotron radiation. Such a substrate-molecule combination for analysis, could in principle be used for a wide array of different measurements. Investigating the effect ultra violet light has on other organic and biological molecules could potentially lead to a much better understanding of how life react to exposure to this radiation. Using synchrotron based measurements has proven as one possibility to study such reactions. These techniques are known for their versatility and usefulness in studying many material systems, also simple biological model systems.

Each research project in this field might seem small and only touch a very narrow part of a vast system. However, even the most tiny obtained knowledge is a small step towards an ultimate goal; understanding the DNA damage by ultra violet light and potentially understanding how to reverse the process. Eventually achieving this would relive the lives of many. This prospect makes even the smallest contribution potentially crucial.

Appendix A.

Orbitals and spin-split area ratios

Table A.1.: Electron shell levels in materials desribed by both X-ray and spectroscopic notation.

Quantum numbers				Spectroscopic notation	X-ray notation
n	l	s	j		
1	0	+1/2, -1/2	1/2	$1s_{1/2}$	K
2	0	+1/2, -1/2	1/2	$2s_{1/2}$	L_1
2	1	-1/2	1/2	$2p_{1/2}$	L_2
2	1	+1/2	3/2	$2p_{3/2}$	L_3
3	0	+1/2, -1/2	1/2	$3s_{1/2}$	M_1
3	1	-1/2	1/2	$3p_{1/2}$	M_2
3	1	+1/2	3/2	$3p_{3/2}$	M_3
3	2	-1/2	3/2	$3d_{3/2}$	M_4
3	2	+1/2	5/2	$3d_{5/2}$	M_5
					et cetera

Table A.2.: After emission from a energy level, the remaining electron may have either spin-up or spin-down state. The magnetic interaction between the orbital momentum and the remaining electron gives the spin-orbit coupling. The intensity differences between states from the same suborbital is presented in this table.

Subshell	l	s	$j = l \pm s$		Area ratio
s	0	1/2	1/2		N/A
p	1	1/2	1/2	3/2	1:2
d	2	1/2	3/2	5/2	2:3
f	3	1/2	5/2	7/2	3:4

The ratio between the areas are calculated using:

$$r = \frac{2(l+s)+1}{2(l-s)+1}. \tag{A.1}$$

Appendix B.

Scan parameters NTNU

The table contains some of the most relevant scan parameters for the acquisitions performed at NTNU. All scans were done with a Mg Kα source, with an energy of 1253.6 eV.

Table B.1.: Relevant scan parameters from XPS measurements at NTNU. Each scan is related to where they are presented in Chapter 5.

Figure	Region	Mode	E_p (eV)	Dwell time (s)	ΔE (eV)
5.1	Widescan	FAT	100	0.5	1
5.2	Mo 3p	FAT	30	0.5	0.1
5.2	Mo 3d	FAT	30	0.5	0.1
5.2	C 1s	FAT	100	0.5	1
5.2	O 1s	FAT	30	0.5	0.1
5.3	Widescan	FAT	100	0.5	1
5.4	C 1s	FAT	30	0.5	0.1
5.4	Mo 3p + N 1s	FAT	30	0.5	0.1
5.4	O 1s	FAT	30	0.5	0.1
5.5	Widescan	FAT	100	0.5	1
5.6	C 1s	FAT	30	0.5	0.1
5.6	Mo 3p + N 1s	FAT	30	0.5	0.1
5.6	O 1s	FAT	30	0.5	0.1

Appendix C.

Scan parameters Matline

Table C.1.: Relevant scan parameters from XPS measurements at Matline. Each scan is related to where they are presented in Chapter 5.

Figure	Region	Photon energy (eV)	E_p (eV)	Energy step (eV)
5.8	C 1s	380	20	0.1
5.8	N 1s	529	20	0.1
5.8	O 1s	620	20	0.1
5.8	Mo 3d	350	20	0.1
5.10	C 1s	380	20	0.1
5.10	N 1s	529	20	0.1
5.10	O 1s	620	20	0.1
5.10	Mo 3d	350	20	0.1
5.11	C 1s	380	20	0.1
5.11	N 1s	529	20	0.1
5.11	O 1s	620	20	0.1
5.11	Mo 3d	350	20	0.1
5.13	VB	100	20	0.1

Table C.2.: Scan parameters from NEXAFS measurements at Matline. Each scan is related to where they are presented in Chapter 5

Figure	Region	Photon energy (eV)	E_p (eV)	Energy-step (eV)
5.14	C 1s K-edge	278 to 302	20	0.2
5.14	N 1s K-edge	390 to 420	20	0.2
5.14	O 1s K-edge	520 to 545	20	0.25

Appendix D.

Thickness of deposited layers

This appendix derives an expression for estimating the thickness of a deposited overlayer by evaluating the intensity from core-levels in photoemission studies.

The following symbols and definitions are used in this derivation:

d = Thickness of deposited layer B.
I_A = The area of an peak emitted from material A
I_B = The area of an peak emitted from material B
σ_A = Cross section of peak in material A
σ_B = Cross section of peak in material B
λ = The inelastic mean free path in the material.

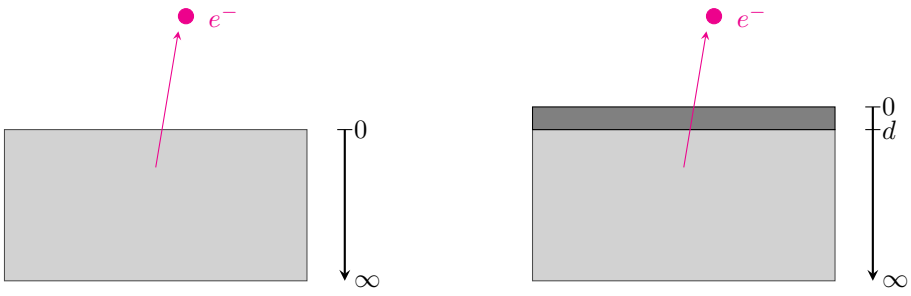

Figure D.1.: Photoemission from the sample before and after deposition of a new layer.

Before deposition, the signal to an given core level from material A is given by,

$$I_A = \sigma_A \int_0^\infty e^{-x/\lambda} \mathrm{d}x.$$

Evaluating the integral with the following substitution,

$$y = \frac{x}{\lambda} \qquad \text{and} \qquad \mathrm{d}x = \lambda \mathrm{d}y,$$

one obtains

$$I_A = \sigma_A \lambda \int_0^\infty e^{-y} \mathrm{d}y = -\sigma_A \lambda e^{-y} \Big|_0^\infty = -\sigma_A \lambda (0 - 1) = \sigma_A \lambda.$$

Now, for evaluating the signals after deposition, one must obviously take the new layer into account. The intensity of the signal from material B is given by,

$$I_B = \sigma_B \int_0^d e^{-x/\lambda} \mathrm{d}x.$$

By using the same substitution as above, this becomes,

$$I_B = \sigma_B \lambda \int_0^{d/\lambda} e^{-y} \mathrm{d}y = -\sigma_B \lambda e^{-y} \Big|_0^{d/\lambda} = -\sigma_B \lambda (e^{-d/\lambda} - 1) = \sigma_B \lambda (1 - e^{-d/\lambda}).$$

Analogously to the previous calculations, the signal from the now covered material A can be calculated as,

$$\begin{aligned} I_A = \sigma_A \int_d^\infty e^{-x/\lambda} \mathrm{d}x = \sigma_A \lambda \int_{d/\lambda}^\infty e^{-y} \mathrm{d}y = -\sigma_A \lambda e^{-y} \Big|_{d/\lambda}^\infty \\ = -\sigma_A \lambda (0 - e^{-d/\lambda}) = \sigma_A \lambda e^{-d/\lambda}. \end{aligned}$$

By simply comparing the ratios I_A and I_B the thickness of layer B can be found as,

$$d = \lambda \ln\left(1 + \frac{I_B/\sigma_B}{I_A/\sigma_A}\right).$$

The end expression for the thickness gives us an estimate of the thickness of the deposited layer, albeit with some very crude approximations. In reality, both the inelastic mean free path (λ) and the cross sections, σ_A and σ_B are heavily dependent on the electron energy. In addition the cross sections could change when a new layer is deposited onto the top of the original material. Despite this, the calculations are deemed as a proper estimate for the deposition thickness.

Another estimate, albeit with even higher uncertainty, would be to evaluate the attenuation of signal the intensity from material A when material B is deposited. Although simpler, this estimate relies on even cruder approximations, such as the cross sections of A and B being the same. The expression for this estimate is derived in (D.1).

$$
\begin{aligned}
I_A^{before} &= \sigma_A \lambda \\
I_A^{after} &= \sigma_A \lambda * e{-}d/\lambda
\end{aligned}
$$

$$
\frac{I_A^{before}}{I_A^{after}} = e^{d/\lambda} \Rightarrow d = \lambda \ln\left(\frac{I_A^{before}}{I_A^{after}}\right) \tag{D.1}
$$

Appendix E.

ASTRID(2) schematic drawing

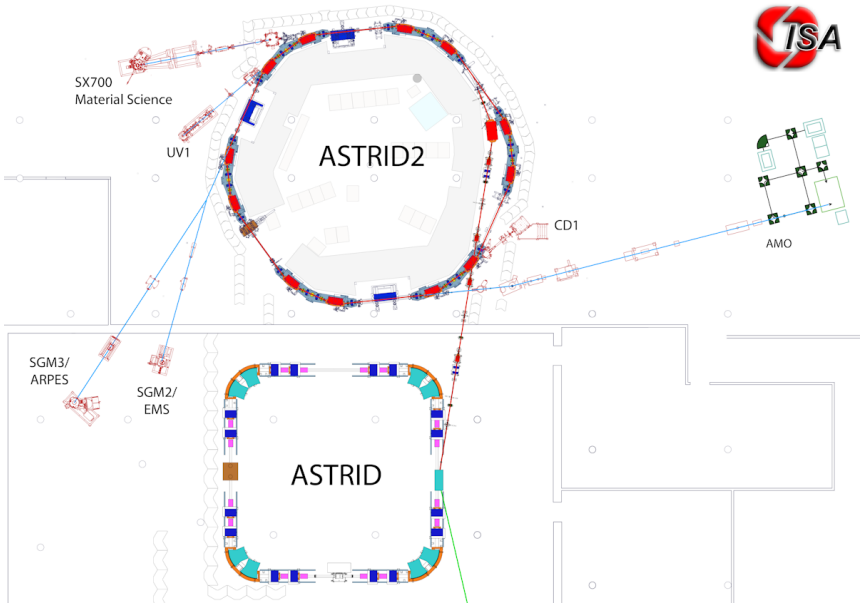

Figure E.1.: Drawing of the two synchrotrons ASTRID and ASTRID2. The beamline SX700 (= Matline) is seen in the top left corner of the image. ASTRID is used as an electron source for ASTRID2 [43].

Appendix F.

Fitted components in PE peaks

Table F.1.: Binding energy of found components in the thymine C 1s, N 1s and O 1s core-level measurements.

		Peak binding energy (eV)		
	Peak	At deposition	After 1 h exposure	After 6.5 h exposure
C 1s	1	289.7	289.7	291.1
	2	289.0	288.6	289.3
	3	288.3	287.7	288.1
	4	286.6	286.6	287.0
	5	286.0	285.8	285.9
	6	285.4	285.1	285.1
	7	284.8	284.1	284.4
N 1s	1	420.7	419.6	419.6
	2	420.1	-	419.0
	3	419.4	417.9	418.0
O 1s	1	531.9	532.7	532.7
	2	531.1	530.8	530.1
	3	530.4	530.0	530.0

Appendix G.

Tautomers of thymine

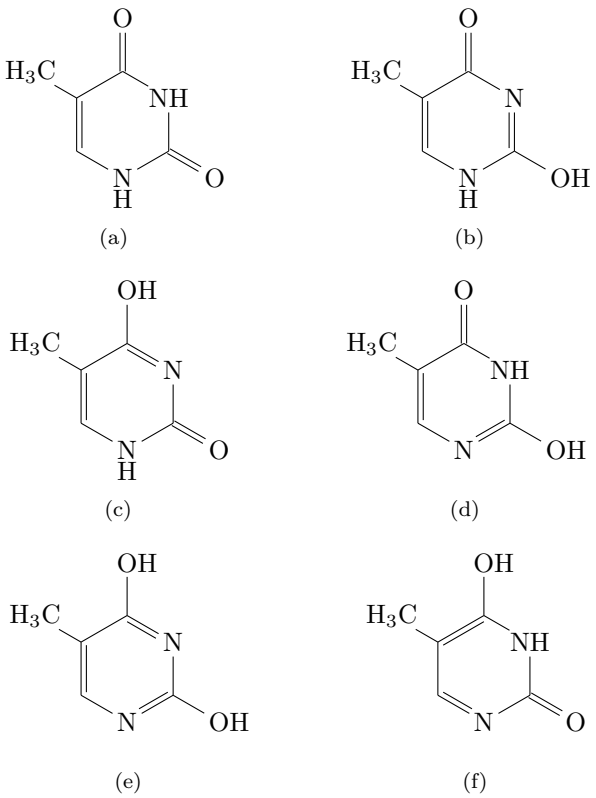

Figure G.1.: Tautomeric forms of thymine. The two most stable forms are believed to be (a) and (b) and according to the literature [105].

Appendix H.

Positions: laterally placed thymine

Figure H.1 shows the simulated orientations of two thymine molecules placed laterally. The difference between the figures, are as visible, the relative orientation between the thymine molecules.

(a) O1

(b) O2

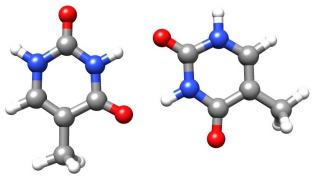

(c) HB1

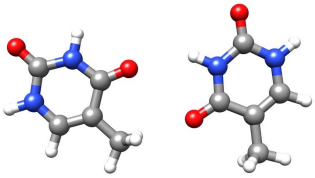

(d) HB2

Figure H.1.: Simualated lateral orientations of two thymine molecules relative to each other.

Bibliography

[1] Akar, A., Gümüş, H., and Okumuşoğlu, N. T. Electron inelastic mean free path formula and CSDA-range calculation in biological compounds for low and intermediate energies. *Appl. Radiat. Isot. 64*, 5 (may 2006), 543–50.

[2] Alberts, B., Johnson, A., Lewis, A., M, R., and K, R. The Initiation and Completion of DNA Replication in Chromosomes. In *Mol. Biol. Cell*. Garland Science, New York, NY, 2002, pp. 281–295.

[3] Albini, A. *Photochemistry - Past, Present and Future*. Springer Berlin / Heidelberg, 2016.

[4] Als-Nielsen, J., and McMorrow, D. *Elements of Modern X-ray Physics*. John Wiley & Sons, 2011.

[5] American Cancer Society. Cancer Facts & Figures 2014. Tech. rep., American Cancer Society, Atlanta, 2014.

[6] Barbatti, M., Aquino, A. J. A., and Lischka, H. The UV absorption of nucleobases: semi-classical ab initio spectra simulations. *Phys. Chem. Chem. Phys. 12*, 19 (may 2010), 4959–67.

[7] Beech, M. The physics of invisibility: A story of light and deception. *Phys. Invisibility A Story Light Decept. 9781461406* (2012), 1–206.

[8] Bernardi, M., Palummo, M., and Grossman, J. C. Photovoltaics using Two-Dimensional Monolayer Materials Extraordinary Sunlight Absorption and 1 nm-Thick Photovoltaics using Two-Dimensional Monolayer Materials. *Nano Lett.* (2013), 1–10.

[9] Bertolazzi, S., Brivio, J., and Kis, A. Stretching and breaking of ultrathin MoS2. *ACS Nano 5*, 12 (2011), 9703–9709.

[10] Bertram, J. S. Molecular Aspects Of Medicine. *Mol. Biol. Cancer 21*, 6 (2000), 167–223.

[11] Bilderback, D. H., Elleaume, P., and Weckert, E. Review of third and next generation synchrotron light sources. *J. Phys. B At. Mol. Opt. Phys. 38*, 9 (may 2005), S773–S797.

[12] Bischoff, F., Seufert, K., Auwärter, W., Joshi, S., Vijayaraghavan, S., Cija, D., Diller, K., Papageorgiou, A. C., Fischer, S., Allegretti, F., Duncan, D. A., Klappenberger, F., Blobner, F., Han, R., and Barth, J. V. How surface bonding and repulsive interactions cause phase transformations: Ordering of a prototype macrocyclic compound on Ag(111). *ACS Nano 7*, 4 (2013), 3139–3149.

[13] Brash, D. E., and Haseltine, W. A. UV-induced mutation hotspots occur at DNA damage hotspots. *Nature 298*, 5870 (jul 1982), 189–192.

[14] Browner, W. S., Kahn, A. J., Ziv, E., Reiner, A. P., Oshima, J., Cawthon, R. M., Hsueh, W. C., and Cummings, S. R. The genetics of human longevity. *Am. J. Med. 117*, 11 (2004), 851–860.

[15] Bunker, G. *Introduction to XAFS: A Practical Guide to X-ray Absorption Fine Structure Spectroscopy*. Cambridge University Press, Cambridge, Massachusetts, 2010.

[16] Carey, F., and Sundberg, R. J. *Advanced Organic Chemistry*. Advanced Organic Chemistry. Springer US, Boston, MA, 2007.

[17] Chung, Y.-W., and Chung, Y.-W. Fundamental concepts in ultrahigh vacuum, surface preparation, and electron spectroscopy. In *Pract. Guid. to Surf. Sci. Spectrosc.* Academic Press, 2001, ch. 1, pp. 1–22.

[18] Clark, D. P., and Pazdernik, N. J. *Biotechnology : academic cell update*. Academic Cell Press, 2012.

[19] Cumpson, P. J., Seah, M. P., and Spencer, S. J. Calibration of Auger and X-ray photoelectron spectrometers for valid analytical measurements. *Spectrosc. Eur. 3* (1998), 2–5.

[20] Damascelli, A. Probing the Electronic Structure of Complex Systems by ARPES. *Phys. Scr. T109*, T109 (2004), 61.

[21] Dixon, J. M., Taniguchi, M., and Lindsey, J. S. PhotochemCAD 2: A Refined Program with Accompanying Spectral Databases for Photochemical Calculations. *Photochem. Photobiol. 81*, 1 (may 2007), 212–213.

[22] Edenberg, H. J. Inhibition of DNA replication by ultraviolet light. *Biophys. J. 16*, 8 (aug 1976), 849–60.

[23] Edwards Limited. RV3, RV5, RV8 and RV12 Rotary Vane Pumps. Tech. rep., Edwards Ltd., 2015.

[24] Einstein, A. Über einen die Erzeugung und Verwandlung des Lichtes betreffenden heuristischen Gesichtspunkt. *Ann. Phys. 322*, 6 (1905), 132–148.

[25] El Ghissassi, F., Baan, R., Straif, K., Grosse, Y., Secretan, B., Bouvard, V., Benbrahim-Tallaa, L., Guha, N., Freeman, C., Galichet, L., and Cogliano, V. A review of human carcinogens—Part D: radiation. *Lancet Oncol. 10*, 8 (aug 2009), 751–752.

[26] Falck, M. *A Study of Thymine to support Experimentalists - Interaction Energies and Core Ionisation Energies.* Master thesis, Norwegian University of Science and Technology, 2016.

[27] Fausto, R., Borba, A., and Gomez-Zavaglia, A. Light induced reactions in cryogenic matrices (highlights 2013-2014). In *Photochem. Vol. 43*, vol. 43. The Royal Society of Chemistry, 2016, pp. 20–82.

[28] Fuggle, J. C., and Alvarado, S. F. Core-level lifetimes as determined by x-ray photoelectron spectroscopy measurements. *Phys. Rev. A 22*, 4 (1980), 1615–1624.

[29] Geim, A. K. Graphene: Status and Prospects. *Science (80-.). 324*, 5934 (2009), 1530–1534.

[30] Geim, A. K., and Novoselov, K. S. The rise of graphene. *Nat Mater 6*, 3 (2007), 183–191.

[31] Grundmann, M. *The physics of semiconductors: An introduction including devices and nanophysics.* Springer Berlin / Heidelberg, 2006.

[32] Gupta, A., Sakthivel, T., and Seal, S. Recent development in 2D materials beyond graphene. *Prog. Mater. Sci. 73* (2015), 44–126.

[33] Hähner, G. Near edge X-ray absorption fine structure spectroscopy as a tool to probe electronic and structural properties of thin organic films and liquids. *Chem. Soc. Rev. 35*, 12 (2006), 1244–1255.

[34] Harra, D. J. Review of sticking coefficients and sorption capacities of gases on titanium films. *J. Vac. Sci. Technol. 13*, 1 (jan 1976), 471.

[35] Hattori, M. Finishing the euchromatic sequence of the human genome. *Tanpakushitsu Kakusan Koso. 50*, 2 (2005), 162–168.

[36] Helbling, E. W. *UV Effects in Aquatic Organisms and Ecosystems.* Royal Society of Chemistry, 2003.

[37] Helveg, S., Lauritsen, J. V., Laegsgaard, E., Stensgaard, I., Noerskov, J. K., Clausen, B. S., Topsoe, H., and Besenbacher, F. Atomic-Scale Structure of Single-Layer MoS2 Nanoclusters. *Phys. Rev. Lett. 84*, 5 (jan 2000), 951–954.

[38] Hertz, H. Ueber einen Einfluss des ultravioletten Lichtes auf die electrische Entladung. *Ann. der Phys. und Chemie 267*, 8 (1887), 983–1000.

[39] Hoffman, D., Singh, B., Thomas, J. H., and III. *Handbook of Vacuum Science and Technology*, vol. 5. Academic Press, 1997.

[40] Hofmann, P. Ion Pump.

[41] Hofmann, S. *Auger- and X-Ray Photoelectron Spectroscopy in Materials Science*, vol. 49 of *Springer Series in Surface Sciences*. Springer Berlin Heidelberg, Berlin, Heidelberg, 2013.

[42] Hüfner, S. *Photoelectron spectroscopy: principles and applications*. Springer Berlin / Heidelberg, 2003.

[43] ISA Centre for Storage Ring Facilities. ASTRID2 – the ultimate synchrotron radiation source, 2012.

[44] Jiang, J.-W. Graphene versus MoS2: A short review. *Front. Phys. 10*, 3 (2015), 287–302.

[45] Kan, M., Wang, J. Y., Li, X. W., Zhang, S. H., Li, Y. W., Kawazoe, Y., Sun, Q., and Jena, P. Structures and Phase Transition of a MoS2 Monolayer. *J. Phys. Chem. C 118*, 3 (2014), 1515–1522.

[46] Kang, J., Cao, W., Xie, X., Sarkar, D., Liu, W., and Banerjee, K. Graphene and beyond-graphene 2D crystals for next-generation green electronics. *Proc. SPIE 9083* (2014), 908305.

[47] Kauzmann, W. *Kinetic Theory of Gases*. Courier Corporation, 2012.

[48] Khosravi, H., Schmidt, B., and Huang, J. T. Characteristics and outcomes of nonmelanoma skin cancer (NMSC) in children and young adults. *J. Am. Acad. Dermatol. 73*, 5 (nov 2015), 785–90.

[49] Kittel, C. *Introduction to Solid State Physics*. Wiley, 2004.

[50] Knapp, W. Vacuum Electronics. In *Vac. Electron. Components Devices*, J. A. Eichmeier and M. K. Thumm, Eds. Springer Berlin Heidelberg, Berlin, Heidelberg, 2008.

[51] Kodym, A., and Afza, R. Physical and chemical mutagenesis. *Methods Mol. Biol. 236* (jan 2003), 189–204.

[52] Kristensen, K., Ettenhuber, P., Eriksen, J. J., Jensen, F., and Jørgensen, P. The same number of optimized parameters scheme for determining intermolecular interaction energies. *J. Chem. Phys. 142*, 11 (mar 2015), 114116.

[53] Kurth, M., Graat, P., and Mittemeijer, E. Determination of the intrinsic bulk and surface plasmon intensity of XPS spectra of magnesium. *Appl. Surf. Sci. 220*, 1-4 (dec 2003), 60–78.

[54] Larmor, J. LXIII. On the theory of the magnetic influence on spectra; and on the radiation from moving ions. *Philos. Mag. Ser. 5 44*, 271 (dec 1897), 503–512.

[55] Lauritsen, J. V., Kibsgaard, J., Helveg, S., Topsoe, H., Clausen, B. S., Laegsgaard, E., and Besenbacher, F. Size-dependent structure of MoS2 nanocrystals. *Nat Nano 2*, 1 (2007), 53–58.

[56] Leybold Vacuum. TRIVAC B Rotary Vane Vacuum Pump S/D 1,6 B. Tech. rep., Leybold Vacuum, 1991.

[57] Li, J., Liu, Z., Tan, C., Guo, X., Wang, L., Sancar, A., and Zhong, D. Dynamics and mechanism of repair of ultraviolet-induced (6-4) photoproduct by photolyase. *Nature 466*, 7308 (aug 2010), 887–890.

[58] Lim, H., Yoon, S. I., Kim, G., Jang, A.-R., and Shin, H. S. Stacking of Two-Dimensional Materials in Lateral and Vertical Directions. *Chem. Mater. 26*, 17 (sep 2014), 4891–4903.

[59] Lindahl, T. Instability and decay of the primary structure of DNA. *Nature 362* (1993), 709–715.

[60] Lodish, H., Berk, A., Zipursky, S. L., Matsudaira, P., Baltimore, D., and Darnell, J. Molecular Cell Biology, 2000.

[61] Lüth, H. *Solid Surfaces, Interfaces and Thin Films*. Graduate Texts in Physics. Springer Berlin Heidelberg, Berlin, Heidelberg, 2010.

[62] Mandl, F. F. *Quantum mechanics*. Wiley, 1992.

[63] Margaritondo, G. Synchrotron light in a nutshell. *Surf. Rev. Lett. 7*, 1995 (2000), 379–387.

[64] Mattila, S., Leiro, J. A., Heinonen, M., and Laiho, T. Core level spectroscopy of MoS2. *Surf. Sci. 600*, 24 (2006), 5168–5175.

[65] Mazzola, F. *Photoemission spectroscopies and their application in solid state and material physics*. Phd thesis, Norwegian University of Science and Technology, 2016.

[66] Meinert, C., Myrgorodska, I., de Marcellus, P., Buhse, T., Nahon, L., Hoffmann, S. V., Hendecourt, L. L. S., and Meierhenrich, U. J. Ribose and related sugars from ultraviolet irradiation of interstellar ice analogs. *Science (80-.). 352*, 6282 (apr 2016), 208–212.

[67] Metcalfe, T. Diagnosing lesions and preventing skin cancer. *Nurs. N. Z. 21*, 11 (dec 2015), 12–3.

[68] Miller, A. J., and Mihm, M. C. Melanoma. *N. Engl. J. Med. 355*, 1 (jul 2006), 51–65.

[69] Miró, P., Audiffred, M., and Heine, T. An atlas of two-dimensional materials. *Chem. Soc. Rev. 43*, 18 (sep 2014), 6537–54.

[70] Mitchell, D. L., and Nairn, R. S. The biology of the (6-4) photoproduct. *Photochem. Photobiol. 49*, 6 (jun 1989), 805–19.

[71] Mobilio, S., Boscherini, F., and Meneghini, C. *Synchrotron radiation: Basics, methods and applications*. Springer-Verlag, 2015.

[72] Møller, C., and Plesset, M. S. Note on an Approximation Treatment for Many-Electron Systems. *Phys. Rev. 46*, 7 (oct 1934), 618–622.

[73] Moran, L. A., Horton, R. A., Scrimgeour, G., Perry, M., and Rawn, D. *Principles of Biochemistry*, 5th ed. Pearson Education Limited, Harlow, United Kingdom, 2013.

[74] Nefedov, A., and Wöll, C. Advanced applications of NEXAFS spectroscopy for functionalized surfaces. *Springer Ser. Surf. Sci. 51*, 1 (2013), 277–303.

[75] Nicolosi, V., Chhowalla, M., Kanatzidis, M. G., Strano, M. S., and Coleman, J. N. Liquid Exfoliation of Layered Materials. *Science (80-.). 340*, 6139 (2013), 1226419.

[76] Niemantsverdriet, J. W. *Also of Interest : Spectroscopy in Catalysis Principles and Practice of Heterogeneous Catalysis Organic Chemistry Principles and Industrial Practice*. WILEY-VCH Verlag GmbH, 2003.

[77] Niu, T., and Li, A. From two-dimensional materials to heterostructures. *Prog. Surf. Sci. 90*, 1 (2015), 21–45.

[78] Nonnenmacher, M., O'Boyle, M. P., and Wickramasinghe, H. K. Kelvin probe force microscopy. *Appl. Phys. Lett. 58*, 25 (1991), 2921.

[79] Novoselov, K. S., and Castro Neto, a. H. Two-dimensional crystals-based heterostructures: materials with tailored properties. *Phys. Scr. T146* (2012), 014006.

[80] Novoselov, K. S., Falko, V. I., Colombo, L., Gellert, P. R., Schwab, M. G., and Kim, K. A roadmap for graphene. *Nature 490*, 7419 (2012), 192–200.

[81] Noyes, W. A. J., Porter, G. B., and Jolley, J. E. The Primary Photochemical Process in Simple Ketones. *Chem. Rev. 56* (1956), 49–94.

[82] OED. Oxford English Dictionary Online, 2016.

[83] Pan, Y., Sahoo, N. G., and Li, L. The application of graphene oxide in drug delivery. *Expert Opin. Drug Deliv. 9*, 11 (2012), 1365–1376.

[84] Perkins, W. G. Permeation and Outgassing of Vacuum Materials. *J. Vac. Sci. Technol. 10*, 4 (jul 1973), 543.

[85] Pfeiffer Vacuum. Working with Turbopumps - Introduction to high and ultra high cauum production. Tech. rep., 2003.

[86] Quirk, M., and Serda, J. *Semiconductor manufacturing technology.* Prentice Hall, 2001.

[87] Reece, J., Urry, L., Cain, M., Wasserman, S., Minorsky, P., and Jackson, R. *Campbell Biology (9th Edition).* Benjamin Cummings, 2010.

[88] Rhodes, A. R., Weinstock, M. A., Fitzpatrick, T. B., Mihm, M. C., and Sober, A. J. Risk factors for cutaneous melanoma. A practical method of recognizing predisposed individuals. *JAMA 258*, 21 (dec 1987), 3146–54.

[89] Sadava, D. E., Hillis, D. M., Heller, H. C., and Berenbaum, M. *Life: The science of Biology.* W. H. Freeman, 2012.

[90] Schreier, W. J., Schrader, T. E., Koller, F. O., Gilch, P., Crespo-Hernández, C. E., Swaminathan, V. N., Carell, T., Zinth, W., and Kohler, B. Thymine dimerization in DNA is an ultrafast photoreaction. *Science 315*, 5812 (feb 2007), 625–9.

[91] Schürmann, R., and Bald, I. Decomposition of DNA Nucleobases by Laser Irradiation of Gold Nanoparticles Monitored by Surface-Enhanced Raman Scattering. *J. Phys. Chem. C 120*, 5 (feb 2016), 3001–3009.

[92] Schwierz, F. Graphene transistors. *Nat. Nanotech 5*, 7 (2010), 487–96.

[93] Seah, M. P., and Dench, W. a. Quantitative electron spectroscopy of surfaces: A standard data base for electron inelastic mean free paths in solids. *Surf. Interface Anal. 1*, 1 (1979), 2–11.

[94] Seah, M. P., Gilmore, I. S., and Spencer, S. J. XPS : Binding Energy Calibration of Electron Spectrometers Assessment of Effects for Different X-ray Sources , Analyser Resolutions , Angles of Emission and Overall Uncertainties. *Surf. Interface Anal. 26*, 9 (1998), 617–641.

[95] Shen, H., Zhang, L., Liu, M., and Zhang, Z. Biomedical applications of graphene. *Theranostics 2*, 3 (2012), 283–294.

[96] Sheneve Z. Butler, Shawna M. Hollen, Linyou Cao, Yi Cui, J. A. G. Opportunities in Two-Dimensional Materials Beyond Graphene. *ACS Nano 7*, 4 (2013), 2898–2926.

[97] Sherwood, P. M. A. Curve fitting in surface analysis and the effect of background inclusion in the fitting process. *J. Vac. Sci. Technol. A Vacuum, Surfaces Film. 14*, 3 (1996), 1424–1432.

[98] Siegel, R., and Howell, J. R. *Thermal radiation heat transfer*. Taylor & Francis, 2002.

[99] Smith, G., Seah, M., and Anthony, M. T. The Calibration of Spectrometers for Auger electron and X-ray Photoelectron Spectrometers: Part I - an absolute traceable energy calibration for electron spectrometers. Tech. rep., European Commission, 1991.

[100] Spirko, J. A., Neiman, M. L., Oelker, A. M., and Klier, K. Electronic structure and reactivity of defect MoS{$_2$}. *Surf. Sci. 542*, 3 (sep 2003), 192–204.

[101] Stoehr, J., and Outka, D. A. Determination of molecular orientations on surfaces from the angular dependence of near-edge x-ray-absorption fine-structure spectra. *Phys. Rev. B 36*, 15 (1987), 7891–7905.

[102] Szatyłowicz, H., and Sadlej-Sosnowska, N. Characterizing the Strength of Individual Hydrogen Bonds in DNA Base Pairs. *J. Chem. Inf. Model. 50*, 12 (dec 2010), 2151–2161.

[103] Tataurov, A. V., You, Y., and Owczarzy, R. Predicting ultraviolet spectrum of single stranded and double stranded deoxyribonucleic acids. *Biophys. Chem. 133*, 1-3 (2008), 66–70.

[104] Thiam, A., Zhao, Z., Quinn, C., and Barber, B. Years of life lost due to metastatic melanoma in 12 countries. *J. Med. Econ. 19*, 3 (jan 2016), 259–64.

[105] Tsuchiya, Y., Tamura, T., Fujii, M., and Ito, M. Keto-enol tautomer of uracil and thymine. *J. Phys. Chem. 92*, 7 (1988), 1760–1765.

[106] Wang, X., and Xia, F. Van der Waals heterostructures: Stacked 2D materials shed light. *Nat Mater 14*, 3 (mar 2015), 264–265.

[107] Watts, J. F., and Wolstenholme, J. *An Introduction to Surface Analysis by XPS and AES*. John Wiley & Sons, Ltd, Chichester, UK, mar 2003.

[108] Willmott, P. *An Introduction to Synchrotron Radiation: Techniques and Applications*, 1st ed. John Wiley & Sons, Ltd, 2011.

[109] Witkin, E. M. Time, Temperature, and Protein Synthesis: A Study of Ultraviolet-Induced Mutation in Bacteria. *Cold Spring Harb. Symp. Quant. Biol. 21*, 0 (jan 1956), 123–140.

[110] Witkin, E. M. Ultraviolet-Induced Mutation and DNA Repair. *Annu. Rev. Genet. 3*, 1 (dec 1969), 525–552.

[111] Yang, Q., Tang, Y., Yang, S. L., Li, Y. S., and Hirose, A. Simultaneous growth of diamond thin films and carbon nanotubes at temperatures less than 500C. *Carbon N. Y. 46*, 4 (2008), 589–595.

[112] Yeh, J. J., and Lindau, I. Atomic subshell photoionization cross sections and asymmetry parameters: $1 < Z < 103$. *At. Data Nucl. Data Tables 32* (1985), 1–155.

[113] Yoshimura, N. *Vacuum Technology*. Springer Berlin Heidelberg, Berlin, Heidelberg, 2008.

[114] Yoshizawa, T. *Handbook of optical metrology : principles and applications*. CRC Press Inc., 2015.

[115] Zhang, W., Wang, Q., Chen, Y., Wang, Z., and Wee, A. T. S. Van der Waals stacked 2D layered materials for optoelectronics. *2D Mater. 3*, 2 (2016), 022001.

[116] Zubavichus, Y., Shaporenko, A., Korolkov, V., Grunze, M., and Zharnikov, M. X-ray absorption spectroscopy of the nucleotide bases at the carbon, nitrogen, and oxygen K-edges. *J. Phys. Chem. B 112*, 44 (2008), 13711–13716.